



Cranston, Laura Jessica (2017) *Structural and functional studies of LH2 complexes having unusual spectroscopic properties*. PhD thesis.

<http://theses.gla.ac.uk/8219/>

Copyright and moral rights for this work are retained by the author

A copy can be downloaded for personal non-commercial research or study, without prior permission or charge

This work cannot be reproduced or quoted extensively from without first obtaining permission in writing from the author

The content must not be changed in any way or sold commercially in any format or medium without the formal permission of the author

When referring to this work, full bibliographic details including the author, title, awarding institution and date of the thesis must be given

Enlighten:Theses
<http://theses.gla.ac.uk/>
theses@gla.ac.uk

Structural and Functional Studies of LH2 Complexes Having Unusual Spectroscopic Properties

Laura Jessica Cranston

BSc (Hons)

Submitted in fulfilment of the requirements for the Degree of Doctor of Philosophy

School of Molecular, Cellular and Systems Biology

College of Medical, Veterinary and Life Sciences

University of Glasgow

2016

Author's declaration

This thesis is an original composition that describes work performed entirely by myself unless otherwise cited or acknowledged. Its contents have not previously been submitted for any other degree. The research for this degree was performed between 2010 and 2014.

Signature:.....

Printed Name:.....

Abstract

The harvesting of light is an important, primary event in photosynthesis, allowing for the transfer of energy to the reaction centre. Purple photosynthetic bacteria use two types of antenna complexes (LH1, LH2) to enhance the efficiency of light harvesting and funnelling energy into the photosynthetic reaction centre. *Marichromatium (Mcr). purpuratum* is an example of a species that can synthesise antenna complexes that have an unusual absorption spectrum. This LH2 complex has a single strong absorption band at approximately 830nm, with a shoulder at 800nm, also known as the B800-B830 LH2 complex

This thesis investigates *Mcr. purpuratum* and the structural basis for the unusual spectrum of the LH2 complex. The LH2 complex was isolated, purified and, after optimising the purification for stability, crystallised. A low-resolution crystal structure of the LH2 complex is presented, which suggests that this LH2 complex is an octamer, similar to *Phaeospirillum (Phs.) molischianum*. During this thesis the genome sequence of *Mcr. purpuratum* became available and I was able to show it contained three *pucBA* operons, which expressed three β and three α polypeptides, respectively. These were all identified in the purified LH2 complex, confirming that it is heterogeneous.

Mcr. purpuratum is not able to produce an LH2 complex in the absence of carotenoid biosynthesis. This was shown by chemical inhibition of phytoene desaturase with DPA, however this chemical is also toxic to the cell. In order to overcome this genetic manipulation by knock-out of the *CrtI* gene was attempted but due to time constraints was not completed

Acknowledgments

I wish to thank, with all my heart, my supervisor Prof. Richard Cogdell. This has been a wonderful opportunity and, without a doubt, the hardest thing I have ever done in my life. I could not have finished without his patience, support and enthusiasm. I wish him the best and many happy years with his grandchildren.

Thank you to EPSRC for the funding, which made this project possible.

I also want to give giant thanks to all of Team Cogdell, especially to Dr. Kirsty Hacking and Dr. Alastair Gardiner. The entire lab was always ready to help and was always so friendly. It was a pleasure to meet and work with every single member. Thanks also Dr. Bill Mullen for all the help with the Mass Spectroscopy and to Prof. Neil Hunter and Dr. Pu Qian, at the University of Sheffield, for the EM images.

A huge amount of gratitude goes out to my friends who never let me give up. I would like to thank the Godhond for their hilarity, frills, kindness and always being there for me when I needed them. Thanks to Annabel and Omar for dog cuddles, wine and many, many nights of board games, which kept me sane (or not in the case of Kingdom Death). Special thanks to Julia for genuinely being the most beautiful person I know, inside and out.

My loving partner, Adrien, has been my constant rock and my personal Batman. I cannot thank him enough. I don't know what I would have done without him, and I hope that we can chase our dreams together.

Finally, I would like to thank my family, my Mum and Dad, for their constant support and love throughout everything. Thank you for always believing and trusting me. I dedicate this to you.

There have been many ups and downs on this journey and I could not have done it alone.

“The Road goes ever on and on
Down from the door where it began.
Now far ahead the Road has gone.
And I must follow, if I can,
Pursuing it with eager feet,
Until it joins some larger way
Where many paths and errands meet.
And whither then? I cannot say”
— J.R.R. Tolkien

Table of Contents

Author's declaration.....	ii
Abstract.....	iii
Acknowledgments.....	iv
Table of Contents.....	v
List of Figures.....	ix
List of Tables.....	xiii
List of Abbreviations.....	xiv
Chapter 1 - Introduction.....	1
1.1 Overview of Photosynthesis in Bacteria.....	1
1.2 The Pigments.....	2
1.2.1 Bacteriochlorophyll.....	2
1.2.2 Carotenoids.....	3
1.3 The Bacterial Photosynthetic Unit.....	5
1.4 LH1-RC. The “Core” Complex.....	6
1.5 The LH2. The Peripheral Complex.....	9
1.6 Energy Transfer.....	15
1.7 Marichromatium (Mcr.) purpuratum.....	16
1.7.1 Discovery.....	16
1.7.2 Light Harvesting.....	16
1.7.3 Okenone.....	17
1.8 Determining the 3-D Structure of Proteins.....	18
1.8.1 3-D Crystallisation of Membrane Proteins.....	18
1.8.1.1 Detergents.....	19
1.8.2 Phase Diagram.....	20
1.8.3 Crystal Growth and Quality.....	21
1.9 Thesis Aims.....	21
Chapter 2 - Methods and Materials.....	22
2.1 Growth of the bacteria.....	22

2.1.1.	Cell Culture and Standard Growth Conditions	22
2.1.2.	Harvesting the Cells and Membrane Preparation.....	22
2.2.	Purification of the LH2 Complex.....	22
2.2.1.	Solubilisation	22
2.2.2.	Anion Exchange Purification and Detergent Exchange.....	23
2.2.3.	Size Exclusion Chromatography.....	23
2.3.	Purification of the LH1-RC Complex	24
2.3.1.	Solubilisation	24
2.3.2.	Anion Exchange Purification and Size Exclusion Chromatography	24
2.4.	Steady- State Absorption Spectroscopy	24
2.5.	SDS-Polyacrylamide Gel Electrophoresis (PAGE)	24
2.6.	Stability of the LH2 Complex in the Presence of Different Detergents.....	25
2.7.	Crystallisation Trials of the LH2 Complex.....	25
2.7.1.	Initial 96 Well Screens	25
2.7.1.1.	Optimisation.....	26
2.7.1.2.	Altering the Purification and Detergent	26
2.8.	Thin Whole Cell Sections	26
2.9.	Reconstitution of <i>Mcr. purpuratum</i> LH2 into Lipid.....	27
2.10.	Molecular Biology	28
2.10.1.	Trials to grow <i>Mcr. purpuratum</i> on Agar plates	28
2.10.2.	Preparation of High Molecular Weight <i>Mcr. purpuratum</i> Genomic DNA	29
2.11.	Investigation of the Carotenoids of <i>Mcr. purpuratum</i>	30
2.11.1.	Diphenylamine Trials.....	30
2.11.1.1.	Bacteria Growth	30
2.11.2.	CrtI Knock Out.....	31
2.11.2.1.	Amplification of Genes for Cloning	31
2.11.3.	Transformation into pJET 1.2/blunt.....	32
2.11.4.	Mobsac Ligation	33
2.11.5.	Conjugation.....	33
2.12.	Analysis of the LH2 polypeptides.....	35

2.12.1.	Mass Spectrometry of <i>Mcr. purpuratum</i>	35
2.12.2.	Peptide Extractions	35
2.12.3.	MALDI-TOF.....	35
2.12.4.	LH60 Column	35
2.12.5.	Tandem MS-MS.....	35
2.12.6.	High-Performance Liquid Chromatography	36
2.12.7.	Deletion of the <i>pucBA2</i> gene.....	37
Chapter 3 - Purification and Crystallisation of the LH2 complex from <i>Mcr. purpuratum</i>		38
3.1.	Purification of the LH2 Complex.....	38
3.1.4.	Optimised Purification of the LH2 Complex	45
3.1.5.	SDS-PAGE of Membranes, Crude LH2 Extracts and Purified LH2 Complex from <i>Mcr. purpuratum</i>	48
3.2.	Electron Micrograph Images of <i>Mcr. purpuratum</i> Whole Cells	49
3.3.	Lipid Reconstitution of the LH2 Complex.....	49
3.4.	Crystallisation of the LH2 Complex from <i>Mcr. purpuratum</i>	53
3.5.	X-ray data collection and processing	58
3.6.	Summary and Analysis	61
Chapter 4 - Analysis of the LH2 Polypeptides from <i>Mcr. purpuratum</i>		63
4.1.	Locating the <i>Mcr. purpuratum</i> <i>puc</i> Operons	63
4.2.	Mass Spectrometry.....	66
4.2.1.	Tandem MS-MS.....	70
4.3.	Peptide Sequences and Alignment	72
4.4.	High Pressure Liquid Chromatography (HPLC).....	78
4.5.	<i>puc</i> Knock out	80
4.6.	Summary and Analysis	82
Chapter 5 - Investigating whether the LH2 complex from <i>Mcr. purpuratum</i> can be synthesised in the absence of carotenoid.....		84
5.1.	Inhibition of Carotenoid Biosynthesis by Diphenylamine.....	84
5.1.1.	Determining the effective DPA concentration	85
5.1.2.	Large scale production of DPA treated cells.....	87
5.2.	Trials to Grow <i>Mcr. purpuratum</i> on Agar Plates and Antibiotic Resistance	91

5.3.	Deletion of the phytoene desaturase (CrtI) gene.....	93
5.3.1.	Primer design and creation of the CrtI KO insert	93
5.3.2.	Transformation into pJET 1.2/blunt.....	95
5.3.3.	Ligation of the CrtI KO into Mobsac.....	96
5.3.4.	Conjugation of the pK18mobsacB + CrtI KO with <i>Mcr. purpuratum</i>	97
5.4.	Summary and Analysis	100
6.	Conclusions and Outlook.....	103
8.	Appendices.....	107
8.1.	<i>Mcr. purpuratum</i> media (Pfennig's Media)	107
8.2.	Detergent Percentages.....	108
8.2.1.	Solubilisation:	108
8.2.2.	Detergent concentrations in buffers:	108
8.3.	Sucrose gradients:	108
8.4.	Dialysis Buffer	109
8.5.	Agar Plates	110
8.6.	Lysis buffer	110
8.7.	LB	110
8.8.	Crystallisation Screens.....	111
8.8.1.	MemGold	111
	References.....	115

List of Figures

Figure 1-1: The general photosynthetic equation derived by van Niel.....	1
Figure 1-2: Chemical structure of Bchl a.....	3
Figure 1-3: Absorption spectrum of Bchl <i>a</i> in organic solvent.....	3
Figure 1-4: Structure of the carotenoid β -carotene.....	4
Figure 1-5: A representation of a purple bacterial photosynthetic membrane.....	5
Figure 1-6: A schematic of the photosynthetic unit viewed perpendicular to the membrane.....	6
Figure 1-7: Cofactor components and arrangement in purple bacterial reaction centres (RC).....	7
Figure 1-8: Model of the LH1-RC from <i>Rps. palustris</i>	8
Figure 1-9: $\alpha\beta$ heterodimer subunit pigments from <i>Rps. acidophila</i> 10050.....	9
Figure 1-10: Absorption spectra showing the red-shift of the Bchl <i>a</i> Q_y bands in the <i>Rps.</i> <i>acidophila</i> LH2 complex in organic solvent.....	11
Figure 1-11: Structural comparison of the LH2 from nonameric <i>Rps. acidophila</i> 10050 (left) with the <i>Phs. molischianum</i> (right) octameric complex.....	12
Figure 1-12: The hydrogen bonding of the B850 LH2 complex of <i>Rps. acidophila</i> 10050 and the B820 LH2 complex of <i>Rps. acidophila</i> 7050.....	14
Figure 1-13: Diagram of an energy level diagram of a carotenoid, B800 Bchl <i>a</i> and B850 Bchl <i>a</i>	16
Figure 1-14: Absorption spectra of <i>Mcr. purpuratum</i> chromatophores at room temperature.....	17
Figure 1-15: Diagram showing the pathway for the synthesis of the carotenoid Okenone.....	18
Figure 1-16: A phase diagram showing the solubility of a protein in solution as a function of the concentration of the precipitant present.....	20
 Figure 2-1: Schematic of SDGs showing the optimised conditions for the best separation of the LH complexes in 20mM Tris-HCl at pH 9.0 containing 0.1 % (v/v) LDAO	23
Figure 2-2: Schematic of SDGs showing the optimised conditions for the best separation of the LH complexes in 20mM Tris-HCl at pH 9.0 containing 0.15 % (w/v) DM	24
Figure 2-3: Diagram showing the location of the primers used to knock out the <i>CrtI</i> gene.....	32

Figure 3-1: <i>Mcr. purpuratum</i> cell culture and absorption spectrum.....	38
Figure 3-2: Comparison of the Q _y absorption of <i>Mcr. purpuratum</i> whole cells grown at their normal light conditions (control) and at low light conditions.....	39
Figure 3-3: Comparison of the spectra of <i>Mcr. purpuratum</i> membranes grown at their normal light conditions (control) and at low light conditions.....	40
Figure 3-4: Sucrose Gradient trials with <i>Mcr. purpuratum</i> membranes solubilised in different detergents.....	41
Figure 3-5: Absorption spectrum of <i>Mcr. purpuratum</i> before and after solubilisation with LDAO	42
Figure 3-6: Absorption spectra of the LH2 complex from <i>Mcr. purpuratum</i> solubilised in LDAO.....	43
Figure 3-7: Absorption spectra of the LH2 complex from <i>Mcr. purpuratum</i> solubilised in DDM.....	44
Figure 3-8: Absorption spectra of the LH2 complex from <i>Mcr. purpuratum</i> solubilised in DM.....	44
Figure 3-9: Chromatogram from the SEC purification of the LH2 complex from <i>Mcr. purpuratum</i>	46
Figure 3-10: Absorption spectra recorded throughout the purification of the LH2 complex.....	47
Figure 3-11: Absorption spectrum of the LH2 complex from <i>Mcr. purpuratum</i> at room temperature.....	47
Figure 3-12: SDS-PAGE gel of samples taken at various points along the LH2 purification protocol.....	48
Figure 3-13: EM image of a thin section of <i>Mcr. purpuratum</i> whole cells.....	49
Figure 3-14 -Negative stained EM image of fully purified, monodisperse LH2.....	50
Figure 3-15: Theorised view of the formation of the proteoliposomes from the <i>Mcr. purpuratum</i> LH2 complex.....	51
Figure 3-16: Electron micrograph (EM) images of gel filtrated LH2 added to a range of different lipids.....	52
Figure 3-17: Crystals of the LH2 complex from <i>Mcr. purpuratum</i>	54
Figure 3-18: Examples of optimising a crystal hit in a 24 well plate (6x4).....	55
Figure 3-19: A collection of images of crystals obtained from the initial optimisation 24 well screens.....	55
Figure 3-20: Promising crystal hits from the MemGold 24-well screen.....	56
Figure 3-21: Optimisation of the crystal hits in the MemGold 24-well screen conditions seen in Figure 3-20.....	57
Figure 3-22: Crystal of the <i>Mcr. purpuratum</i> LH2 complex shown inside the LithoLoop.....	58

Figure 3-23: Diffraction pattern from the <i>Mcr. purpuratum</i> LH2 crystal.....	59
Figure 3-24: Crystal packing for the successful Molecular Replacement (MR) solution in space group <i>I4</i> , which forms the octameric <i>Mcr. Purpuratum</i> LH2 ring around the fourfold axis, viewed along this axis.....	60
Figure 4-1: Contig 82 of the <i>Mcr. purpuratum</i> genome.....	64
Figure 4-2: Mass Spectrometry Chromatograms for the ExP sample from purified LH2 complexes from <i>Mcr. purpuratum</i>	68
Figure 4-3: A-Overview of the MALDI-TOF results from the ExPP sample from <i>Mcr. purpuratum</i> LH2.....	69
Figure 4-4: Raw Tandem MS-MS data from the LH2 complex from <i>Mcr. purpuratum</i>	71
Figure 4-5: Alignment of the final modified expressed β and α LH2 polypeptides of <i>Mcr. purpuratum</i> alongside the original <i>puc</i> gene sequence.....	73
Figure 4-6: Alignment of the final expressed β and α LH2 polypeptides of <i>Mcr. purpuratum</i>	73
Figure 4-7: The six potential α and β peptides from <i>Mcr. purpuratum</i> aligned to the BChl a coordinating histidine of the twelve potential α and β peptides of <i>Alc. vinosum</i> and the B800-850 and B800-820 α and β from <i>Rps. acidophila</i> , and <i>Phs. Molischianum</i>	77
Figure 4-8: HPLC chromatograms for the peptide extracts from purified LH2 complexes from <i>Mcr. purpuratum</i>	79
Figure 4-9: Diagram showing the location of the primers used to knock out the <i>pucBA2</i> gene.....	80
Figure 4-10: Agarose DNA gel of the amplified upstream (UP) and Downstream (DN) fragments for the <i>pucBA2</i> KO.....	81
Figure 4-11: Diagram showing the PJET 1.2 vector with the <i>pucBA</i> KO insert.....	81
Figure 5-1: <i>Mcr. purpuratum</i> culture grown in the presence of DPA between 0 μ M and 100 μ M.....	85
Figure 5-2: The absorption spectra normalised at the Q _y 830 nm showing the effect of different concentrations of DPA on <i>Mcr. purpuratum</i> for the small scale test.....	86
Figure 5-3: <i>Mcr. purpuratum</i> culture grown in the presence of DPA at 0 μ M (C), 40 μ M, 60 μ M and 80 μ M.....	87
Figure 5-4: The absorption spectra of <i>Mcr. purpuratum</i> membranes grown in the presence of DPA at 0 μ M (Control), 40 μ M, 60 μ M and 80 μ M.....	88
Figure 5-5: <i>Mcr. purpuratum</i> LH complexes grown in the presence of DPA at 0 μ M (Control), 40 μ M, 60 μ M and 80 μ M.....	89

Figure 5-6: Absorption spectrum showing the effect of different concentrations of DPA on the LH complexes of <i>Mcr. purpuratum</i>	90
Figure 5-7: <i>Mcr. purpuratum</i> growing on 1.5% agar plates in a series of culture dilutions.....	91
Figure 5-8: Antibiotic trials of <i>Mcr. purpuratum</i>	92
Figure 5-9: Diagram showing the location of the primers used to knock out the <i>CrtI</i> gene.....	94
Figure 5-10: Agarose gel of the amplified upstream (UP) and Downstream (DN) DNA fragments for the <i>CrtI</i> KO.....	94
Figure 5-11: Agarose DNA gel image of the <i>CrtI</i> KO PCR.....	95
Figure 5-12: Diagram showing the PJET 1.2 vector with the <i>CrtI</i> KO insert.....	95
Figure 5-13: Agarose DNA gel of the Eco I and Hind III digestion of the <i>CrtI</i> KO-pJET1.2/blunt plasmid for the 4 different colonies selected.....	96
Figure 5-14: Diagram showing the pK18mobsacB vector before and after the ligation of the <i>CrtI</i> KO insert.....	97
Figure 5-15: Conjugation of <i>Mcr. purpuratum</i> with the pK18mobsacB + <i>CrtI</i> KO in λ pir.....	98
Figure 5-16: Sucrose dilutions plates of the <i>Mcr. purpuratum CrtI</i> KO.....	99
Figure 5-17: Grid plates to test for the presence of the vector pk18mobsacB.....	100

List of Tables

Table 2-1: The [Lipid]/[Protein] ratio and the concentration of each in the final solution of 0.1 ml for reconstitution.....	28
Table 2-2: The different antibiotics tested in this experiment. The concentration used across different plates can also be seen.....	29
Table 2-3: Names and sequences of the primers used to knock out the <i>CrtI</i> gene.....	31
Table 2-4: Amounts of <i>Mcr. purpuratum</i> culture and pK18mobsacB + <i>CrtI</i> KO in λ pir added to make the conjugation dilutions.....	34
Table 2-5: Names and sequences of the primers used to knock out the <i>pucBA2</i> gene.....	37
Table 4-1: The amino acid sequences of the <i>Mcr. purpuratum puc</i> genes, numbered for the order they appear on contig 82.....	65
Table 4-2: A list of masses detected by MALDI-TOF from the LH2 complex of <i>Mcr. purpuratum</i> and the <i>puc</i> amino acid sequence they correspond to.....	67

List of Abbreviations

2D	2- dimensional
3D	3-dimensional
1 *	Singlet excited state
3 *	Triplet excited state
α	Alpha
β	Beta
AEX	Anion Exchange Chromatography
Alc.	Allochromatium
AU	Arbitrary units
B800	Bchl with absorption maximum at ~ 800 nm
B820	Bchl with absorption maximum at ~ 820 nm
B830	Bchl with absorption maximum at ~ 820 nm
B850	BChl with absorption maximum at ~ 850 nm
BChl	Bacteriochlorophyll
Blc.	Blastochloris
Cyt C	Cytochrome c
DE52	Diethylaminoethyl cellulose
DDM	n-Dodecyl β-D-Maltopyranoside
DM	n-Decyl-β-D-maltopyranoside
DMSO	Dimethyl sulfoxide
DNA	Deoxyribonucleic acid
DPA	Diphenylamine
DS	Downstream
DTT	Dithiothreitol
EDTA	Ethylenediaminetetraacetic acid
EM	Electron microscopy
ET	Energy transfer
ETT	Electronic energy transfer
IC	Internal conversion
ICM	Intracytoplasmic membranes
KO	Knock-out
LB	Luria Broth
LDAO	lauryldimethylamineoxide
LH	Light Harvesting
LH1	Light Harvesting complex 1

LH2	Light Harvesting complex 2
Mcr.	Marichromatium
MES	2-ethanesulfonic acid
MR	Molecular replacement
NIR	Near infrared
OD	Optical density
OR	Optical ratio
PCR	Polymerase chain reaction
Phs.	Phaeospirillum
PNSB	Purple non-sulphur bacteria
PSB	Purple sulphur bacteria
Rba.	Rhodobacter
RC	Reaction centre
Rps.	Rhodopseudomonas
RT	Room temperature (25°C)
SDC	Sucrose density centrifugation
SDS PAGE	Sodium dodecyl sulphate polyacrylamide gel electrophoresis
SEC	Size Exclusion Chromatography
SOE	Splice, Overlap, Extension
US	Up stream

Chapter 1 - Introduction

Sunlight is the primary source of energy that supports and maintains the variety of life on Earth. Solar energy is an essential component in one of the most significant and ancient biochemical process known: photosynthesis. Conversion of captured sunlight to chemical energy by photosynthetic organisms has changed the Earth and life on it. Organisms such as plants and algae have evolved to perform photosynthesis whereby solar energy is absorbed and used to fix carbon dioxide and reduce it into carbohydrates with oxygen as the by-product. The evolution of oxygenic photosynthesis and the following rise of atmospheric oxygen has revolutionised the energetic and enzymatic fundamentals of life. Understanding the mechanisms and underlying details of photosynthesis is an important topic in research. A full understanding of how light energy is harvested by photosynthetic organisms has the potential to help solve several problems facing humanity. These problems range from food security to fuel for transportation to a demand for renewable energy sources. Studying how Nature is able to harvest and utilise sunlight will, hopefully, lead to greater insights into how to create our own artificial solar biomimetic devices (Cogdell, Brotsudarmo et al. 2010).

1.1 Overview of Photosynthesis in Bacteria

It is fascinating to know that the reason for nearly all life existing on Earth is due to a simple equation (Figure 1-1). Cornelis Bernardus van Niel studied basic photosynthetic reactions and was able to see a pattern amongst the different groups: purple bacteria, green sulphur bacteria and green plants (van Neil 1941, Clayton 1980).

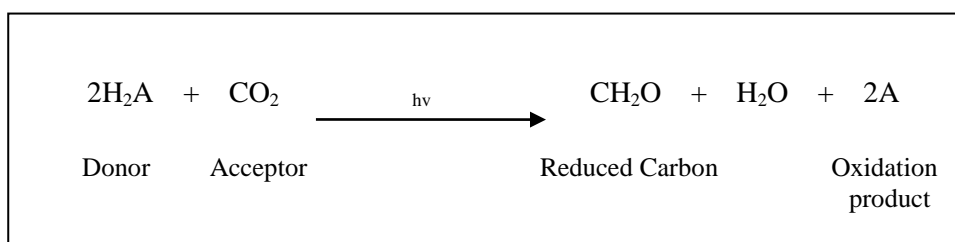


Figure 1-1: The general photosynthetic equation derived by van Niel. Where H_2A is the electron donor and can be H_2S in purple sulphur bacteria or succinic acid in purple no-sulphur bacteria, or H_2O in plants and cyanobacteria (van Neil 1941).

Purple bacteria were found to be able to utilise H_2S , other sulphur-containing compounds, or a variety of organic reductants (Malik 1983, Blankenship 2013). It was shown that this equation could be applied to all photosynthetic species that were studied. The oxidation product (2A) produced is dependent on the organism and the chemical composition of the starting donor. In sulphur bacteria it is sulphur, in plants it is oxygen and in non-sulphur bacteria, it is an organic compound, such as fumarate.

Photosynthetic bacteria have been used to study photosynthesis due to their simplicity and ease of growth. Purple photosynthetic bacteria are anoxygenic and belong to the phylum *proteobacteria*. Purple sulphur bacteria (PSB) belong to the γ class, whereas purple non-sulphur bacteria (PNSB) belong to the α and β classes (Stackebrandt, Murray et al. 1988, Williams, Sobral et al. 2007). They are gram-negative bacteria and their photosynthetic apparatus is located in special membranes called intracytoplasmic membranes (ICM). These membranes are synthesised when the bacteria are exposed to low partial oxygen pressure and light (Oelze and Drews 1972). They are not present when the purple photosynthetic bacterium is grown chemoheterotrophically (Madigan and Jung 2009). Photosynthetic bacteria inhabit aquatic environments below aerobic phototrophs, such as algae, plants and cyanobacteria. This means they are limited in the wavelengths of light that they can absorb due to it being filtered through the oxygenic, chlorophyll-containing phototrophs. As a result of this, they require pigments, which can absorb the wavelengths in the green and near-infrared (NIR) regions of the spectrum (Kirk 1994).

1.2. The Pigments

Pigments function within the photosynthetic bacteria to absorb electromagnetic radiation. The pigments are arranged into photosynthetic units (PSU). The major light-absorbing pigments in purple photosynthetic bacteria are bacteriochlorophyll and carotenoids.

1.2.1. Bacteriochlorophyll

Bacteriochlorophyll (Bchl) can be considered in two parts – the hydrophobic tail and the bacteriochlorin ring. There are two types that exist in purple bacteria, Bchl *a* and Bchl *b* (Scheer, Svec et al. 1974). The structure of Bchl *a* can be seen in Figure 1-2. It has a Mg^{2+} central metal ion. It is the bacteriochlorin ring that contains the conjugated double bond system (conjugated π -electron system), which forms the chromophore and is responsible for the absorption of light energy (Scheer, Svec et al. 1974). The absorption spectrum of Bchl *a* in an organic solvent can be seen in Figure 1-3. It shows that it contains three major peaks, which are known as the Soret, the Q_x and the Q_y (Telfer, Pascal et al. 2008). The chromophore of the BChl contains the Q_x and Q_y transition dipole moments. These are found perpendicular to each other. The position of the Q_y absorption peak can be shifted by several factors. These include the polarity of the solvent and its aggregation state. When two Bchl molecules aggregate to form a dimer, this causes a red shift in the position of Q_y . Coordination between the Mg^{2+} and hydrogen bonding of the acetyl group to amino acid residues of protein scaffolds can also alter the absorption of the Q_y . (Fowler, Sockalingum et al. 1994, McLuskey, Prince et al. 2001, Papiz, Prince et al. 2003).

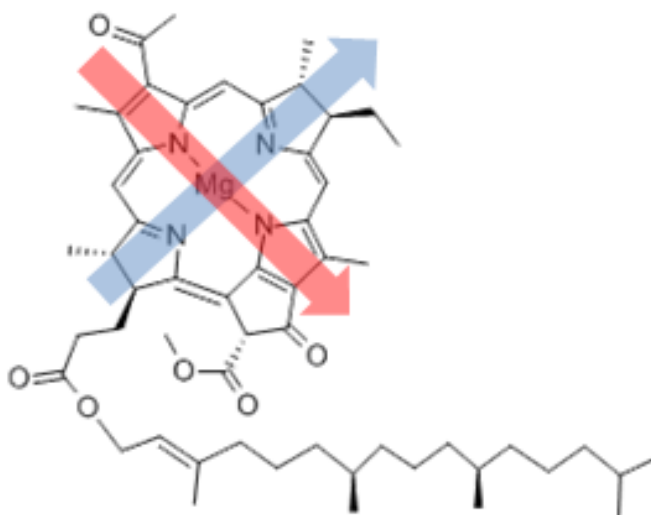


Figure 1-2: Chemical structure of Bchl a. The red arrow donates the Q_x and the blue arrow donates the Q_y dipole moments.

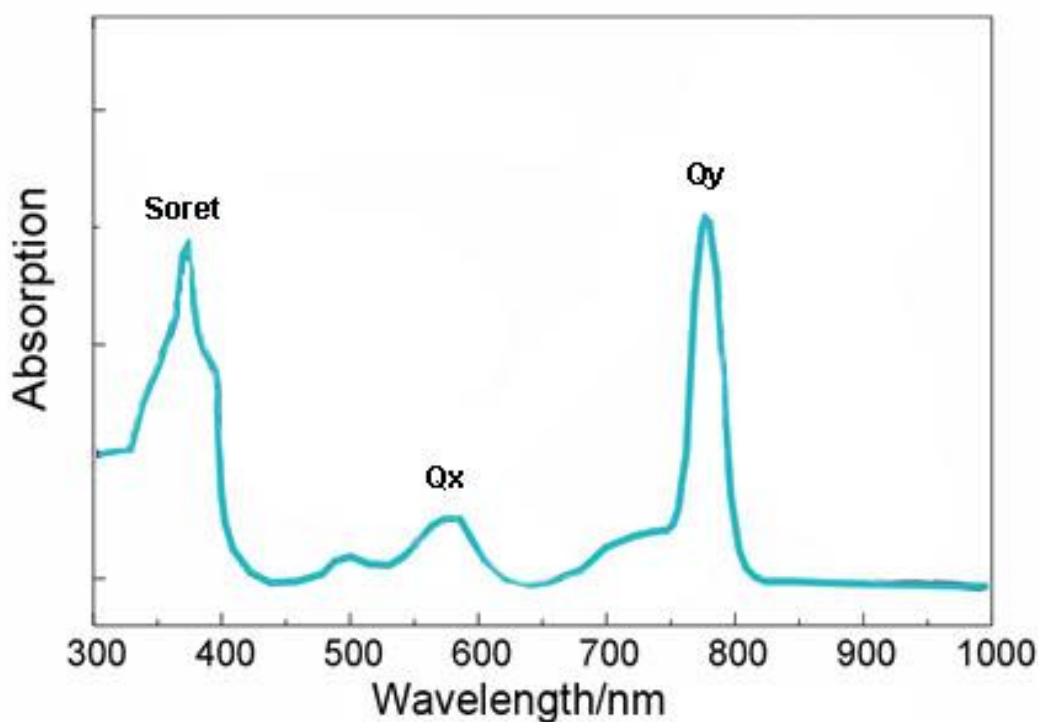


Figure 1-3: Absorption spectrum of Bchl a in an organic solvent. Three distinct peaks can be seen, the Soret at ~370 nm, the Q_x at 580 nm and the Q_y at 770 nm. The position of the peaks depends on the solvent and the environment.

1.2.2. Carotenoids

The variability of structures of carotenoids is vast, however, there are features and characteristics that they all share. Carotenoids are long chain hydrocarbons that contain a central conjugated double bond system (conjugated π -electron system). As in Bchl a, is it the conjugated π -electron system in carotenoids that forms the chromophore (Young and Britton 2012). An example of the carotenoid β -carotene can be seen in Figure 1-4.

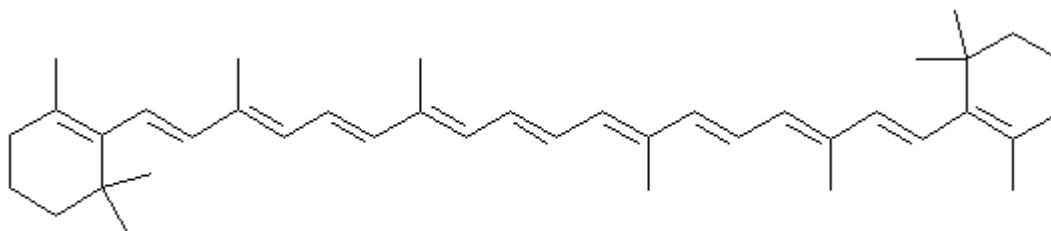


Figure 1-4: Structure of the carotenoid β -carotene. The alternating single and double bonds, which make up the chromophore can be seen.

They are hydrophobic and are divided into two major groups. Xanthophylls are carotenoids that contain oxygen and carotenes that contain no oxygen. Carotenoids play multiple roles in living systems. In photosynthesis, they have 3 main functions:

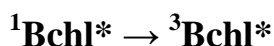
1. light harvesting
2. photoprotection
3. structural

Carotenoids absorb solar radiation at wavelengths that are inaccessible to Bchl molecules (Polivka and Frank 2010). Typically, they absorb between 450 nm and 550 nm depending on the number of conjugated double bonds. Carotenoids have two main, well described excited singlet states, S_1 and S_2 . When a carotenoid absorbs a photon excitation of an electron from the ground state (S_0) into the S_2 state occurs. There is no excitation from S_0 to S_1 as this is forbidden due to symmetry (Polivka and Sundström 2004). The length of the conjugated double bond system affects the absorption, as well as any chemical modifications present on the chromophore. The longer the conjugated π -electron system the more red-shifted the peaks are in the absorption spectrum (Frank and Cogdell 1996, Magdaong, LaFountain et al. 2014).

The photoprotective mechanism works by quenching of triplet excited states of Bchl ($^3\text{Bchl}^*$) and the dissipation of excess energy. Triplet Bchl can pass the excitation on to triplet oxygen, forming the singlet excited state of molecular oxygen. Singlet oxygen is very reactive and harmful to living matter. (Borland, Cogdell et al. 1989). This is outlined below in a series of equations.



This singlet state can then become a triplet excited state by a change in the spin multiplicity, whereby the electron spin reverses direction, termed intersystem crossing.



The triplet Bchl can then pass the energy to form singlet oxygen, however, the carotenoids are able to quench the triplet state of the Bchl and release the energy as heat (Cogdell, Howard et al. 2000). Carotenoids are able to quench both triplet Bchl and singlet oxygen thereby preventing oxidative damage of photosynthetic systems (Cogdell & Frank 1985).

1.3 The Bacterial Photosynthetic Unit

Purple photosynthetic bacteria use two types of light-harvesting (LH) complexes to harvest solar energy. These LH complexes are pigment-protein complexes arranged in arrays within the ICM. The pigments, BChl and carotenoid, absorb light energy and funnel it down an energy gradient to a central reaction centre (RC) where a charge separation occurs across the membrane, effectively ‘trapping’ the solar energy in a chemical form (Cogdell, Isaacs et al. 1999). A schematic of this can be seen in Figure 1-5. The LH1 complex forms a stoichiometric 1:1 complex with the RC in most photosynthetic bacteria and is termed the ‘core’ complex or the LH1-RC (Roszak, Howard et al. 2003). The LH2 antennas are arranged peripherally around the ‘core’ complex (Figure 1-6) (Cogdell, Isaacs et al. 1999). All purple photosynthetic bacteria contain the LH1 complex but not all contain the LH2 complex.

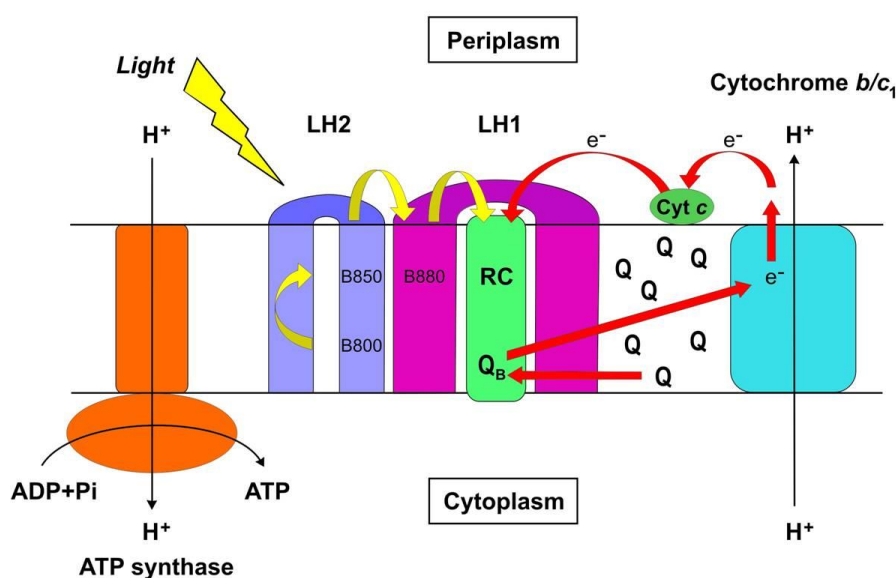


Figure 1-5: A representation of a purple bacterial photosynthetic membrane. The Light harvesting (LH) complexes, LH2 and LH1 harvest the energy of a captured photon. The Bchl a (B800-B850) pigment in the LH2 complex captures the photon and funnels the energy down an energy gradient until it reaches the reaction centre (RC). The RC uses this energy to generate a charge separation across the membrane and reduce a quinone molecule (QB). The QB is further reduced and doubly protonated. The resultant quinol molecule then diffuses through the membrane to the cytochrome b/c1 complex where it is oxidised and a proton motive force is generated, which is subsequently used by ATP synthase to produce ATP from ADP. (Roszak, Howard et al. 2003)

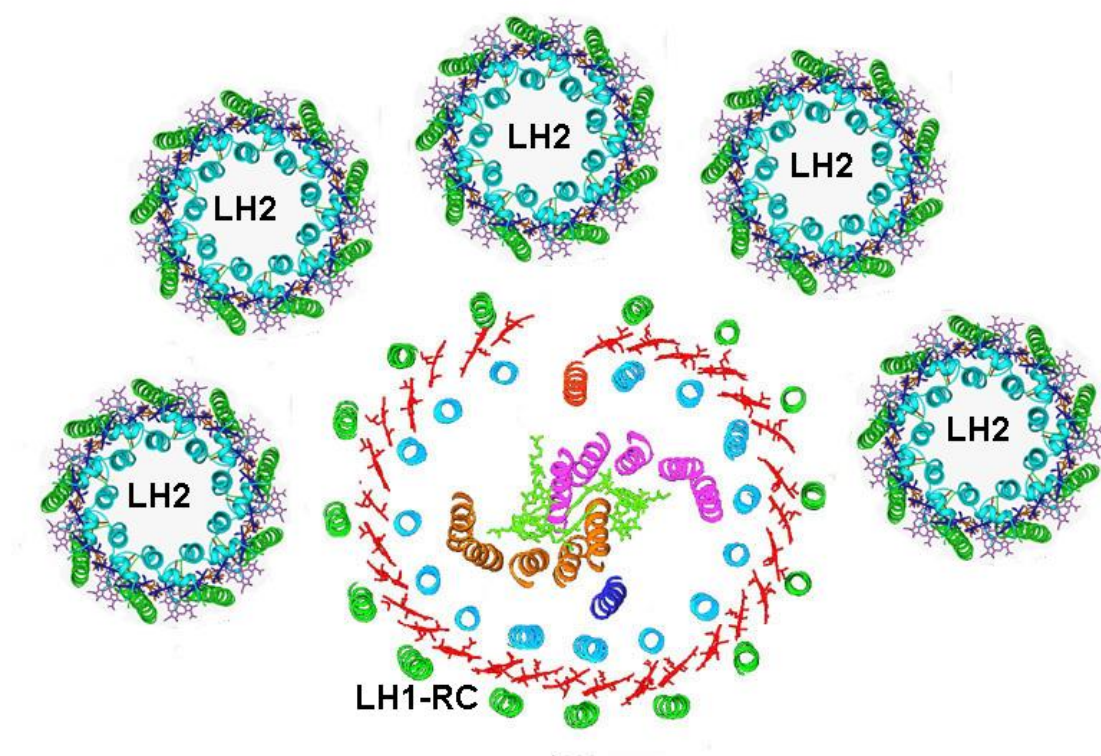


Figure 1-6: A schematic of the photosynthetic unit viewed perpendicular to the membrane.

(Deisenhofer, Epp et al. 1985, Papiz, Prince et al. 2003, Roszak, Howard et al. 2003) The multiple smaller nonameric rings on the outside are LH2 complexes from *Rhodospseudomonas (Rps.) acidophila*. The peptide can be seen in cyan (β), and green (α). The pigments are in blue, pink (Bchl), and orange (carotenoid). The LH2 complexes surround the larger LH1 complex that contains the RC, known as the LH1-RC (structure from *Rps. palustris*)

The LH1 and LH2 form rings that are based on a similar structural principle. Biochemical studies have shown that the LH complexes are composed of circular associations of α and β heterodimers of low molecular weight apoproteins (5-7 kDa) and associated pigments Bchl a and carotenoid (Cogdell, Fyfe et al. 2004). These polypeptide chains share a three-domain organisation. They contain an N-terminal hydrophilic cytoplasmic domain, followed by a transmembrane helical region and a C-terminal hydrophilic periplasmic domain. The $\alpha\beta$ heterodimers form a scaffold for the pigments to non-covalently bind to. The binding of the Bchl a to the protein alters the wavelength at which they absorb. (McLuskey, Prince et al. 2001, Papiz, Prince et al. 2003)

1.4. LH1-RC. The “Core” Complex

In principle, it is possible that photosynthesis could have evolved only with RCs. However, this would only have been viable under high-intensity illumination. The LH complexes provide a much larger surface area available for photon capture and increase the efficiency of the process, and allow it to occur over a wide range of incident light intensities (Cogdell, Gardiner et al. 2008). The

very first membrane protein to have its structure determined by X-ray crystallography was the RC of *Blastochloris (Blc.) viridis* (previously *Rps. viridis*) (Deisenhofer, Epp et al. 1985). Prior to this work membrane proteins were thought to be near impossible to crystallise and so high-resolution structures could not be determined. These authors won the Nobel Prize in Chemistry in 1988 and opened the door for many other structures of membrane proteins to be solved by X-ray crystallography.

The RC structure is made up of proteins and cofactors. The RC is composed of three polypeptides, the Light (L), Medium (M) and Heavy (H) in a ratio of 1:1:1 (Okamura, Steiner et al. 1974). In some species, there is a fourth protein known as bound Cytochrome c (cyt c). For example, this protein is present in *Blc. viridis* but not in *Rba. sphaeroides*. (Clayton and Haselkorn 1972). The L and M polypeptides have 5 hydrophobic transmembrane α -helix (A-E) (Deisenhofer, Epp et al. 1985). These are arranged in the order; A, B, C, E, D and have a type of pseudo two-fold symmetry. The H subunit is located on the cytoplasmic side of the membrane and consists of a single transmembrane α -helix and a globular hydrophilic domain. Cyt c is found on the periplasmic side of the membrane. There are nine cofactors in total that are non-covalently bound to the RC (Deisenhofer, Epp et al. 1985, Michel, Epp et al. 1986). The nine cofactors located within the protein scaffolding are organised into two branches (A and B) and are directly responsible for the electron transfer reactions. Those in branch A are more closely associated with the L subunit and those in branch B are more closely associated with the M subunit. In particular, the cofactors are: four BChl, two of these are strongly coupled to form a BChl dimer (D) (Allen, Feher et al. 1987) located on the periplasmic side, two ubiquinone molecules (Q) and one non-heme Fe^{2+} ion and two bacteriopheophytins (BPh) consisting of a free bacteriochlorin ring. A schematic of the layout of these cofactors can be seen in Figure 1-7.

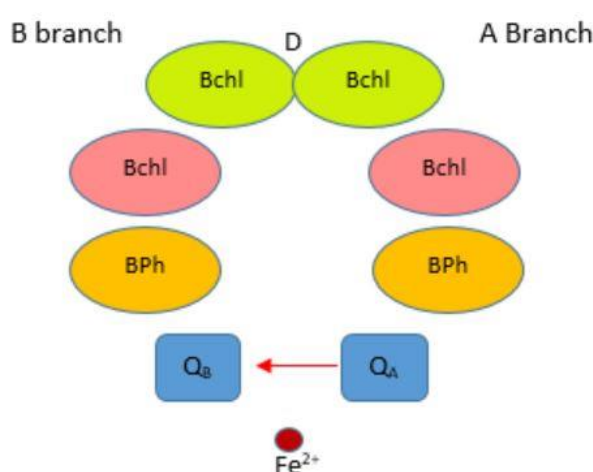


Figure 1-7: Cofactor components and arrangement in purple bacterial reaction centres (RC). The primary electron donor is a dimeric BChl (D). This is then transferred to the BPh, then to the first ubiquinone molecule, Q_A. This occurs along the A Branch, which is associated with the L subunit of the RC. The electron is finally then transferred to the second ubiquinone molecule, Q_B.

Electron transfer only occurs down the A Branch. Light-induced electron transfer within the RC consists of a cascade of reactions. When a photon is absorbed the primary electron donor D is excited and very fast electron transfer from D* to BPh occurs. Then an electron is transferred to the primary ubiquinone acceptor Q_A. When the quinone (Q_B) is reduced by the first electron, charge separation is generated across the membrane. The Q_B is subsequently further reduced and doubly protonated. The resultant Q_B molecule then diffuses through the membrane to the cytochrome b/c₁ complex where it is oxidised and the release protons to generate the proton motive force that is used by ATP synthase to produce an ATP molecule. (Mitchell 1961, Holten, Windsor et al. 1978, Michel, Epp et al. 1986, Kirmaier and Holten 1987, Li, Gilroy et al. 1998).

The first structure of an LH1-RC to be determined was at 4.8 Å from *Rps. palustris*- seen in Figure 1-8. (Roszak, Howard et al. 2003). The RC is surrounded by an open elliptical ring of LH1, which consists of 15 αβ polypeptides. LH1 consists of α and β polypeptides, which are paired and surround the RC. One pair of αβ-polypeptide binds two Bchl *a* molecules and one carotenoid. The Bchl *a* molecules are strongly coupled, giving rise to the strong Q_y absorption band in the 870 nm to 890 nm region. The gap, shown in the LH1 complex of *Rps. palustris* is introduced by protein W. It is currently unknown what the function of this is, but it has been suggested that protein W is similar to a protein found in *Rba. sphaeroides* and *Rba. capsulatus* called Puf X (Parkes-Loach, Law et al. 2001). The LH1-RC structures of *Thermochromatium (Tcr.) tepidum* was also recently solved at 3.0 Å. As mentioned previous, the LH1-RC is usually found in a 1:1 stoichiometric ratio but there are also examples of dimeric cores complexes (Qian, Neil Hunter et al. 2005).

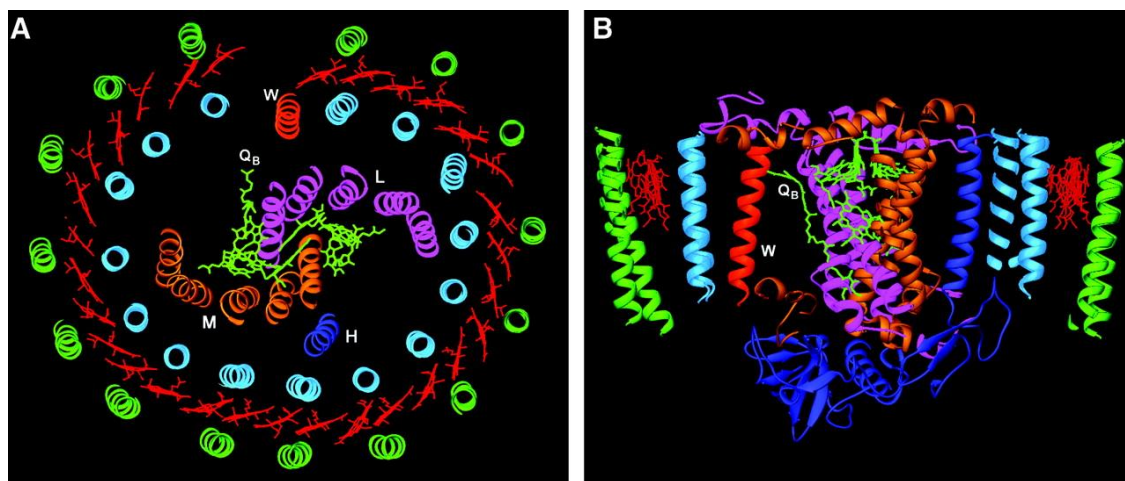


Figure 1-8: Model of the LH1-RC from *Rps. palustris*. The transmembrane α and β polypeptides can be seen in cyan (β), and green (α) and the Bchl *a* are seen in red. The protein W is shown as the single red helix at the gap of the LH1. The RC subunits are labelled and the bound pigments are shown as green molecules. A): View from the periplasmic side of the membrane looking through the complex. B) Through the membrane view of the complex. (Roszak, Howard et al. 2003)

In most purple photosynthetic bacteria the PSU is composed of the LH2 and core complexes (Cogdell, Fyfe et al. 1996). There are some species, however, such as *Blc. viridis* and *Rhodospirillum (Rs.) rubrum*, which only contain LH1-RC complexes. These species adapt to light changes by altering the number of ICM and, therefore, the number of PSU that are present in each

cell.

1.5. The LH2. The Peripheral Complex

The LH2 complexes do not deliver excitation energy directly to the RC, but to the LH1 antennae that they surround. As with the LH1 complex, the LH2 is made up of repeating $\alpha\beta$ heterodimers and associated pigments (Zuber 1985). The LH2 complexes bind two Bchl *a* molecules within their transmembrane domains per apoprotein pair. These Bchl *a* are tightly coupled and form a dimer. A single molecule of carotenoid binds per apoproteins pair as well. The LH2 complex contains an additional more peripheral Bchl *a* binding site per apoprotein pair (McDermott, Prince et al. 1995, Cogdell, Isaacs et al. 1999). This heterodimer subunit can be seen in Figure 1-9.

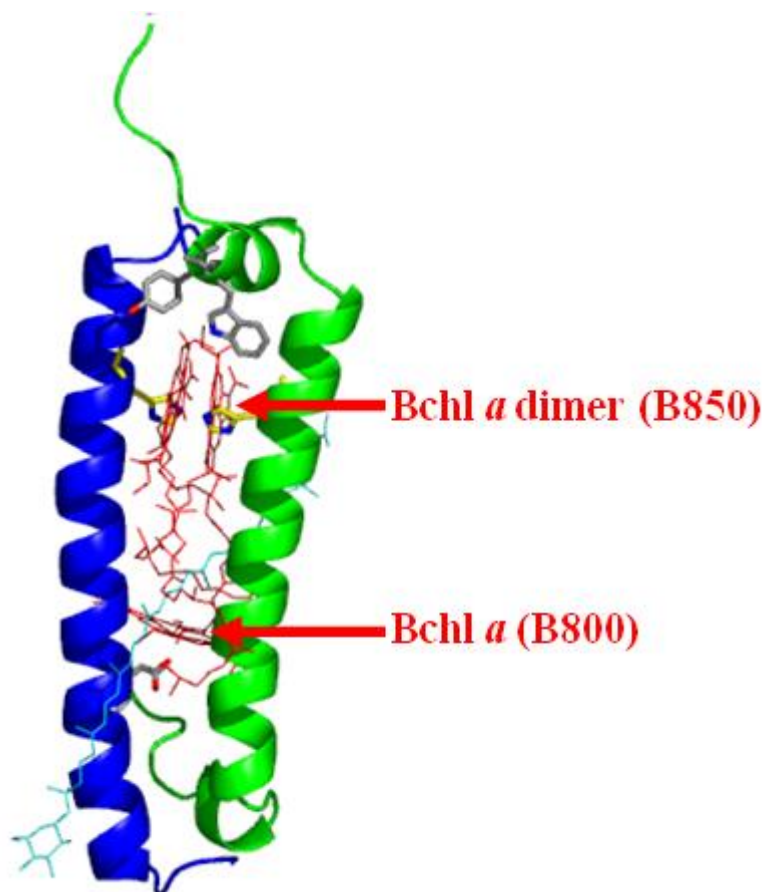


Figure 1-9: Side view of the $\alpha\beta$ heterodimer subunit pigments from *Rps. acidophila* 10050. (Papiz, Prince et al. 2003). The $\alpha\beta$ polypeptides can be seen in blue and green. The Bchl *a* molecules can be seen in red and the carotenoid molecule in cyan. The Bchl *a* dimer (B850) sit perpendicular to the membrane, whilst the Bchl *a* monomer sits parallel to the membrane.

The first LH2 crystal structure to be solved was from *Rps. acidophila* strain 10050 (McDermott, Prince et al. 1995). This was improved upon and is now available at 2 Å resolution (Papiz, Prince et al. 2003) (Figure 1-11). It is a nonamer, with nine $\alpha\beta$ heterodimers. The pigments non-covalently bind to the $\alpha\beta$ heterodimers, which act as scaffolds. There are minimal protein-protein interactions but very prominent protein-pigment interactions that hold the complex together (Prince, Papiz et al. 1997). This structure of the LH2 complex can be easily correlated with the bands present in the absorption spectrum. Figure 1-10 shows the absorption spectrum of the LH2 complex of *Rps. acidophila*. The BChl *a*s have two transition dipole moments that produce the main absorption bands, Q_y and Q_x . The 590 nm peak corresponds to the Q_x and is the same for the LH1 and LH2. The Q_y is distinct between the two LH complexes and also varies between different LH2 complexes from different species and different growth conditions (Gardiner, MacKenzie et al. 1996, Carey, Hacking et al. 2014). The differences in the positions of the Q_y bands of the BChl *a* populations are due to differences in their site energies, as well as due to pigment-pigment interactions. The site energy of the BChl is defined by the binding site, hydrogen bonding and the electrostatic interactions. These can vary depending on the amino acid residues present within the BChl *a* binding site and around it (Cogdell, Howard et al. 2002). When a Bchl *a* dimer is formed, the two first excited singlet states of the Q_y bands of each Bchl *a* mix, producing two exciton bands. There is one at lower energy and one at higher energy. Most of the oscillator strength resides in the lower exciton band and, therefore, the Q_y absorption of the dimer is red-shifted relative to that of the monomers. In general, as the size of the coupled aggregate increases so does the extent of the red shift (Cogdell, Gall et al. 2006). The Soret peak at 390 nm corresponds to the absorbance of all Bchl *a* molecules. The three peaks at 450-550 nm are due to the carotenoid absorbance. In the case of *Rps. acidophila*, the carotenoid is rhodopin glucoside (RG).

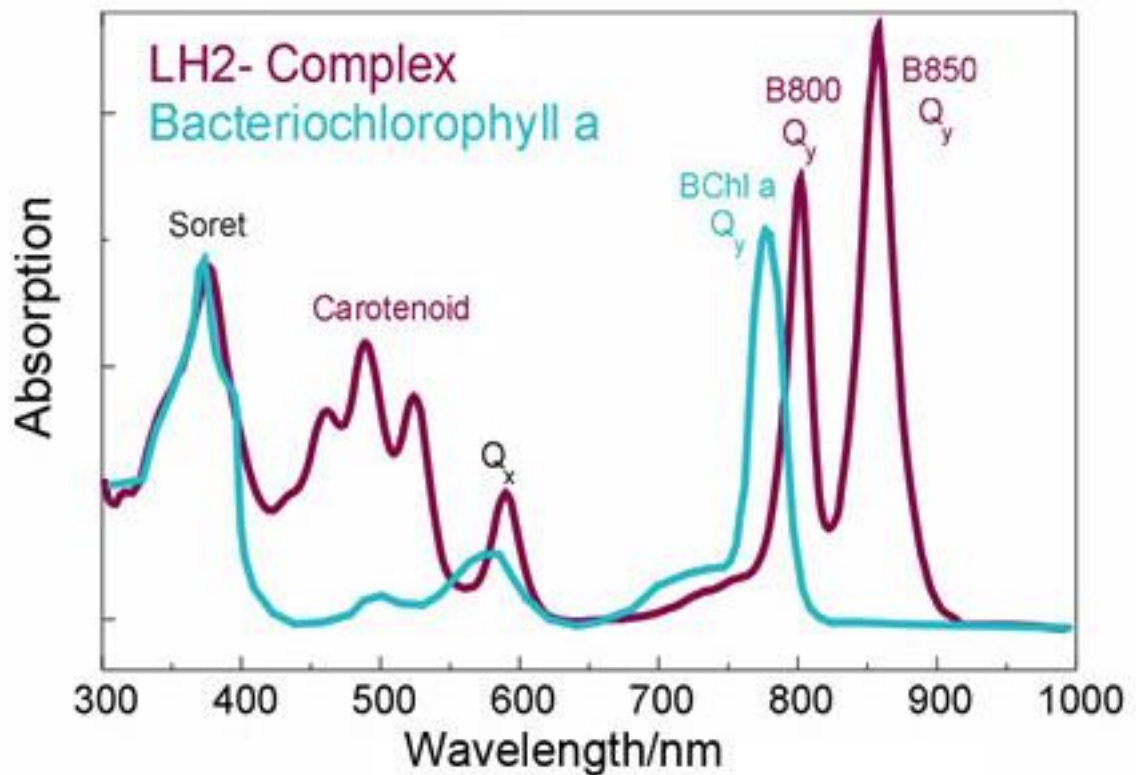


Figure 1-10: Absorption spectra showing the red-shift of the Bchl *a* Q_y bands in the *Rps. acidophila* LH2 complex in an organic solvent. The 850 nm band arises from the ring of excitonically coupled Bchl *a* molecules bound on the α and β polypeptides, 18 in total (2 per dimer). The 800 nm band arises from the monomeric Bchl *a* bound only on the β chain, 9 in total.

Concentrating on the long wavelength region, the absorption spectrum shows two strong near-IR absorption bands, one at 800 nm and one at 850 nm. The 800 nm absorption band comes from monomeric Bchl *a* molecules (B800) (Cogdell, Isaacs et al. 1999). These monomeric Bchl *a* molecules form a ring of weakly interacting molecules and are responsible for the absorption transition at 800 nm. The 850 nm absorption band comes from the strongly exciton coupled Bchl *a* molecules (B850). The nine Bchl *a* pairs are strongly excitonically-coupled and responsible for a range of absorption, depending on the complex studied, (from ~840 ~890 nm). The structure from the LH2 of *Phaeospirillum* (*Phs.*) *molischianum* (previously *Rhodospirillum molischianum*) has been solved to 2.4 Å (Koepke, Hu et al.) and, interestingly, the ring structure of this LH2 turned out to be octameric. A comparison of the structures can be seen in Figure 1-11. The LH2 of *Phs. molischianum* exhibits two absorption maxima at 800 and 846 nm at the Q_y (also known as the B800-B850). Compared to the nonameric *Rps. acidophila* this is less than the B800-B850 absorption band. This makes sense since there is one fewer $\alpha\beta$ heterodimer that will form the LH2 ring.

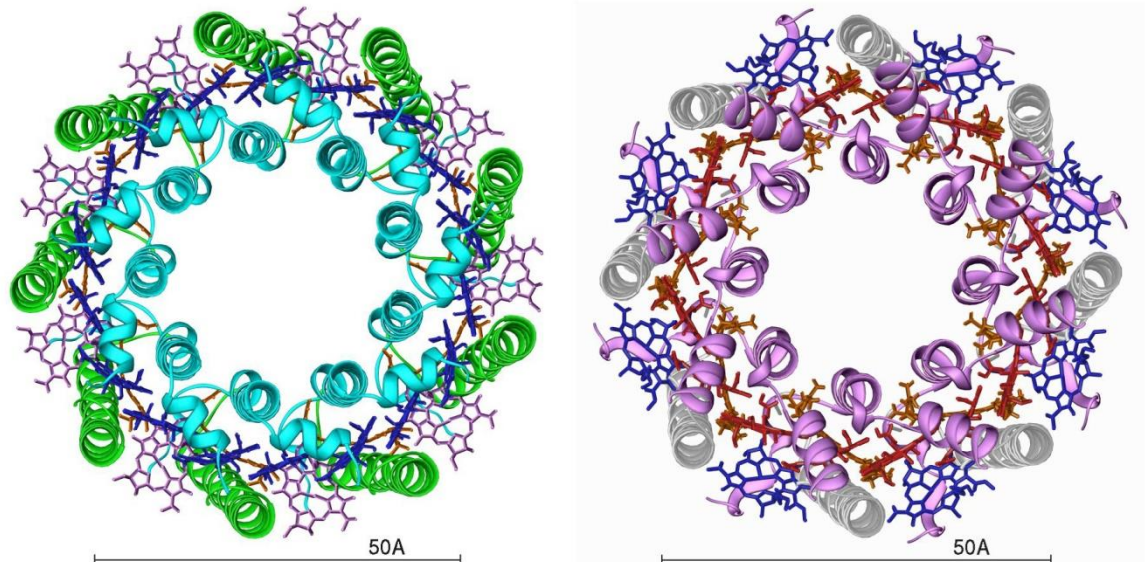


Figure 1-11: Structural comparison of the LH2 from nonameric *Rps. acidophila* 10050 (left) with the *Phs. molischianum* (right) octameric complex. Nine repeating $\alpha\beta$ heterodimers can be seen for *Rps. acidophila* and eight for *Phs. molischianum* (right). For *Rps. acidophila* cyan = β polypeptides, green = α polypeptides, orange = carotenoid). The single binding peripheral B800 BChl *a* can be seen in pink, whilst the dimer B850 Bchl *a* can be seen in dark blue following the ring structure. (Papiz, Prince et al. 2003). For *Phs. molischianum* pink = β polypeptides, grey = α polypeptides, orange = carotenoid). The single binding peripheral B800 BChl *a* can be seen in dark blue, whilst the dimer B850 Bchl *a* can be seen in orange following the ring structure (Koepke, Hu et al. 1996). The B850 ring can also be seen in each structure. In each case, the bacteriochlorin rings of the B850 BChl *a* sit perpendicular to the membrane and so they appear side on. This shows the overlap between all the B850 BChl *a* that allows the excitonic coupling of the molecules.

There has also been a report of LH2 rings as large as 12-13 subunits as in *Allochrochromatium* (*Alc.*) *vinosum* (Kereïche, Bourinet et al. 2008). When *Alc. vinosum* is purified in detergent it is seen that the 800 nm transition exhibits a split and the 850 nm sees a broadening (Hayashi, Nozawa et al. 1981, Cogdell and Scheer 1985). It has also been observed that the LH2 from *Alc. vinosum* has at least three different spectral forms, which are produced in response to variations in growth conditions. These are the B800-B850, the B800-B840 and the B800-B820 LH2 complexes. These all maintain the unusual split 800 nm peak in their low-temperature absorption spectra. It was also determined that they have different polypeptide compositions and a mixed carotenoid composition. (Carey, Hacking et al. 2014)

The LH2 polypeptides are coded by the *puc* operon and their expression is controlled by light intensity (Kiley and Kaplan 1987). This allows for varying amounts of LH2 relative to LH1 to be produced. *Puc* operon usually contains the *pucBA* genes, where the β and α apoproteins are encoded for respectively. There is homology across multiple species LH2 α polypeptides and β polypeptides. There are regions of conserved amino acids especially found in the binding pocket (Zuber 1985). In some species, there have been multiple *puc* operons observed. These contain multiple *pucBA* gene pairs that allow different genes to be switched on and off to produce LH2 complexes with different α and β polypeptides present (Gardiner, MacKenzie et al. 1996). This can, in principle, result in both different homogeneous and heterogeneous LH2 rings. The heterogeneity

or homogeneity of the peptides also affects the Q_y absorption of the strongly coupled Bchls and therefore the resultant spectra. *Rps. palustris* expresses different alpha and beta polypeptides to produce a heterogeneous LH2 complex (Tadros and Waterkamp 1989, Brotosudarmo, Kunz et al. 2009). It has five *puc* operons and produces an alternate LH2 when grown under low light conditions compared with that seen at high light (Nishimura, Shimada et al. 1993). Even though *Rps. acidophila* 10050 has multiple *puc* genes only 1 type of LH2 is expressed. *Alc. vinosum* has multiple *puc* genes, which encode the LH2 apoproteins (Weissgerber, Zigann et al. 2011). As mentioned it above, it is well documented that *Alc. vinosum* can produce a variety of spectrally different LH2 depending on the growth conditions. This is also seen in species of *Rps. palustris* and some of *Phs. molischianum* (Tadros and Waterkamp 1989, Brotosudarmo, Kunz et al. 2009, Mascle-Allemand, Duquesne et al. 2010). The genes expressed under very low light conditions often give rise LH complexes with having near-IR absorption maxima at 800 nm and 820 nm as opposed to the standard high-light complexes with absorption maxima at 800 nm and 850 nm. The molecular origin of the spectral difference between B800–B820 and B800–B850 type LH2 is well-understood thanks to crystal structures. In *Rps. acidophila* it the B800 Bchl *a*s are stabilised by coordination between the Mg^{+2} of the Bchl *a* and α -methionine1, and an H-bond between the acetyl group of Bchl *a* and β -Arginine20 (Papiz, Prince et al. 2003). The B850 Bchl are coordinated through their central Mg^{2+} ions to the imidazole ring side chain of the conserved histidine residues, α -histidine31 and β -histidine30 (McDermott, Prince et al. 1995, Papiz, Prince et al. 2003). They also form hydrogen bonds to α -tyrosine44 and α -tryptophan45. These hydrogen bonds were not present with the B820 Bchl *a*. This is because the amino acid sequence was different. Changes from α -tyrosine44 to α -phenylalanine44 and α -tryptophan45 to α -leucine45 mean no hydrogen bonding takes place at these positions. The crystal structure of the B800–B820 form of the *Rps. acidophila* strain 7050 shows that the B820 instead forms hydrogen bonds with α -tyrosine41 and this locks the acetyl group of Bchl *a* into an out-of-plane position (McLuskey, Prince et al. 2001). When the acetyl group is in the plane the Q_y transition is red shifted due to the inclusion of a double bond in the conjugated system. When it is out of plane there is a blue shift due to the loss of this double bond. (Cogdell, Howard et al. 2002). (Gardiner, MacKenzie et al. 1996, McLuskey, Prince et al. 2001). This can be seen in Figure 1-12. A similar effect was seen in *Rba. sphaeroides* when the α -tyrosine44 and α -tyrosine45 of its B850 LH2 complex were mutated (Fowler, Sockalingum et al. 1994).

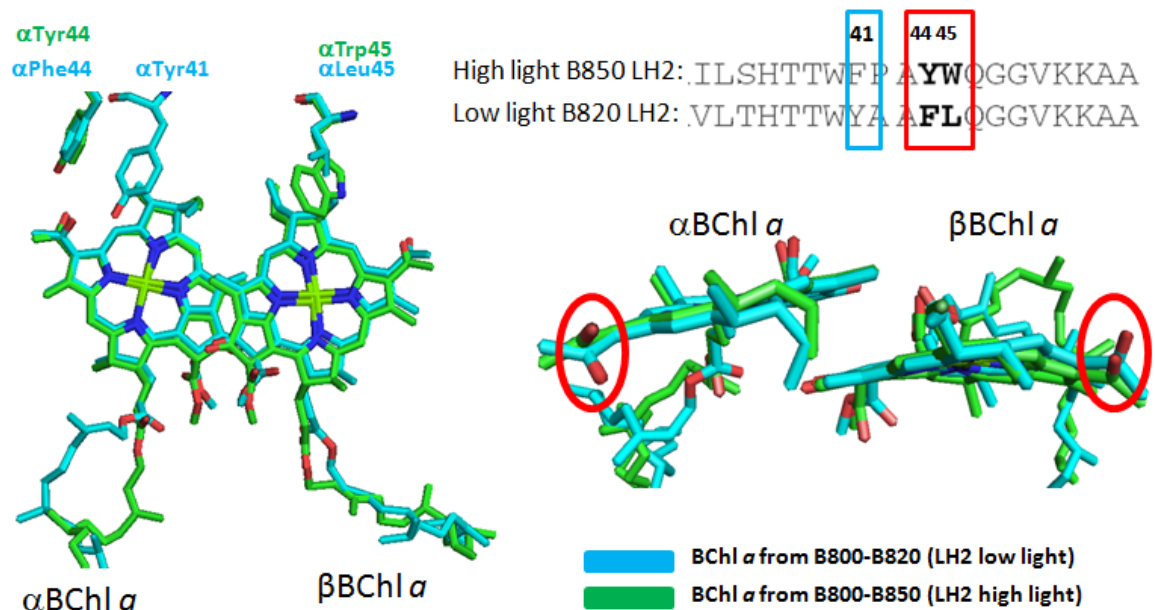


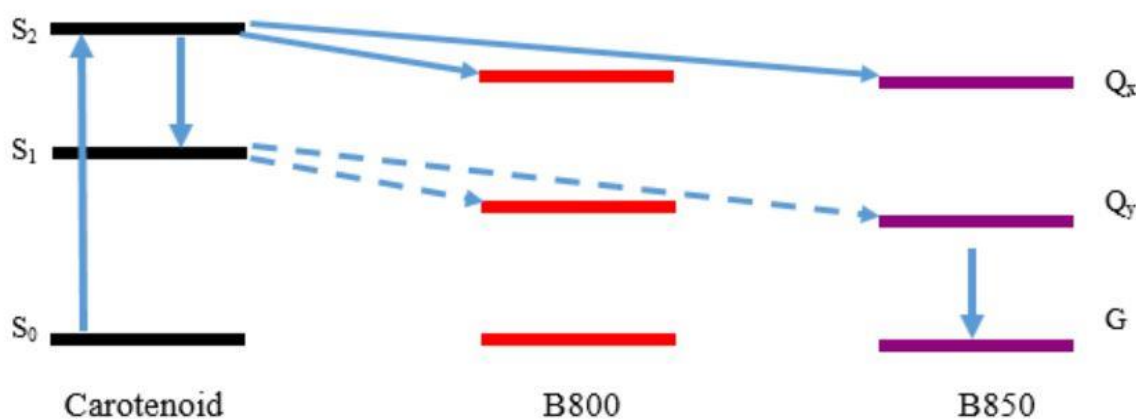
Figure 1-12: The hydrogen bonding of the B850 LH2 complex of *Rps. acidophila* 10050 and the B820 LH2 complex of *Rps. acidophila* 7050. It can be seen in the B850 LH2 that the α Tyr44 (Y) residue makes an H-bond to the C3-acetyl group of α -BChl α molecule and the α Trp45 (W) is H-bonded with the C3-acetyl group of β -BChl α . In the B800-820 LH2, these residues are replaced by α -Phe44 and α -Leu45 that do not make H-bonds. Instead, there is α -Tyr41 in B800-820 LH2, which makes an H-bond and this locks the acetyl group of α -BChl α into an out-of-plane position. The acetyl group of β -BChl α is also not H-bonded and out-of-plane (McLuskey, Prince et al. 2001).

The $\alpha\beta$ heterodimers are essentially protein scaffolds that hold the pigments in their fixed locations. This ensures they are in the correct positions and at the correct distances for efficient energy transfer. There are minimum protein-protein interactions between the transmembrane apoproteins (McDermott, Prince et al. 1995, Prince, Papiz et al. 1997, McLuskey, Prince et al. 2001). As mentioned previously, carotenoids are also known to play a role in the structure of the LH2. Experiments of trying to remove carotenoids or inhibit carotenoid biosynthesis in photosynthetic organisms are by no means new (Cohen-Bazire and Stanier 1958, Fuller and Anderson 1958). There are carotenoidless mutants, the most well-known case being a mutant of *Rps. sphaeroides* called R.26 (Crounse, Feldman et al. 1963). Not only does it lack carotenoids, but also the B800-850 LH2 complex. In most cases, the LH2 complex cannot form without carotenoid (Sistrom and Clayton 1964, Ghosh, Hauser et al. 1988, Gall, Henry et al. 2005). There seems to be no such problem for the LH1-RC complex. The inhibitor Diphenylamine (DPA) has also been used to study the formation of Light Harvesting Complexes without carotenoid (Moskalenko and Makhneva 2012) (Gall, Henry et al. 2005). DPA inhibits the activity of phytoene desaturase and causes a build-up of phytoene and related precursors. The consensus at this point in time seems to be that the LH1 can survive structurally without the need for carotenoid and the LH2 can only in very few rare cases (Moskalenko and Makhneva 2012, Carey, Hacking et al. 2014). Carotenoids also play a role in the location of the Q_y maximum. An example is seen with the carotenoidless mutant G9+ of *R. rubrum*. The wild-type strain has a Q_y maximum of 881nm compared with the mutant is 872 nm.(Parkes-Loach, Sprinkle et al. 1988)

1.6 Energy Transfer

There are several processes possible after the absorption of a photon with regards to photosynthesis and the energy transfer (ET) between the pigments. Some of these can be seen in Figure 1-13. It is now well-established that carotenoids have two excited states that serve as energy donors: the S_2 state, responsible for the strong absorption in the 400–550 nm region and the dark S_1 state, which is located below the absorbing state and is forbidden for one-photon transitions from S_0 (Polívka and Sundström 2004).

The energy absorbed by a chromophore can be transferred efficiently to a neighbour chromophore through electronic energy transfer (EET) or Förster energy transfer (Förster 1948). This process is a transition dipole-dipole interaction between a donor molecule and an acceptor molecule (Scholes 2003). The efficiency, or speed, of EET depends on several factors. The first is the energy gap between the donor and the acceptor - an overlap in energy between the donor emission and the acceptor absorption is required. The second is the distance -if the donor and acceptor are not close enough then the energy will decay before the transfer can occur. The third is that the dipole moments must be parallel. This is a simple model, and the ET seen within the LH complexes is far more complicated (Scholes, Jordanides et al. 2001). In LH2 complexes, the S_2 and S_1 states of the carotenoids act as energy donors, passing the energy down the energy gradient. Transfer from the S_2 to the Q_x is constant but if the energy level of the S_1 is higher than the Q_y , then energy transfer from S_1 to the Q_y pathway is also observed. The internal conversion (IC) is a transition between two electronic states of the same spin multiplicity (S_2-S_1 or S_1-S_0) (Rondonuwu, Taguchi et al. 2004) (Polli, Cerullo et al. 2006) (Cogdell, Howard et al. 2002). The pigments within the LH complexes are arranged closely together, sometimes touching, which allows for strong interaction and leads to the formation of excitons. This is seen with the Bchl a pairs that form dimers. When the dimer is formed the two first excited singlet states mix, producing two exciton bands. In the LH2 ring structure, the Bchl a pigments are excitonically coupled over 18 molecules so the Q_y band is even lower (Dau and Sauer 1996).



Internal Conversion

Energy Transfer

Figure 1-13: Diagram of an energy level diagram of a carotenoid, B800 Bchl *a* and B850 Bchl *a*. When a photon is absorbed by the carotenoid it is promoted from ground state to the first excited singlet state, S_2 . This state is very short and the energy is transferred to B850 and B800 Q_x transitions respectively. The majority of transfer between the carotenoids and the Bchl *a* occurs this way but the energy can also decay from S_2 to S_1 within the carotenoid. This is called internal conversion (IC). If the energy level of the S_1 is higher than the Q_y , then energy transfer from S_1 to the Q_y pathway is also observed.

Rps. acidophila, as an example, transfer between B800-B800 molecules is $0.8\text{--}1.6\text{ ps}^{-1}$, EET B800 -B850 molecules is $0.7\text{--}0.9\text{ ps}^{-1}$. EET from B850-B850 is very fast at $100\text{--}200\text{ fs}^{-1}$. Energy can then be transferred from B850 to the B850 of a neighbouring LH2 complex at 5 ps^{-1} and from there to the LH1 at $3\text{--}5\text{ ps}^{-1}$. Finally, the EET from the LH1 complex to the RC occurs with the rate constant of $30\text{--}40\text{ ps}^{-1}$ (Yang, Yoon et al. 2012). The time frame for IC in carotenoids and then ETT to the Bchl *a* is different depending on the carotenoid and the LH2 complex (Polli, Cerullo et al. 2006).

Energy transfer times are unique to each LH complex. There are still many species of photosynthetic bacteria that have not yet been discovered or investigated. This means that there are still many LH complexes yet to be characterised.

1.7 *Marichromatium (Mcr.) purpuratum*

1.7.1 Discovery

Marichromatium (Mcr.) purpuratum is a small, marine, purple sulphur photosynthetic bacterium first described by Imhoff and Truper in 1980 (Imhoff and Trüper 1980). It was isolated from the Red Sea and until 1998 was known as *Chromatium purpuratum* (Imhoff, Suling et al. 1998). The complete genome of *Mcr. purpuratum* 984 was very recently sequenced and became available towards the end of this project. (Nordberg, Cantor et al. 2014).

1.7.2 Light Harvesting

The unusual LH2 complex spectrum from *Mcr. purpuratum* produces a single strong absorption band at approximately 830 nm with a shoulder at 800 nm, for which there is presently no structural explanation (Figure1-14). This is also known as the B800-B830 LH2 complex. This has been isolated and purified previously (Cogdell, Hawthornthwaite et al. 1990, Kerfeld, Yeates et al. 1994). Another interesting fact about this species is that it belongs to a small group of *Chromatiaceae* that synthesise an unusual carotenoid called Okenone. This carotenoid gives the culture an intense purple colour and results in an atypical, for purple photosynthetic bacteria, broad absorption band in the 400 nm-600 nm region.

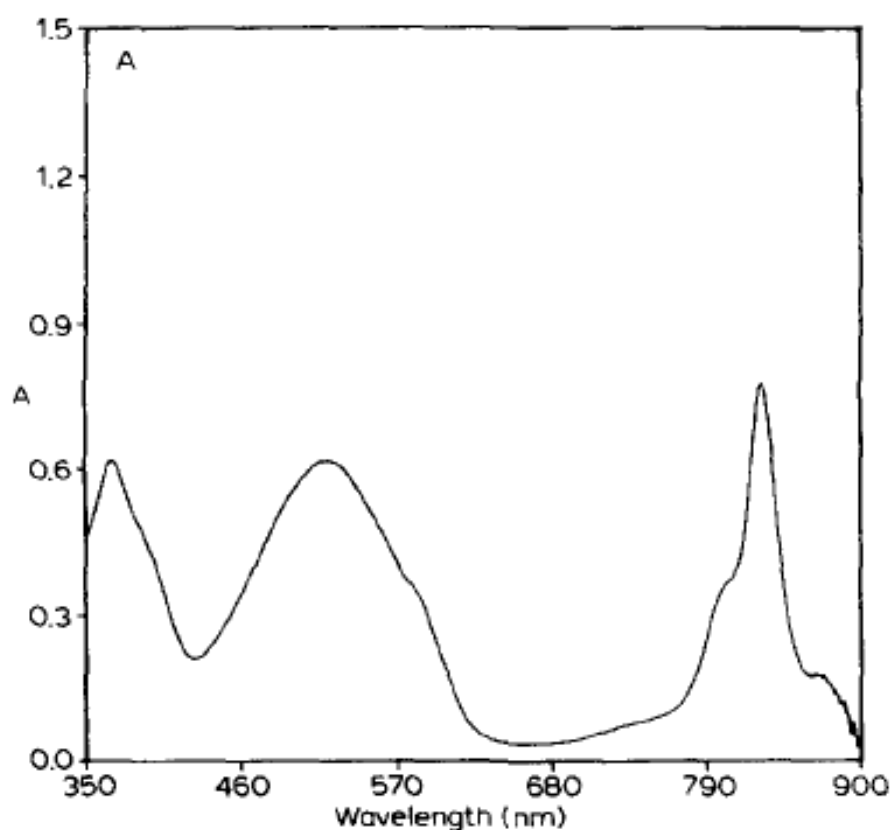


Figure 1-14: Absorption spectra of *Mcr. purpuratum* chromatophores at room temperature. The strong 830 nm peak with the shoulder at 800 nm of the LH2 can be seen, as well as the shoulder at 875 nm, which relates to the LH1. The broad peak at ~460 nm to 560 nm is the carotenoid okenone (Cogdell, Hawthornthwaite et al. 1990).

1.7.3 Okenone

The elucidation of the biochemical pathway for okenone has also been recently published (Vogl and Bryant 2011). The *CrtI* gene encodes for the enzyme phytoene desaturase, which catalyses the conversion of phytoene to neurosporene (Figure 1-15).

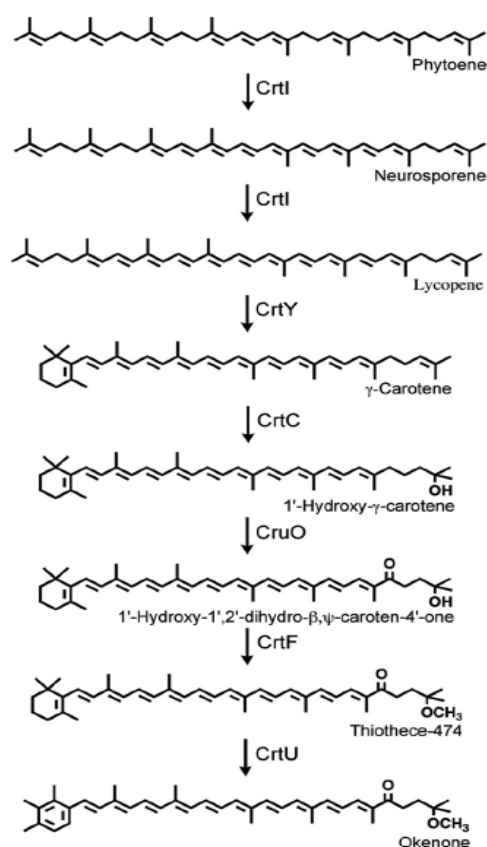


Figure 1-15: Diagram showing the pathway for the synthesis of the carotenoid Okenone. Also shown are the genes that encode for the enzymes involved in each step of the pathway. The *CrtI* gene can be seen right at the beginning. (Imhoff and Trüper 1980, Vogl and Bryant 2011)

Okenone belongs to a distinct group of carotenoids that contain a carbonyl group (CC). This group includes spheroidenone, found in *Rba. sphaeroides* and *Roseobacter* sp. The presence of this oxygen atom has a strong influence on the properties of the whole molecule as oxygen has the second highest value of electronegativity among elements. This electronegativity allows it to withdraw electrons from the adjacent atoms. This results in a broadening of the absorption peak of okenone, which can be seen in Figure 1-14.

1.8. Determining the 3-D Structure of Proteins

The function of a protein is directly dependent on its three-dimensional (3-D) structure. Solving the structure of a protein will lead to a greater understanding and insight into its detailed function. One of the most powerful and favoured techniques in resolving detailed structural information of proteins is X-ray crystallography (Blundell and Johnson 1976, Smyth and Martin 2000). This method allows for the 3-D molecular structure of a molecule to be obtained from crystallised protein by exposing the crystals to an X-ray beam. This results in a diffraction pattern which, once processed, reveals an electron density map (Drenth 2007).

1.8.1. 3-D Crystallisation of Membrane Proteins

Obtaining a protein crystal of necessary quality for structure determination is the most time consuming and least understood aspect of protein crystallisation. Membrane proteins are one of the most difficult targets for crystallisation due to their hydrophobic nature and location within the

lipid bilayer of the cell. For many years it was thought that crystallising them was not possible at all (Carpenter, Beis et al. 2008). This all changed in 1985 when the first 3-D structure of a membrane protein, the reaction centre of *Blc. viridis*, was resolved using X-ray crystallography (Deisenhofer, Epp et al. 1985). This was groundbreaking work and has paved the way for many more membrane protein structures to be solved by X-ray crystallography (Preusch, Norvell et al. 1998, White and Wimley 1999). Nevertheless, the total number of membrane protein structures which are available online is tiny when compared to those available for water soluble proteins. As of February 2017, there are over 120000 macromolecule structures stored on the PDB of which only 870 are classified as membrane proteins (Berman, Westbrook et al. 2000).

1.8.1.1. Detergents

The use of detergent is required to extract a membrane protein from the lipid bilayer. Detergents are amphipathic molecules, possessing a hydrophilic head and hydrophobic alkyl chain tail. This amphipathic property allows the formations of a detergent micelle around the protein. The concentration of detergent molecules needed to spontaneously form micelles is the critical micelle concentration (CMC). This micelle mimics the natural lipid bilayer, hiding the hydrophobic sections of the membrane proteins (Carpenter, Beis et al. 2008). Detergents can be put into different categories relating to their structure. Ionic detergents contain a head group with a positive or negative net charge. Non-ionic detergents, such as n-Dodecyl β -D-Maltopyranoside (DDM) and n-Decyl- β -D-maltopyranoside (DM), have a net neutral charge. Zwitterionic detergents, such as lauryldimethylamineoxide (LDAO) have the characteristics of both non-ionic and ionic detergents and have a net neutral charge, similar to non-ionic detergents. They are more efficient than non-ionic detergents at disrupting protein-protein bonds.

The longer the alkyl chain length of the detergent, the bigger the micelle that is formed. A large micelle means a milder detergent with less chance of denaturing the protein, however, it leaves less of the protein exposed. Crystal formation is dependent on a section of the protein which is exposed to the soluble phase. These exposed hydrophilic domains form the intermolecular contacts within the crystal lattice. Detergents with short chain lengths are of a harsher nature and destabilise the protein, as the small micelle leaves the hydrophobic regions exposed to solvents (Tate 2010). Short chain detergents can induce a loss of function and protein aggregation, because of this they are generally not used in membrane protein crystallisations (Prive 2007, Sonoda, Newstead et al. 2011). Ionic detergents are generally not favoured for a similar reason. They are harsh and can strip essential lipids from the surface of the protein resulting in a functionality and structural loss (Hjelmeland 1990). Non-ionic detergents are considered to be milder detergents and can solubilize membrane proteins without denaturation, depending on the length of the alkyl chain.

Choosing a suitable detergent is an very important step in the crystallisation process. The protein must be stable in the detergent over the purification process and for the period of time required for crystallisation. The temperature, pH, and ionic strength of the system should also be

taken into consideration. It is often difficult to predict which particular detergent type will work best for solubilization of the membrane and for crystallisation. As such, it is best to try as many as possible. (Hjelmeland 1990)

1.8.2. Phase Diagram

Crystals are regular arrays of precipitated material, in this case, protein. A protein will stay in solution only up to a certain concentration. Once this concentration is reached, the solution will no longer remain homogenous and will precipitate. The basics of protein crystallography operate because of this phenomenon. A schematic diagram of a solubility curve, illustrating how the solubility varies with the concentration of a precipitant is shown in Figure 1-16

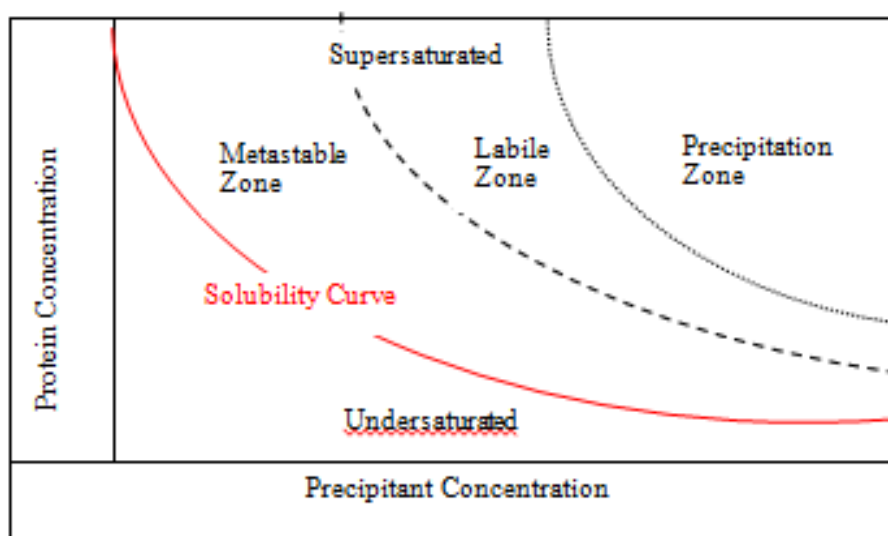


Figure 1-16: A phase diagram showing the solubility of a protein in solution as a function of the concentration of the precipitant present.

The concentration of protein in the solution at equilibrium is the proteins solubility and this varies with the solution conditions. Crystals dissolve in the undersaturated region where the concentration is below the protein solubility. In theory, crystals will form in any solution that is supersaturated, which is the case when the protein concentration exceeds the solubility. This is not the case in practice (Asherie 2004) due to the large degree of supersaturation that is required to overcome the activation energy barrier and allow nucleation to occur. (De Yoreo and Vekilov 2003). Nucleation takes time and, if the supersaturation level is too small, can end up taking too much time. If this occurs then crystals formation will not take place and the system has entered the metastable zone as seen in the phase diagram in Figure 1-16. In the opposite scenario, if the supersaturation is too large then it will cause aggregates and precipitates to form. This is the Precipitation zone. That only leaves the Labile zone, otherwise known as the Crystallisation zone. The system enters this phase when the solution is supersaturated and the conditions are specific to allow protein nuclei to form. If these nuclei remain stable and don't aggregate, they will recruit more and more molecules of protein allowing for the growth and the beginnings of a crystal (Asherie 2004).

1.8.3. Crystal Growth and Quality

Vapour diffusion is one of the most widely used techniques to obtain protein crystals (Chayen 1998). There are two types of vapour diffusion: hanging drop and sitting drop. Both these techniques utilise a protein drop containing precipitant and buffer, which is allowed to equilibrate with a larger reservoir containing the precipitant and buffer at higher concentrations. Water vaporises from the drop to the reservoir causing the precipitant concentration to increase. Crystals will begin to form if the conditions are reached in the Labile zone as described above but usually, the protein will simply precipitate out of solution as an amorphous aggregate (the Precipitation Zone). The hanging drop method is not favoured when crystallising membrane proteins as the detergent reduces the surface tension of the drop.

The quality of crystals produced depends on the strength of the protein-protein interactions within the crystal lattice. These can be affected by the temperature, pH, detergent, and the type of buffer present, ionic concentration, and additives (McPherson 1990). Crystal growth can be helped by the use of additives or small molecules. These can decrease the micelle size and to shift the phase diagram to allow nucleation at conditions in which were not previously possible (Deisenhofer and Michel 1989). It is crucial that crystal growth occurs in controlled, non-denaturing conditions. This ensures that once crystallisation conditions are discovered they can be repeated and improved.

1.9. Thesis Aims

The overall aim of this work is to investigate the bacteria species *Mcr. purpuratum* and the B800-B830 LH2 complex. This work will try to understand the origin of this unusual Q_y NIR absorption and explain it. This will help us to recognise the basis of the variations observed between the LH2 complex of *Mcr. purpuratum* and the LH2 of other species.

Chapter 2 - Methods and Materials

2.1. Growth of the bacteria

2.1.1. Cell Culture and Standard Growth Conditions

Marichromatium (Mcr.) purpuratum strain BN5500 (also designated as DSM1591 or 984) was grown anaerobically in the light at 30 °C in Pfennig's media using incandescent bulbs (Imhoff and Trüper 1980). The light intensity was kept constant at $80 \mu\text{mol m}^{-2} \text{s}^{-1}$ in a dedicated growth room. This was frequently measured and checked using an LI-250A light meter. Initially, the liquid cultures were grown from glycerol stocks (50 % (v/v) glycerol in a 1:1 ratio with a culture that had been stored in the deep freeze at -80 °C. Inoculation of media occurred in a sterile laminar flow hood. Liquid culture was established in 500 ml media sealed bottles and grown for 12 h. Cultures were maintained by inoculating fresh 500 mls of media every 48 h. Once this culture was fully grown it was used to inoculate a large scale 10 L flask.

Previous work on other purple photosynthetic bacteria has shown that some bacteria produce different light-harvesting complexes under different growth conditions (Gardiner, MacKenzie et al. 1996, Carey, Hacking et al. 2014). It was thought that the *Mcr. purpuratum* may be similar. A culture was grown anaerobically at 30 °C at a light intensity of $2 \mu\text{mol m}^{-2} \text{s}^{-1}$, low light conditions (LL) for 2 weeks.

2.1.2. Harvesting the Cells and Membrane Preparation

The bacteria were harvested at 4 °C by centrifuging at 4000 x g for 25 min in a Beckman J6B centrifuge and washed with MES 100mM KCl buffer at pH 6.8. The pelleted cells were re-suspended in 20 mM Tris-HCl buffer at pH 9.0 and broken by three passages through a French Press at 950 lb in^{-2} (6550.0125 kPa) in the presence of DNase (bovine Deoxyribonuclease I, Sigma-Aldrich) and MgCl_2 . The broken cells were centrifuged at a slow spin of 2000 x g for 10 min to remove cell debris before a spin of 200000 x g for 1 h. The pelleted membranes were then re-suspended in 20 mM Tris-HCl buffer at pH 9.0 to an optical density (OD) of 50 at 830 nm (OD_{830} 50). The membranes were then either used immediately or stored at -20 °C.

2.2. Purification of the LH2 Complex

The purification method of the LH2 complex from *Mcr. purpuratum* was based on previous work (Cogdell, Hawthornthwaite et al. 1990).

2.2.1. Solubilisation

The membranes at OD_{830} 50 were solubilized at room temperature for 1 h using lauryldimethylamineoxide (LDAO) at 1.0% (v/v). The solubilized membranes were spun at 200000 x g for 1 h to pellet un-solubilised protein. Separation of the LH1 complex and LH2 complex was

accomplished using a sucrose density gradient (SDG) centrifugation (Figure 2-1). Sucrose at different concentrations in 20mM Tris-HCl at pH 9.0 containing 0.1 % (v/v) LDAO was layered in Beckman ultracentrifuge tubes and 2.5 mls of solubilized protein was carefully layered on top. The tubes were spun at 200000 x g for 16 h in a Beckman Ti70 rotor. The LH fractions were collected from the gradients using a Pasteur pipette and the absorption spectra recorded to assess the stability, purity and concentration.

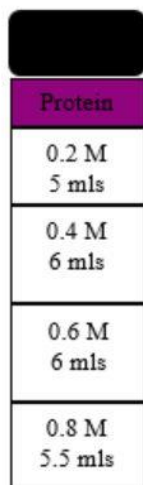


Figure 2-1: Schematic of SDGs showing the optimised conditions for the best separation of the LH complexes in 20mM Tris-HCl at pH 9.0 containing 0.1 % (v/v) LDAO.

2.2.2. Anion Exchange Purification and Detergent Exchange

Crude LH2 fractions from SDG were further purified by anion exchange chromatography (AEX) using diethylaminoethyl cellulose (DE52) (Whatman). 25 g of the adsorbent was slurry packed into a glass chromatography column with a diameter of 3.3 cm. The column was packed and run using gravity flow. The first stage is the wash stage, in which the adsorbent is washed with 20 mM Tris-HCl at pH 9.0 to remove residual contaminants. The protein was then loaded, and once bound, buffer exchanged into 20mM Tris-HCl at pH 9.0 containing 0.15% (w/v) n-Decyl- β -D-maltopyranoside (DM). The LH2 complex was then eluted using a step gradient by adding increasing concentrations of NaCl containing 0.15% (w/v) DM in Tris-HCl at pH 9.0. The bound LH2 protein was eluted at 50 mM of NaCl.

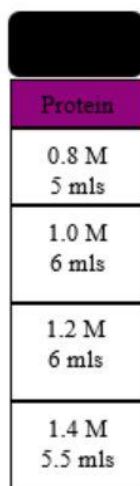
2.2.3. Size Exclusion Chromatography

Additional purification was achieved by size exclusion chromatography (SEC) on a Superdex G200 column (GE Healthcare). This was connected to AKTA prime (GE Healthcare Life Sciences) system with a flow rate of 0.5 ml/min. A 1 ml sample at OD_{830 nm} 100 was loaded onto the column, which had been equilibrated with 20 mM Tris-HCl pH 9.0 0.15 % DM. The optical ratio (OR) was used to assay the purity of the complexes present. This was deduced by the ratio of the NIR BChl maximum to the A₂₈₀. 0.5 ml fractions were collected and those with an A₈₃₀ /A₂₇₀ ratio of 2.2 or higher were and concentrated to an OD₈₃₀ of 100.

2.3. Purification of the LH1-RC Complex

2.3.1. Solubilisation

The membranes at OD₈₃₀ 50 were solubilized at room temperature for 1 h using DM at 2.0% (v/v). The solubilized membranes were spun at 200000 x g for 1 h, to pellet un-solubilised protein. Separation of the LH1 complex and LH2 complex was accomplished using SDG centrifugation as for the LH2. The concentration and volume of different sucrose solutions can be seen in Figure 2-2



Protein
0.8 M 5 mls
1.0 M 6 mls
1.2 M 6 mls
1.4 M 5.5 mls

Figure 2-2: Schematic of SDGs showing the optimised conditions for the best separation of the LH complexes in 20mM Tris-HCl at pH 9.0 containing 0.15 % (w/v) DM

2.3.2. Anion Exchange Purification and Size Exclusion Chromatography

Crude LH1-RC fractions from SDG were purified by AEX as described for the LH2. Elution occurred at 100 mM NaCl. The AEX elution was then further purified by SEC, as described for the LH2.

2.4. Steady- State Absorption Spectroscopy

Absorbance spectroscopy was used to assess the quality of the light harvesting complexes. LH complex samples were diluted using 20 mM Tris-HCl pH 9.0 with 0.15 % (w/v) DM. When measuring the membrane samples the detergent was not added to the buffer. This dilution was used to sample ODs of 1 and 0.1 at the NIR maximum. Steady-state absorption spectra were recorded in 1 cm path length cuvettes using a Shimadzu 1700 spectrophotometer.

2.5. SDS-Polyacrylamide Gel Electrophoresis (PAGE)

SDS-PAGE was used to analyse the purity and the polypeptide composition of the LH complexes. SDS-PAGE was performed using samples taken at various stages throughout the

purification procedures; membranes, SDG, anion exchange and gel filtration. This was to complement the absorbance spectrum assessment of purity.

Each sample was prepared by adding 1 µl of 1M DTT, 5 µl of NuPAGE (Invitrogen) sample buffer and varying amounts of protein (calculated to ensure a known final OD₈₃₀) and dH₂O to bring the total volume to 20 µl. The samples were heated at 80 °C for 10 min. The samples were then loaded on a Pre-cast 4-12 % NuPAGE Bis-Tris (Invitrogen) gel, with Novex Sharp Protein Standard molecular weight markers (220 kDa – 10 kDa) (Invitrogen). (Laemmli 1970). The gel was run at 200 V for 30 min in BIO-RAD SDS-PAGE running buffer (Invitrogen) and washed twice with 100 ml of dH₂O for 10 min before staining. The gel was stained for 1 h using SimplyBlue SafeStain (Invitrogen), and then de-stained overnight in dH₂O, as per the manufacturer's instructions.

2.6. Stability of the LH2 Complex in the Presence of Different Detergents

Previous work had shown that the LH2 complex was unstable in LDAO (Kerfeld, Yeates et al. 1994). In order to investigate the stability of the complex, thermostability assays were carried out. This is important for crystallisation as the protein must be stable over a long period of time.

Mcr. purpuratum LH2 protein was solubilized in three different detergents: LDAO, DM and n-Dodecyl β-D-Maltopyranoside (DDM). These were then purified using SDG centrifugation, to separate the LH1-RC and LH2 complex (see appendix for DDM SDG). 1 ml samples of the LH2 complex, in the different detergents, were heated to a temperature of 50°C in a heating block. The absorbance spectrum of the complex was measured every 15 min. The reduction of the 830 peak implies the degradation of the protein, as it can no longer appropriately bind the BChl *a*. Plotting the 830 nm absorption over time indicates which detergent provided the most stability for the LH2 complex.

2.7. Crystallisation Trials of the LH2 Complex

The goal of crystallisation is to produce a well-ordered crystal which is large enough to provide a high-resolution diffraction pattern when exposed to X-rays. The tertiary structure of a protein can be determined from analysis of this diffraction pattern (Ostermeier and Michel 1997). Membrane proteins are one of the most difficult targets for crystallisation due to their hydrophobic nature and location within the lipid bilayer of the cell. (Carpenter, Beis et al. 2008)

2.7.1. Initial 96 Well Screens

Crystallisation trials were initially carried out using the sitting drop vapour diffusion method. Primary screens of MemGold and MemStart/MemSys (Molecular Dimensions) crystal

trials were set up with OR > 2.2 LH2 protein at OD₈₃₀ 100 and OD₈₃₀ 50. These initially set up with the LH2 protein solubilised in the detergent DDM and were then repeated using protein solubilised in DM. A Cartesian HoneyBee 8+1 nanovolume robot was used to set these 96 well MRC crystallisation plates (Molecular Dimensions). This allowed rapid screening of these sparse matrix screens and identification of many possible crystallisation conditions. These trays were then placed in the Crystallisation Hotel Rhombix Imager (Thermo Fisher Scientific). Crystals were kept at a constant temperature of 20°C and monitored over the course of several weeks.

2.7.1.1. Optimisation

Conditions that produced crystals in the 96 well plates were optimised in 24 well MRC crystallisation trays. These hold a larger volume of protein in the well than the 96 well screen, 10µl compared to 2µl, allowing for the production of larger crystals. Optimisations were made using solutions from Molecular Dimensions where possible. The screens were set up using a Hamilton robot. The initial crystallisation conditions were optimised by changing the salt concentration, the buffer pH and the precipitant concentration around those of the initial 96 well plate hit conditions. Crystals were kept at a constant temperature of 16 °C and were identified using a MEIJI EMZ light microscope. Crystals that were three-dimensional were cryo-protected using well solution supplemented with 40% (v/v) PEG 400 and were cryo-cooled in a liquid nitrogen stream. The crystals were then tested on the University of Glasgow in-house X-ray Diffractometer, Rigaku MicroMax-007 and Mar345 dtb detector by Dr Aleksander Roszak. Crystals that presented good diffraction with clear diffraction spots and defined lunes were stored in liquid nitrogen for further testing at Diamond Light Source (DLS).

2.7.1.2. Altering the Purification and Detergent

This was done as part of the optimisation process due to finding crystallisation was variable. The purification procedure of *Mcr. purpuratum* LH2 was altered after the primary 96 sparse matrix screens described above. The detergent used for solubilisation was changed to LDAO followed by exchange into 0.15% (w/v) DM with a buffer of 20 mM Tris-HCl pH 9.0. Purified LH2 protein at OD₈₃₀ 100 and OD₈₃₀ 50 vapour diffusion crystal trays were set up in 24 well plates using the MemGold and MemStat screens (Molecular Dimensions). The trays were kept at a constant temperature of 16°C. The Cartesian crystallisation robot and 96 well plates were no longer used due to the limited size of the wells and the impact on crystal formation. Seeding was also tried as part of the optimisation procedure using the Hampton Seed Beed kit. This was done as described in the manufacturer's instructions and in Chapter 3.

2.8. Thin Whole Cell Sections

A fresh culture of *Mcr. purpuratum* was taken to Sheffield, as part of a collaboration with Prof Neil Hunter. 3 ml of fresh cell culture was pelleted on a table top microcentrifuge. The supernatant was removed and the cells were resuspended in 0.1 M sodium phosphate to wash them and pelleted

again for 1 min at the same speed. The washed cells were then fixed in 1 ml of primary fixant (44 ml of 0.1 Sodium phosphate pH 7.0 and 6 ml of 25 % (v/v) glyceraldehyde (EM grade)) and left overnight at 4 °C. The mixture was spun down for 2 min at low speed to pellet the cells and washed twice with the 0.1 M sodium phosphate. For staining, 0.5 ml 2 % osmium VIII oxide solution was added and left to stand for 2 h. The cells were pelleted and washed again with the 0.1 M sodium phosphate, allowing the pellet to soak for 10 min before pouring off the supernatant and repeating. The pellet was resuspended in 75 % ethanol and then repelleted. This was repeated with 95 % and 100 % ethanol and finally, 100 % ethanol dried over anhydrous CuSO₄. 1 ml of the intermediate solvent propane oxide was added, the pellet was dislodged from the side tube and the mixture was decanted into a 7 ml glass specimen vial. It was left for 15 min before fresh propane oxide was added. Once this was removed a 50:50 mixture of propane oxide: resin was added and mixed gently overnight at room temperature. The 50:50 mixture was removed and excess resin added to the pellet in addition to BDMA, ensuring it was fully coated, with 1 drop of benzyldimethylamine (BDMA) per 1 ml of resin. It was stirred with a change of resin every 3 h to dilute out the remaining solvent. Finally, the pellet was transferred to the edge of the thin section mould and fresh resin was added. After the mould was baked for 48 h at 60 °C the cells were sectioned and viewed under an electron microscope (EM).

2.9. Reconstitution of *Mcr. purpuratum* LH2 into Lipid

As part of a collaboration with Prof Neil Hunter in Sheffield, it was thought that Atomic Force Microscopy (AFM) could be utilised to view the ring size and structure of the *Mcr. purpuratum* LH2. This work was done with the aid of Dr Pu Qian. Native membranes were sent down for AFM but clear pictures could not be obtained. Therefore, the purified LH2 was reconstituted into lipid. Stock solutions of the lipids 1,2-Dioleoyl-*sn*-glycero-3-phosphocholine (DOPC), 1,2-Dihexanoyl-*sn*-Glycero-3-Phosphocholine (DMPC) L- α -phosphatidylglycerol (PG), 1-palmitoyl-2-oleoyl-*sn*-glycero-3-phosphocholine (POPC) were made at 4mg/ml in 1ml of 20mM Tris-HCl at pH 9.0 with 0.15% DM. The lipids were acquired from Avanti (avantilipids.com). Using a BSA protein Bradford assay kit it was determined that OD_{830 nm} 10 was equal to 0.612 mg/ml of protein. Purified LH2 was added to the range of different lipids at different [Lipid]/[Protein] ratios, which can be seen in the table below (Table 2-1).

The solutions were dialysed over a week to remove the detergent, using a specially prepared dialysis buffer (see appendices). The samples were then viewed on grids under an electron microscope.

Table 2-1: The [Lipid]/[Protein] ratio and the concentration of each in the final solution of 0.1 ml for reconstitution

Ratio	[Lipid]/ [Protein] mg/ml
0.33	0.15/0.5
0.50	0.25/0.5
0.80	0.4/0.5
1	0.5/0.5
1.20	0.6/0.5
1.50	0.75/0.5

2.10. Molecular Biology

During this work, new information became available with the recent sequencing of the *Mcr. purpuratum* genome (Grigoriev, Nordberg et al. 2011). This identified several possible *puc* genes that code for the LH2 polypeptides. This opened up possibilities regarding the genetic manipulation of the *puc* genes and the carotenoid genes. All protocols were carried out as per the manufacturer's instructions and the Molecular Cloning manuals (Sambrook, J. and et. al 2000).

2.10.1. Trials to grow *Mcr. purpuratum* on Agar plates

Trials were conducted using *Mcr. purpuratum* media to find whether *Mcr. purpuratum* was able to grow on agar plates. Once this has been optimised, several agar plates containing different antibiotic concentration were set up to test the sensitivity of the bacteria to the antibiotics (Table 2-2). The agar plates were prepared (see appendices), then 50 µl of liquid culture at OD_{830 nm} 1 - which had been grown the day before - was added to the plates and left to grow overnight at 30 °C under anaerobic conditions.

Table 2-2: The different antibiotics tested in this experiment. The concentration used across 3 different plates can also be seen.

Antibiotic	[STOCK] mg/ml	[Control Plate] µg/ml	[Plate 1] µg/ml	[Plate 2] µg/ml	[Plate 3] µg/ml
Ampicillin	100	0	50	75	100
Kanamycin	30	0	10	30	50
Chloramphenicol	100	0	100	150	200
Tetracycline	25	0	25	50	75
Streptomycin	100	0	25	50	100

2.10.2. Preparation of High Molecular Weight *Mcr. purpuratum* Genomic DNA

Mcr. purpuratum genomic DNA was required for PCR to create mutants and was extracted from liquid culture. The pipette tips (1.5 ml eppendorfs) were autoclaved as well as stock buffers (1M Tris-HCl at pH 8.0 and 0.5 M EDTA) to remove any DNase. A culture of *Mcr. purpuratum* was first plated out on 1.5 % agar plates to ensure its purity. Single colonies were picked and then grown overnight in a 500 ml flat bottle. 10 ml of this culture was pelleted at 4 °C then the supernatant was removed, and the cells re-suspended in 20 mM Tris-HCl at pH 8.0 as a wash. This was spun down again, the supernatant was removed and then the cells were re-suspended in 1 ml fresh lysis buffer (see appendices). The mixture was incubated at 37 °C for 1 h. Proteinase K was then added to a final concentration of 100 µg/ml (5 µl per ml from a 20 mg/ml stock) and incubated at 50 °C overnight. When the sample had clarified RNase A was added to a final concentration of 20 µg ml⁻¹ (2 µl per ml of a 10 mg/ml stock) and the tubes were further incubated at 37 °C for 1 h.

The 1 ml sample was split into two 500 µl aliquots and an equal volume of phenol:chloroform:isoamyl alcohol(IAA) (25:24:1) was added to each. The tubes were inverted gently several times until the aqueous and solvent layers formed a milky suspension. The samples were then centrifuged for 10 min in a Jencons-PLS spectrafuge 24D at 16300 x g. The upper phase was removed and transferred to a fresh eppendorf without disturbing the lower phase and the white protein pellicle at the interface. To the aqueous upper phase 100 µl of 10 M ammonium acetate and

600 µl absolute ethanol (Analytical reagent (AR) grade) was added. The tubes were gently inverted until the solutions fully mixed and the ‘clouds’ of DNA became visible. The tubes were placed on ice for 10 min before the DNA was centrifuged at 16300 x g for 10 min. The supernatant was then removed completely from the tubes and then the pellets were re-suspended in 1 ml of 70 % ethanol. This was then centrifuged at 16300 x g for 5 min, the supernatant removed and excess ethanol blotted from the tube upside down on blue roll. The pellets were air dried until all the ethanol had evaporated and then they were re-suspended in 50 µl of DNase & RNase free water. This was incubated at 4 °C overnight to help the DNA go back into solution. This method was adapted from Molecular Cloning: A Laboratory Manual (Sambrook and al 2000) by Andrea Mitchell.

2.11. Investigation of the Carotenoids of *Mcr. purpuratum*

2.11.1. Diphenylamine Trials

Diphenylamine (DPA) inhibits the activity of phytoene desaturase, causing a build-up of phytoene and related precursors (Fuller and Anderson 1958). DPA also disrupts the biogenesis pathway that produces ubiquinol, making it toxic at high concentrations. This experiment was designed after seeing the effect of the DPA on other phototrophic (Cohen-Bazire and Stanier 1958) (Gall, Henry et al. 2005) (Moskalenko and Makhneva 2012).

2.11.1.1. Bacteria Growth

Mcr. purpuratum was grown phototrophically overnight at 30 °C with an average illumination intensity of 10 µmol m⁻² s⁻¹. This freshly grown culture was then used as the inoculum for the DPA trials. The first sets of trials were conducted on a small scale, using 100 ml flat bottles. The concentration range chosen to be tested was as follows: 0 µM (control), 20 µM, 40 µM, 60 µM, 70 µM and 100 µM DPA. The stock concentration of DPA was 10 mM in 100 % ethanol. The final volume of the culture mixture was 120 ml, consisting of the media, DPA treatment and 20mls of inoculum. This was agitated before finally being poured into a 100 ml flat bottle. In the case of the control, some of the 100 % ethanol, equal to the same volume of DPA was added. For 24 h the cultures were grown in closed flasks wrapped in tinfoil, to ensure all oxygen was respired away. This prevented the production of destructive oxygen radicals which the carotenoid would normally protect from. Following this, the foil was removed and the cultures were grown for a further 48 h behind a red filter. This filter prevents the photo-destruction of the DPA by white light. The temperature in the growth chamber was kept constant at 30 °C.

The initial small-scale experiments were designed to help narrow down the range of DPA concentrations to use before moving up to larger scale 500 ml flat bottles. However, when a similar ratio of media to the inocula was tested, 500 mls of media to 100 mls of inoculum, the DPA did not have the same effect on growth at the same concentrations. Therefore, the same range of concentrations had to be investigated again with different ratios of inocula to media. In the end, 30

mls of inoculum was used with 530 mls of media and treatment giving a total volume of 560 mls. The concentrations of DPA used were 0 μM (control), 40 μM , 60 μM , 80 μM and 100 μM . These cells were harvested and the membranes prepared. 1.5 % DM was used to solubilize the membranes. The light-harvesting complexes separated by overnight SDG centrifugation (as described in detail above). DM is a gentle detergent and was used to allow the core complex to remain intact. The LH2 and LH1-RC were removed and the individual absorption spectra were recorded for each of them at the different DPA concentrations.

2.11.2. *CrtI* Knock Out

The removal of the *CrtI* gene would result in the build-up of phytoene, stopping the synthesis of okenone and therefore the loss of the deep purple colour of the *Mcr. purpuratum* culture. This part of the study is a compliment to the DPA trials described above.

Table 2-3: Names and sequences of the primers used to knock out the *CrtI* gene. The restriction sites sequences are marked in bold red

	Primer Name	Primer Sequence
1	MPcrtI_for2_eco	ATAGA GAATTC GTCGACCTCTATCGCCGTCTCGTC
2	MPCrtI_rev2_Hind	ACT AAGCTT GAAGACCGGATCCTTCAACCACTC
3	MPcrtI_US_rev	GTGTTAGACGTCCATGAGTGTCAAGTCTAC
4	MPcrtI_DS_for	CTCATGGACGTCTAACACCATGACCGAAGC

2.11.2.1. Amplification of Genes for Cloning

The first stage was to design primers that would amplify up an upstream fragment and a downstream fragment surrounding the *CrtI* gene. There were designed with the help of Dr Sarah Henry. The method used was the splice-overlap extension method (Horton, Hunt et al. 1989). This required flanking primers and internal primers to be designed. A summary of the location of these primers in relation to the *CrtI* gene and their sequences can be seen in Figure 2-3 and Table 2-3. Restriction sites for EcoRI and a HindIII were designed into primers 1 and 4, respectively. Primers 3 and 4 incorporated the start codon of the *CrtI* gene in their sequences as well as the stop codon so that they would share an overlap of 18 base pairs, which could be used to anneal them together. The upstream fragment's length was calculated to be 500 bp and the downstream fragment was 630 bp.

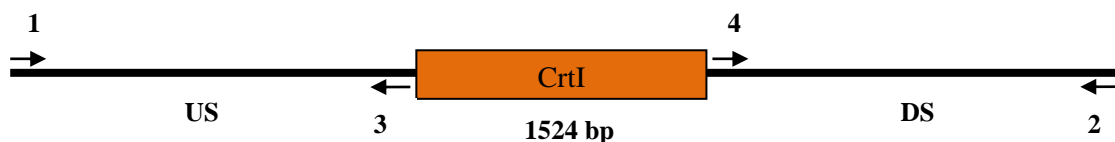


Figure 2-3: Diagram showing the location of the primers used to knock out the *CrtI* gene. The numbers correspond to the names of the primers in Table 2-3. US- Upstream, DS- Downstream

A Phusion PCR program was created on a C-1000 thermal Cycler from Bio-Rad. This program sets a melting temperature of 95 °C for 10 s followed by annealing at 55 °C for 15 s and extension for 30 s at 72 °C. This cycle was set to repeat 30 times before a final 5 min extension. Two different reaction tubes were set up that only differed in the combination of primers which were added; 1 µl genomic DNA (gDNA), 0.5 µl Phusion® DNA Polymerase (Finnzymes), 10 µl of Phusion buffer, 1.5 µl Dimethyl sulfoxide (DMSO) and 1 µl Deoxynucleotide Triphosphates (dNTPs). The sequences were very GC rich and the addition of DMSO was used to relax the secondary structures of the DNA, allowing the primers to anneal and amplify the DNA with a greater efficiency. To the upstream reaction tube, 1 µl of the primers 1 and 3 were added. To the downstream reaction tube, 1 µl of primers 2 and 4 were added. Each tube was made up to 50 µl with sterile dH₂O. The PCR product was run on a DNA gel and the 2 bands, 1 from the upstream and 1 from the downstream were cut out. The Qiagen, QIAquick gel extraction kit was used to extract the DNA from the bands, following the protocol from the manufacturer to achieve maximum DNA concentration. 5 µl of each of the extracted DNA from the upstream and downstream reactions was added to 10 µl of Phusion buffer, 1.5 µl Dimethyl sulfoxide (DMSO) and 1 µl Deoxynucleotide Triphosphates (dNTPs) and made up to 45 µl with sterile dH₂O to prevent contamination. A splicing by overlap extension/splicing by overhang extension (SOE) PCR program was then run, which had a melting temperature of 95 °C for 10 s, an annealing temperature of 37 °C for 20 s and an extension time of 60 s at 72 °C. Upon completion, 2.5 µl of 1 and 4 were added to the mixture, along with 0.5 µl Phusion® DNA polymerase. The Phusion program mentioned previously was started once again and another analytical DNA gel was run at its end. The band at 1 kb was equal to the predicted mass of the *CrtI* KO and was cut out and extracted as described previously.

2.11.3. Transformation into pJET 1.2/blunt

The next step was to clone the *CrtI* KO into pJET1.2/blunt (Fermentas). A ligation was set up on ice, using 1 µl *CrtI* KO DNA, 1 µl pJET1.2/blunt 10 µl of ligation buffer, 1 µl of T4 Ligase (Fermentas) and made up to 20 µl with dH₂O. This was left at room temperature for 1h. This ligation mixture was then transformed into JM 109 competent *E. coli* cells by adding 2 µl of it to a 50 µl aliquot of cells and leaving the mixture on ice for 10 min. The cells were then heat shocked for 25 s at 42 °C, before being placed back on ice for 2 min. 250 µl of fresh LB broth (see appendices), which had been heated to 42 °C, was then added. The cells recovered for 1 h in a 37

°C shaker incubator. The cells were then spread on a 1.5 % LB agar plate that contained 50µg/ml of the antibiotic Ampicillin and left to grow at 37 °C overnight. 4 colonies were picked from the plate and each grown up separately in 5 mls of LB that contained 50 µg/ml of Ampicillin before 3 mls of each culture was taken and pelleted. Then using the Thermo Scientific GeneJET plasmid miniprep kit the pJet 1.2/blunt plasmid containing the *CrtI* KO was extracted and eluted. The 4 different plasmids were then digested separately, using EcoI and HindIII for 2 h at 37 °C. 16 µl of plasmid, 2 µl of Buffer B (10X) ((Roche) and 1 µl of each enzyme was added. At this stage, the pK18mobsacB (BV Tech) (Schafer, Tauch et al. 1994) cloning vector was also digested with the same enzymes.

2.11.4. Mobsac Ligation

The digested *CrtI* KO was then ligated into the digested pK18mobsacB. A ligation was set up on ice, using 1 µl digested *CrtI* KO, 1 µl pK18mobsacB 10 µl of ligation buffer, 1µl of T4 Ligase (Fermentas) and made up to 20 µl with dH₂O. This was left at room temperature for 1 h. This ligation mixture was then transformed into JM 109 strain competent *E. coli* cells. The cells were then spread on a 1.5 % LB agar plate that contained 30 µg/ml of the antibiotic Kanamycin, 6 µl of 1 M IPTG and 2 % X-gal. If plain pK18mobsacB is successfully transformed into a cell, then the cell will express functional β-galactosidase. However, if the pK18mobsacB+*CrtI* KO is transformed into a cell, then it will express non-functional B-galactosidase due to the disruption of the lac Z-alpha gene by the insert. The plate was left to grow at 37 °C overnight. 5 white colonies were picked from the plate and each grown up separately in 5 mls of LB that contained 30µg/ml of kanamycin. 3 mls of each culture was taken and the cells pelleted, then using the Thermo Scientific GeneJET plasmid miniprep kit the PJet 1.2/blunt plasmid containing the *CrtI* KO was extracted and eluted in 50 µl of dH₂O. The 5 different plasmids were then digested separately, using a restriction enzyme that cuts within the insert at least once and outside the insert at least once. 10 µl of DNA was added to 2 µl Buffer J (10x) and 1 µl of the restriction enzyme kpnI. This was made up to 20 µl with dH₂O and kept at 37 °C for 2 h. A DNA gel confirmed that all 5 colonies had successfully incorporated the pK18mobsacB + *CrtI* KO. DNA 5 was selected and sent for sequencing.

2.11.5. Conjugation

The DNA extracted from colony 5 was then transformed λpir competent *E. coli* cells. This strain of cells has been modified so when it is used as specific host strain into which the transposon vector DNA is transformed, the transfer occurs by biparental mating. They can utilise any gram-negative bacterium as a recipient for conjugative DNA transfer. The cells were then spread on a 1.5 % LB agar plate that contained 30 µg/ml of the antibiotic kanamycin. The plate was left to grow at 37 °C overnight and then 2 colonies were picked from the plate and each grown up separately in 5 mls of LB that contained 30 µg/ml of kanamycin. At this time, a scrapping of *Mcr. purpuratum* colonies from an agar plate was taken and grown up in 10 mls of *Mcr. purpuratum* (CP) media aerobically and in the dark at 30 °C overnight.

A series of dilutions were made in 1.5 ml eppendorfs, as can be seen in table 2-4

Table 2-4: Amounts of *Mcr. purpuratum* culture and pK18mobsacB + *CrtI* KO in λ pir added to make the conjugation dilutions

Dilution	<i>Mcr. purpuratum</i> added / μ l	pK18mobsacB + <i>CrtI</i> KO in λ pir added / μ l
0 (Control)	1000	0
5	995	5
10	990	10
50	950	50
100	900	100
200	800	200

The samples were centrifuged at 33000 x g for 1 min then supernatant removed and the pellet was resuspended in 50 μ l of fresh LB. An LB agar plate with no antibiotic was split into 6 sections using a marker pen. Each of the conjugation dilutions was pipetted onto a different section, making sure no contact occurred between them. This was allowed to dry for 20 min before being grown at 37 °C for 6 h.

CP media and CP media agar plates were prepared with no yeast extract (-YE). Without this, the *E. coli* can only grow slowly. Twelve agar plates in total were made, all containing 30 μ g/ml of kanamycin except 1, which would be used for the control. After 6 h had passed a scraping of each conjugation mixture was taken and resuspended in 200 μ l of CP media -YE. All the dilutions were plated in duplicates, using 100 μ l per plate. The control was plated on 2 CP media plates, one containing kanamycin and one without. These were grown under anaerobic conditions in the light.

12 single colonies were then picked and grown in 8 mls of CP media -YE containing 30 μ g/ml of kanamycin. Of these 12, only 7 managed to grow. Serial 1 in 10 dilutions were made for each colony. CP media 1.5 % agar plates -YE were made with 10% sucrose and the 10^{-4} , 10^{-5} , 10^{-6} and 10^{-7} dilutions plated. Different growth conditions of the sucrose plates were attempted to try and optimise the production of the *CrtI* mutant.

1. The plates were grown anaerobically in the dark for 24 h before being exposed to light.
2. The plates were grown aerobically in the dark.
3. The plates were grown anaerobically in the light.

2.12. Analysis of the LH2 polypeptides

2.12.1. Mass Spectrometry of *Mcr. purpuratum*

Mass spectroscopy was used to identify which α and β peptides are expressed in the *Mcr. purpuratum* LH2 complex.

2.12.2. Peptide Extractions

To begin with, 500 μ l of OD 100 at 830 nm of purified *Mcr. purpuratum* LH2 was flash frozen using liquid nitrogen and then freeze-dried overnight. The sample was then dissolved in 1 ml of 1:1 Chloroform: methanol with 100 mM ammonium acetate (Chl: MeOH 0.1AA) and left at room temperature for 10 min. The mixture was spun at 5,000 rpm in a Sorval centrifuge for 10 min to collect cell debris. The sample was then carefully pipetted off and transferred to a brown glass vial wrapped in tinfoil to protect it from light.

2.12.3. MALDI-TOF

The extracted peptides were taken for Matrix-assisted laser desorption/ionisation – Time of Flight (MALDI- TOF) mass spectrometry. MALDI is a very soft ionisation technique which allows the detection of the mother ion and its mass. Samples were recorded using an Ultraflex III TOF/TOR (Bruker). By examining the genomic sequence of *Mcr. purpuratum*, more specifically its *puc* genes, the DNA sequence and therefore the amino acid sequence of the all the possible LH2 peptides can be determined. Using this sequence of amino acids the average mass can be calculated and compared to the masses detected from the MALDI-TOF giving a possible identification.

All MALDI-TOF measurements were done with the aid of Dr William Mullen at the University of Glasgow. A series of dilutions of the sample were made using Chl: MeOH 0.1AA. 1 μ l of each sample and dilution was loaded onto an Anchorchip Target plate, and 0.8 μ l of α -Cyano-4-hydroxycinnamic acid (CHCA) was added after the sample had dried.

2.12.4. LH60 Column

Extracted peptides were separated from the pigments using a glass column containing Sephadex 60 resin. This column was equilibrated in Chl: MeOH 0.1AA with a flow rate of 2 ml min^{-1} for 30 min. The extracted peptides were loaded onto the column and immediately 0.5 ml fractions were collected until coloured pigments began to elute. All the fractions before the pigment front had their absorption spectra measured at 280 nm. Samples with an $\text{OD}_{280 \text{ nm}}$ 0.1 and higher were pooled together. This was then dried down using nitrogen gas. The dried down sample was resuspended in 300 μ l of Chl: MeOH 0.1AA and then a series of dilutions were made which were then loaded on the plate as described previously.

2.12.5. Tandem MS-MS

Using LH2 *Mcr. purpuratum* samples were analysed on a Dionex Ultimate 3000 RSLC nano flow system (Dionex, Camberly UK). The samples (5 μ l) were loaded onto a Dionex 100 μ m

x 2 cm 5 μ m C18 nano trap column at a flow rate of 5 μ l/min by a Ultimate 3000 RS autosampler (Dionex, Camberley UK). The composition of the loading solution was 0.1 % formic acid and acetonitrile (98:2). Once loaded onto the trap column the sample was then washed off into an Acclaim PepMap C18 nano column 75 μ m x 15 cm, 2 μ m 100 Å at a flow rate of 0.3 μ l/min. The trap and nano flow column were maintained at 35 °C in a column oven in the Ultimate 3000 RSLC. The samples were eluted with a gradient of solvent A: 0.1 % formic acid versus solvent B: acetonitrile starting at 5 % B rising to 50 % B over 20 min. The column was washed using 90 % B before being equilibrated prior to the next sample being loaded. The eluant from the column was directed to a Proxeon nanospray ESI source (Thermo Fisher Hemel UK) operating in positive ion mode then into an Orbitrap Velos FTMS. The ionisation voltage was 2.5 kV and the capillary temperature was 200 °C. The mass spectrometer was operated in MS-MS mode scanning from 380 to 2000 amu. The top 5 multiply charged ions were selected from each full scan for MS-MS analysis.

The fragmentation method used was Electron-transfer dissociation (ETD). ETD induces fragmentation of cations by transferring electrons to them. Singly charged reagent anions transfer an electron to multiply protonated peptides within an ion trap mass analyser to induce fragmentation. ETD cleaves along the peptide backbone while side chains and modifications such as phosphorylation are left intact. The fragmentation method was ETD at 75 ms activation. The ions were selected for MS² using a data dependent method with a repeat count of 1 and repeat and exclusion time of 15 s. Precursor ions with a charge state of 1, 2 and 3 were rejected. The resolution of ions in MS¹ was 60,000 and 7,500 for ETD MS².

2.12.6. High-Performance Liquid Chromatography

Adsorption chromatography depends on the chemical interactions between solute molecules and specifically designed ligands chemically grafted to a chromatography matrix. Different types of ligands have been immobilised to exploit a variety of biochemical properties for purification. Reversed phase chromatography utilises hydrophobic interactions by an immobilised aromatic ligand or n-alkyl hydrocarbon. This means that hydrophobic molecules, such as proteins, peptides and nucleic acids, can be separated by reversed phase chromatography with excellent recovery and resolution.

Several methods were attempted using a Waters Alliance RP-HPLC system with an e2695 solvent module and UV detector. Primarily the Tharion method 1 was used (Tharion, Nightingale et al. 1999) dissolving the peptides in formic acid and running a gradient from a starting solvent of 30 % acetonitrile with 0.1 % trifluoroacetic acid (TFA). A C8 XBridge column was equilibrated at 0.7 cm³ min⁻¹ in the starting solvent. The dried down sample was resuspended in 200 μ l formic acid and filtered using a Spartan 0.2 μ m PTFE filter before injecting onto the HPLC column. No peaks were seen and on further investigation, it was found that the sample was not

soluble in formic acid or in 30% acetonitrile. In contrast, it was found that the peptides would not bind to the column at all when dissolved in Chl: MeOH 0.1AA.

The next method to be tried was described by Parkes-Loach (Parkes-Loach, Sprinkle et al. 1988). Solution A was dH₂O with 0.1 % TFA and Solution B was Acetonitrile: Isopropanol (2:1) with 0.1 % TFA. The peptides were dissolved in 100 µl hexafluoroacetone(hydrate) (HFA) which was then mixed with 100 µl of mobile phase (50:50 Solution A: Solution B). The gradient was adapted from (Makhneva, Bolshakov et al. 2008) and altered over a few different runs to see which would give the best separation. The detection wavelength was set at 280 nm.

2.12.7. Deletion of the *pucBA2* gene

Previous sequence data indicated that there were multiple peptides being expressed in the *Mcr. purpuratum* LH2 complex. MALDI data helped to narrow down which alpha and beta pairs were being expressed and their amino acid sequences were located using Uniprot and NCIB.

The first knock was selected as *pucBA2*, which transcribes the β₂ and α₂ polypeptides. This was done as described previously for the *CrtI* KO. The primers designed and used can be seen in Table 2-5. The *pucBA2* KO insert has been cloned into pJET1.2/blunt and was ready to be digested with BamHI and HindIII. It was then to be cloned into pK18mobsacB.

Table 2-5: Names and sequences and of the primers used to knock out the *pucBA2* gene. The restriction sites sequences are marked in bold red

	Primer Name	Primer Sequence
1	PucBA2_forUS_bam	ATAG GGATCC GAGAGGTCGCGTTAGTTTATG
2	PurBA2_revDS_hin	ATAT TTCGA AGTGGACACGAACAACAGGTGAT
3	PucBA2_Rev_US	TTCTTACTTGGCCATTAGAGGTATCTCCAAG
4	PucBA2_For_DS	CTAATGGCCAAGTAAGAACTCTCGGGTCCG

Chapter 3 - Purification and Crystallisation of the LH2 complex from *Mcr. purpuratum*

This chapter will look at *Mcr. purpuratum* from whole cells to purified protein. The major points will be the purification and crystallisation trials of the LH2 complex. The main aim was to optimise the purification method for the LH2 complex and use this purified protein for crystal trials in the hope of obtaining three-dimensional (3D) crystals that would diffract to a high resolution. This would make it possible to obtain a structure of this unusual LH2 complex. In a previous study only very tiny crystals had been grown that diffracted poorly (Kerfeld, Yeates et al. 1994).

3.1. Purification of the LH2 Complex

The purification method was based upon and optimised from previous work. (Cogdell, Hawthornthwaite et al. 1990) The details of the purification method of this complex can be read in section 2.2 of the Materials & Methods.

3.1.1. Growth of the Bacteria

One of the most striking things about *Mcr. purpuratum* is the colour. This beautiful purple colour remains throughout the entire purification process, from cell culture all the way to the final purification step of LH2. A photograph of the cell culture can be seen in Figure 3-1A and the absorbance spectrum in Figure 3-1B.

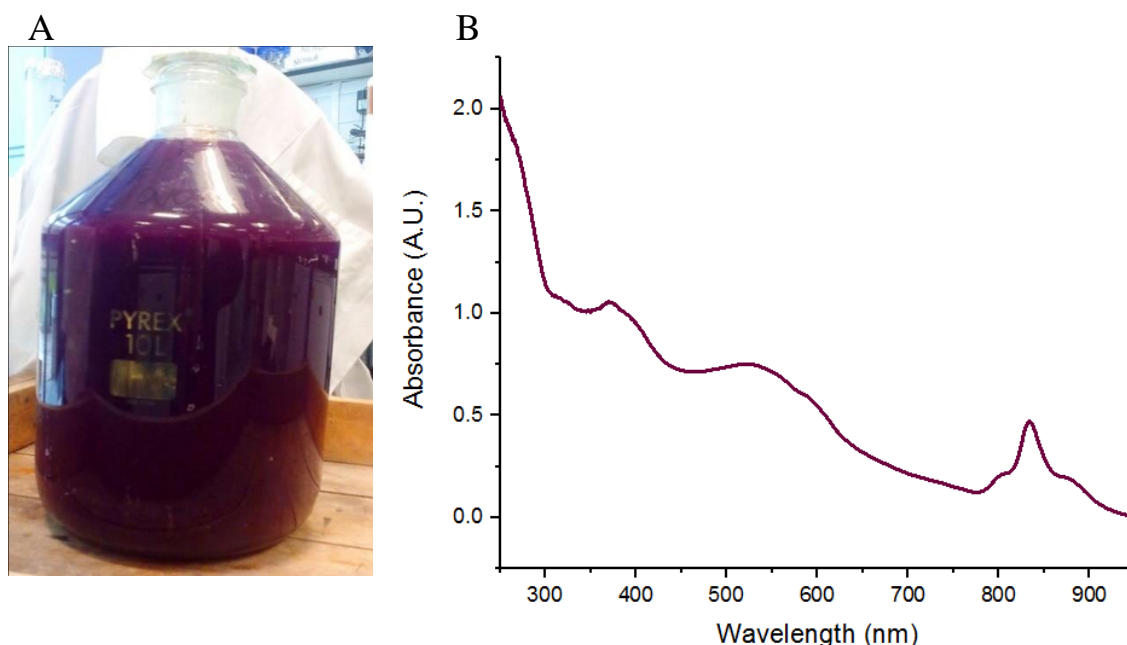


Figure 3-1: *Mcr. purpuratum* cell culture and absorption spectrum. A) The culture was grown in a 10 L pyrex® flask and ready to harvest. B) The room temperature absorption spectrum of the cells. The 800 nm shoulder, 830 nm LH2 peak and the 875 nm can be clearly seen. In the visible region, there is a broad absorption band between 580 and 460 nm, which is mainly due to the major carotenoid present (okenone) and then the Bchl a Soret band between 360-370 nm

3.1.2. Growth under Low Light Conditions

An attempt was made to grow the *Mcr. purpuratum* culture under low light conditions. Several other bacteria species have been shown to produce alternate LH complexes when the growth conditions have been altered (Carey et al. 2014; Gardiner, Cogdell, and Takaichi 1993; Tharia et al. 1999). Figure 3-2 below shows a comparison of the spectra of *Mcr. purpuratum* whole cells grown at their normal light conditions (control) and at low light conditions (LL). For this experiment, normal light conditions, the control, is defined at a light intensity of $80 \mu\text{M m}^{-2} \text{s}^{-1}$ and low light conditions is defined as $2 \mu\text{M m}^{-2} \text{s}^{-1}$

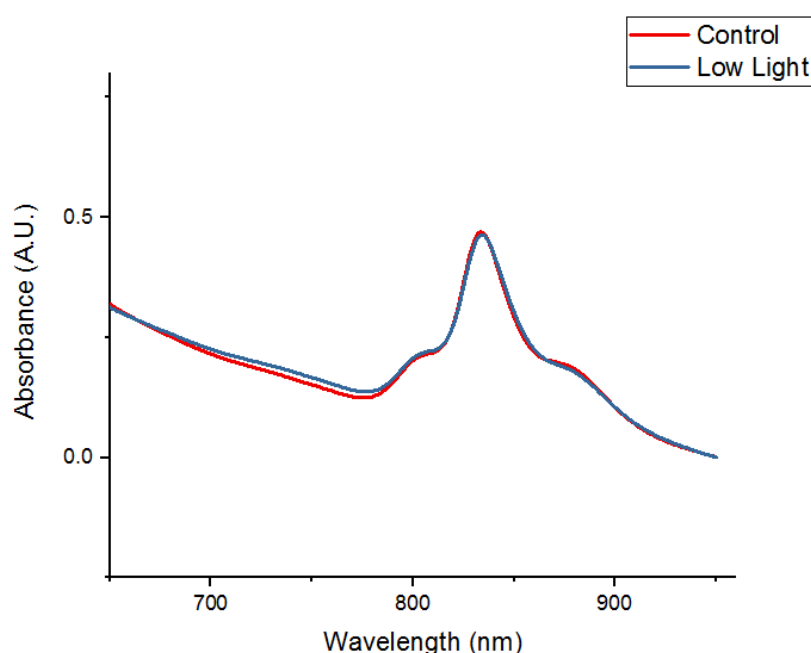


Figure 3-2: Comparison of the Q_y absorption of *Mcr. purpuratum* whole cells grown at their normal light conditions (control) and at low light conditions. The control growth line can be seen in red and the low light growth in blue. There is a perfect overlap, indicating no difference between the absorption spectra

Figure 3-2 focuses and compares the area of *Mcr. purpuratum* absorption spectrum where the Q_y absorption is seen. This is due to previous studies revealing that the majorly seen change is in the Q_y absorption of the LH2 complex. If there was a different LH2 complex being produced under the low light growth conditions for *Mcr. purpuratum*, then a shift would be expected at the 830 nm peak. It can be clearly seen that there is a perfect overlap of the control conditions and low light conditions. The main 830 nm peak of the LH2, the 800 nm shoulder and the 875 nm shoulder for the LH1-RC all remain unchanged.

To confirm this observation in the bacteria culture, the cells were harvested from both the control and the low light conditions. The cells were broken by passage through a French Pressure cell and the photosynthetic membranes were collected from the broken-cell mixture by centrifugation and re-suspended in the Tris-HCl solution at pH 9.0 to an OD_{830} of 50. The absorption spectra were then measured and the results can be seen in Figure 3-3

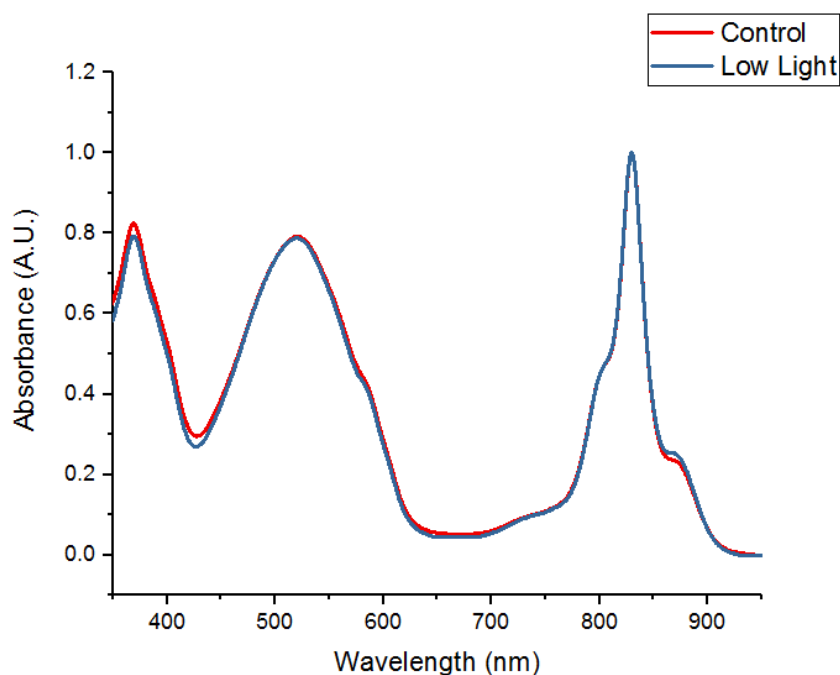


Figure 3-3: Comparison of the spectra of *Mcr. purpuratum* membranes grown at their normal light conditions (control) and at low light conditions. The control growth line can be seen in red and the low light growth in blue. There is a perfect overlap, as seen in the whole cell spectra, indicating no difference between the absorption spectra.

A comparison of the full absorption spectra of *Mcr. purpuratum* membranes revealed no major changes between the normal light conditions and the low light conditions. There does appear to be a small increase in the absorption at the 875 nm shoulder. This indicated that there is an increase in the amount of LH1-RC produced when grown in LL. This is to be expected as the bacteria is compensating for the low light intensity by increasing the amount of LH complexes to harvest the available light. At this stage, there was no need to proceed further with this investigation as the results confidently showed that an alternate LH complex was not produced under low light growth conditions.

3.1.3. Stability of the LH2 Complex in the Presence of Different Detergents

To determine the optimum detergent for solubilization and stability of the LH2 complex, *Mcr. purpuratum* membranes were solubilized separately in different detergents and loaded onto SDGs. DM, LDAO and DDM were used in these detergent trials at concentrations can be viewed in the appendix.

It can be seen in Figure 3-4 that the LH1-RC band is completely missing from the SDG when LDAO was used to solubilize the membrane. The zwitterionic detergent LDAO has the harshest properties of the three detergents tried and, due to this, the LH1-RC complex in this detergent is not stable. This was investigated further by measuring the absorption of the LDAO solubilized membranes (Figure 3-5). This showed the loss of the LH1-RC peak at 875nm, indicating that LDAO was too harsh and, hence, denaturing the LH1-RC during solubilization.

Solubilization was attempted at room temperature and at 4 °C with the same results. In the cases of DDM and DM, the LH1-RC and LH2 bands could both be clearly seen in the SDGs. However, there was a slight overlap of the LH complexes in DDM. A much better separation of the LH1-RC and LH2 complex was achieved with DM compared to DDM. The complexes migrate the same distances in both DDM and DM. A good separation between LH complexes on the SDGs was very important as it reduced the amount of cross contamination between the LH1-RC and the LH2 that was recovered. The two complexes have a different colour as they preferentially bind different carotenoids (Codgell, Southall et al. 2006). The upper orange band contains denatured complexes and free carotenoid.

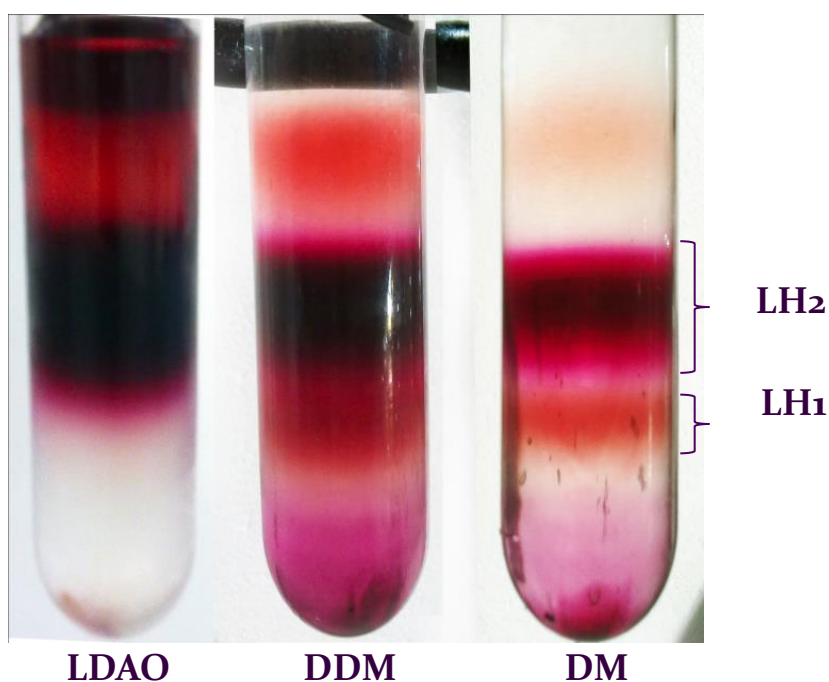


Figure 3-4: Sucrose Gradient trials with *Mcr. purpuratum* membranes solubilized in different detergents. n-Dodecyl β -D-Maltopyranoside (DDM) and n-Decyl- β -D-maltopyranoside (DM) and lauryldimethylamineoxide (LDAO) Separation of the LH complexes can be seen in DM and DDM. The LH1-RC complex is absent in LDAO as it has denatured due to the harsh nature of this detergent.

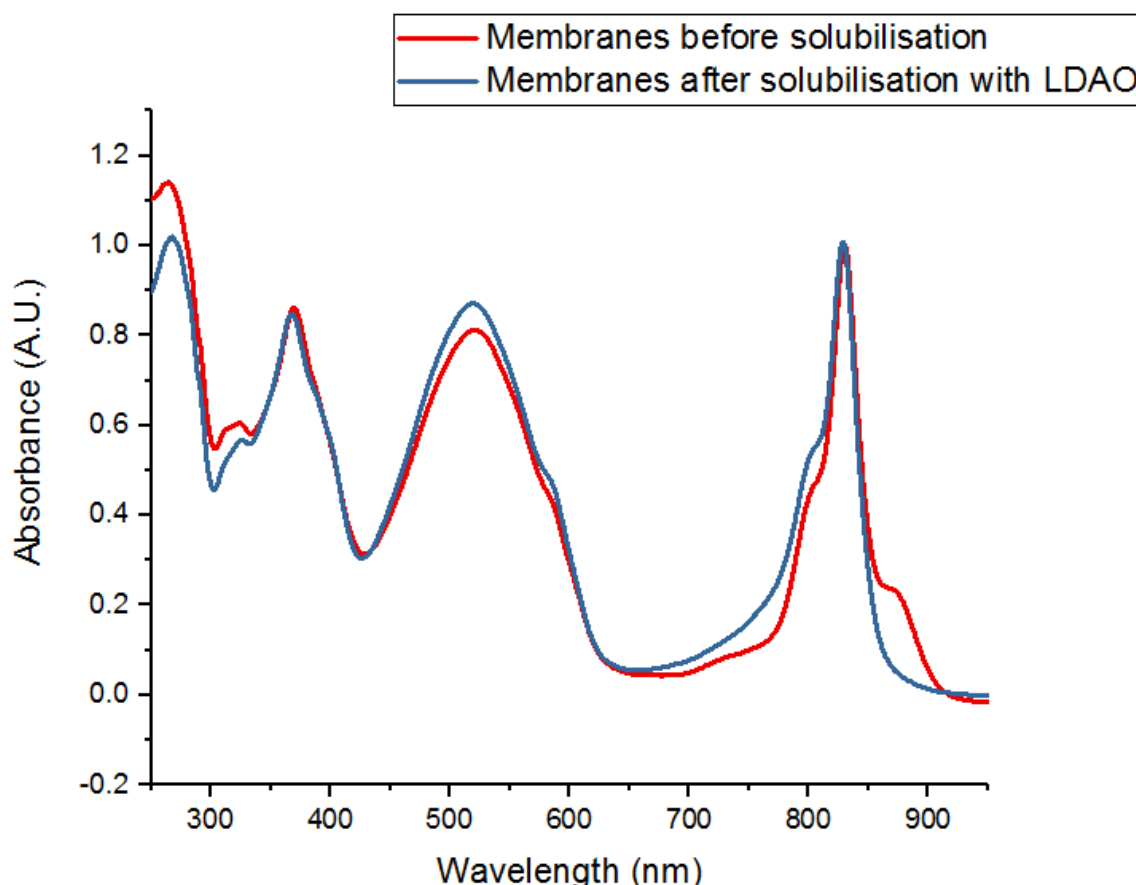


Figure 3-5: Absorption spectrum of *Mcr. purpuratum* before and after solubilization with LDAO. The LH1-RC shoulder at 875 nm can be clearly seen before solubilization. However, after solubilisation with LDAO for 1 hour at room temperature, this 875nm peak is no longer present.

Thermo-stability trials were then carried out using the LH2 protein taken from the above sucrose gradients (Figure 3-4). This involved heating the protein to 50 °C and taking a sample to measure the absorption spectrum every 15 min. The trial on LDAO confirmed that it was too harsh, and rapidly destabilised the LH2 complex over a short period of time, as seen previously (Cogdell, Hawthornthwaite et al. 1990) Heating the complex to 50°C caused the 830 nm peak to degrade completely within 30 mins (Figure 3-6). The loss of the 450-550 nm okenone peak was also observed. The complex is completely degrading as the major protein-protein and protein-pigment interactions, which hold it together are being compromised LDAO is a zwitterionic detergent and is very efficient at disrupting protein-protein bonds. In comparison, the complexes solubilised in DM (Figure 3-8) and DDM (Figure 3-7) showed no sign of denaturation when placed under the same conditions for an hour. The 830 nm peak did not alter throughout the whole time frame. This indicated that the LH2 complex from *Mcr. purpuratum* is much more stable in these detergents in comparison to LDAO. This makes sense as DM and DDM are non-ionic detergents and much milder in comparison to LDAO.

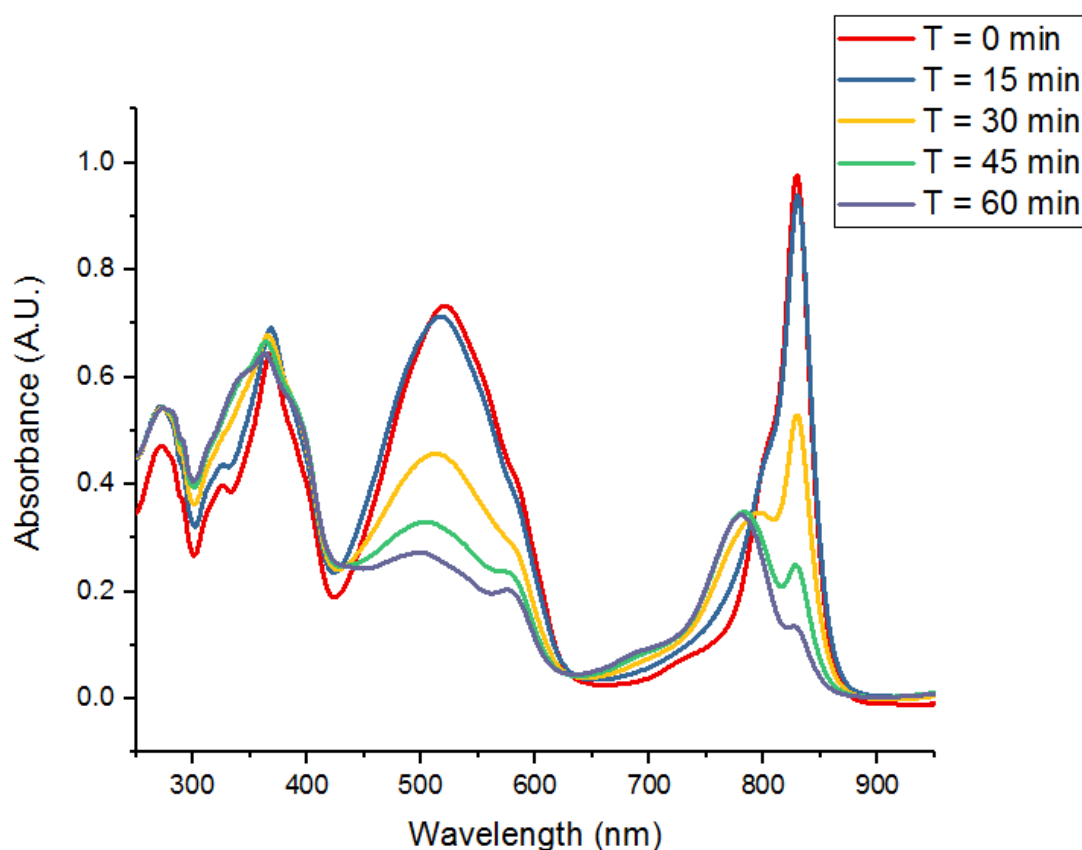


Figure 3-6: Absorption spectra of the LH2 complex from *Mcr. purpuratum* solubilised in LDAO. The spectrum has been recorded every 15 mins whilst the protein was incubated at 50 °C. The deterioration of the LH2 protein can be clearly seen in this case. In LDAO the 830 nm peak is almost completely gone after an hour. It begins to deteriorate at 30 mins. The okenone peak also decreases. This indicated that the complex has completely denatured.

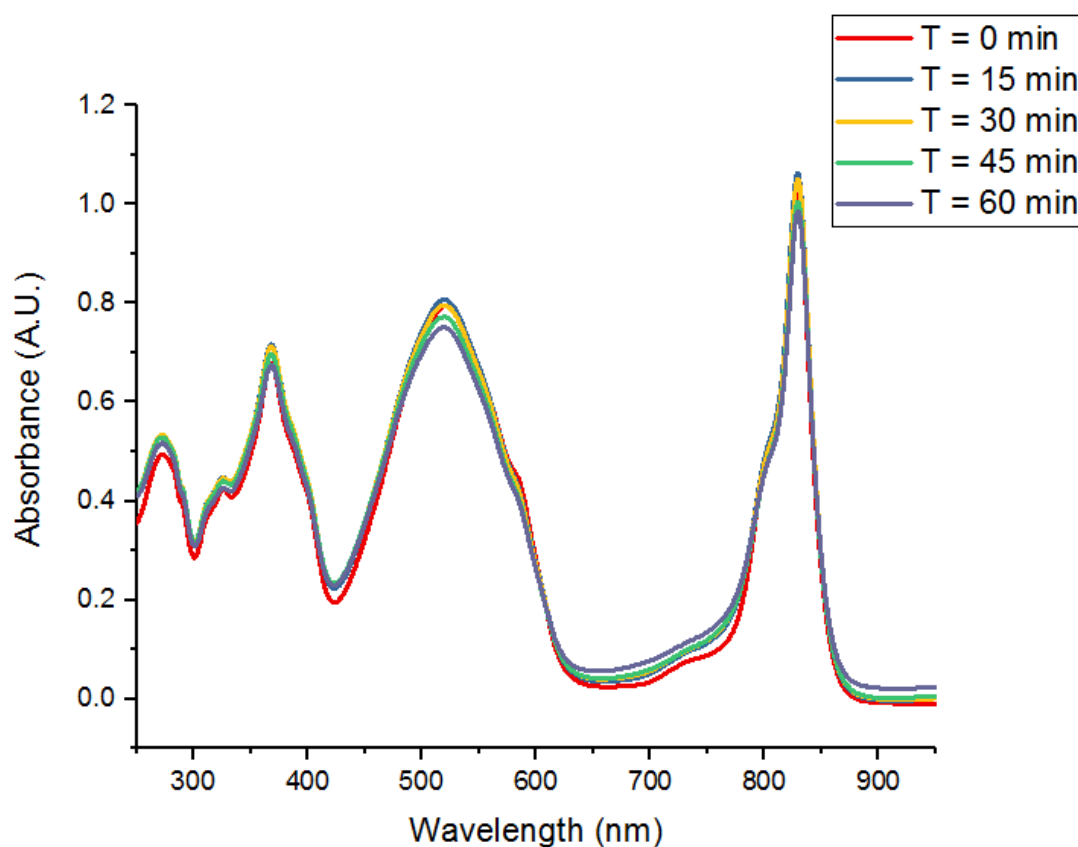


Figure 3-7: Absorption spectra of the LH2 complex from *Mcr. purpuratum* solubilised in DDM. The spectrum has been recorded every 15 mins whilst the protein was incubated at 50 °C. The 830 nm peak of the complex remains intact in DDM, as does the carotenoid, okenone, peak at ~500 nm.

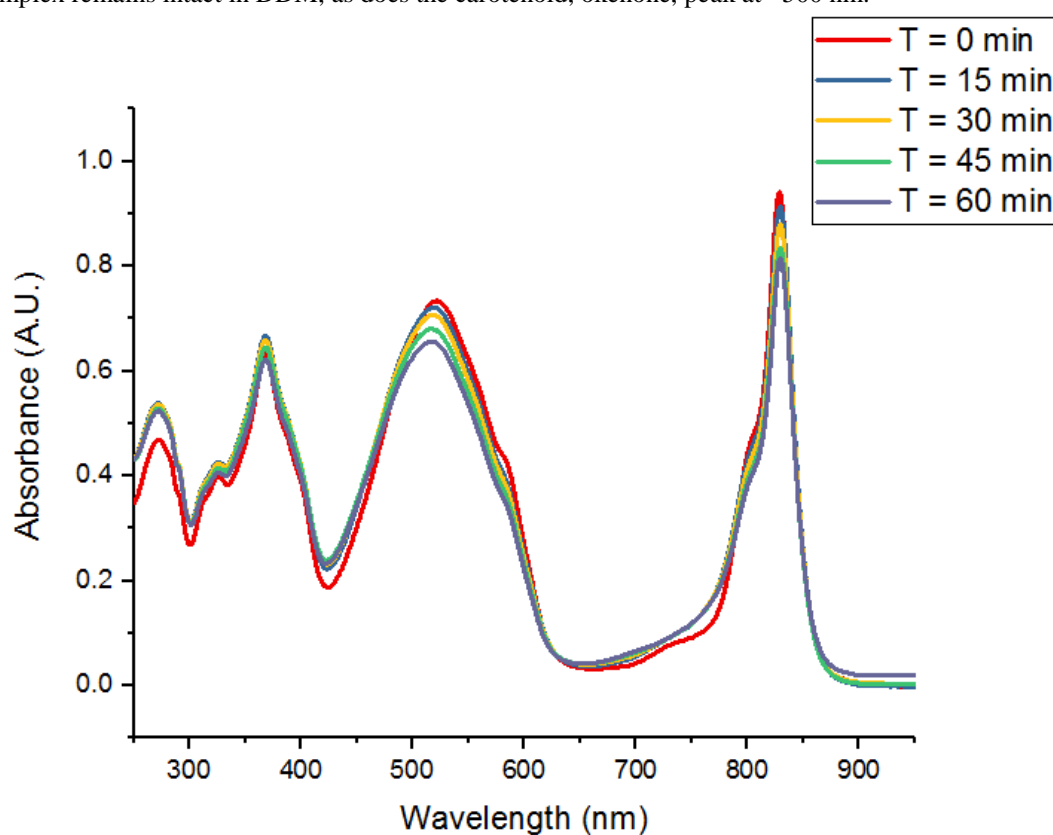


Figure 3-8: Absorption spectra of the LH2 complex from *Mcr. purpuratum* solubilised in DM. The spectrum has been recorded every 15 mins whilst the protein was incubated at 50 °C. The 830 nm peak of the complex remains intact in DM.

The thermos-stability assay for the LDAO solubilized sample suggests that prolonged exposure to LDAO may cause the LH2 complex to denature. Short chain detergents are known to induce a loss of function and protein aggregation and are generally not used in membrane protein crystallisations (Prive 2007, Sonoda, Newstead et al. 2011). Long term stability is important for crystallisation trials of the LH2 complex. The milder detergents, DM and DDM have very different physicochemical properties to LDAO and these assays suggest that these detergents help long term protein stability. Studies have shown that they both have high success rates with crystallising α -helical membrane proteins (Newstead, Ferrandon et al. 2008). DDM has a longer alkyl chain length and, therefore, a larger micelle. This means a smaller region of the protein is exposed to make crystal contacts. As this would make crystallisation less favourable it was decided to continue the LH2 purification in DM.

3.1.4. Optimised Purification of the LH2 Complex

In many cases, choosing to completely solubilize the membrane in a stronger, harsher detergent is better because this ensures that the target protein is fully extracted from the membrane (Joanne Lemieux, Reithmeier et al. 2002, Guan, Smirnova et al. 2006, Sonoda, Newstead et al. 2011). LDAO has been used for the successful crystallisation of bacterial reaction centres and LH complexes (Michel 1982, Welte, Wacker et al. 1985, Wacker, Gad'on et al. 1986). However, several membrane protein complexes are quickly denatured by LDAO (Timmins, Leonhard et al. 1988), including the LH1-RC of *Mcr. purpuratum*. A detergent that is efficient for the solubilisation of a membrane protein may not ensure the functionality and stability. This detergent may not be suitable for crystallisation due to long term stability. It can, therefore, be exchanged during or after purification by another detergent, which is more suitable for the long-term stability of the protein and crystallisation. Therefore, it was decided to solubilise the *Mcr. purpuratum* membranes in LDAO and then immediately exchange them into DM. The integrity of the purified LH2 complex was checked spectrophotometrically at the beginning of the purification process and after every purification step by measuring the absorption spectrum from 250 to 950 nm with a spectrophotometer (Shimadzu UV-1700). No denaturation was observed. The LDAO solubilized membranes were subjected to SDG to fully separate the LH2 and the LH1-RC, but as previously shown the LH1-RC was absent after solubilisation in LDAO (Figure 3-4 and 3-5). The LH2 fraction was then further purified and detergent exchanged by anion-exchange chromatography (AEX) using diethylaminoethyl cellulose (DE52, Whatman). The bound protein was washed with 20 mM Tris-HCl pH 9.0 containing 0.15% DM to exchange the LDAO detergent and then eluted by adding increasing concentrations of NaCl also containing 0.15% DM. The LH2 complex from *Mcr. purpuratum* binds with a relatively low affinity to the resin and is eluted with 50 mM NaCl in the purification buffer. The OR of the LH2 fractions collected at this stage was ~1.8.

An additional purification step was achieved by size exclusion chromatography (SEC) using a Superdex S-200 column (XK 16/100, GE Healthcare) that had been equilibrated overnight

with 20 mM Tris–HCl pH 9.0 plus 0.15% DM. The chromatogram of the LH2 complex from *Mcr. purpuratum* after SEC showed an almost symmetrical peak, which suggests that they are uniform within the detergent-protein complex (Figure 3-9). If the peak had shown smaller, broad peaks before or after the main elution peak it would indicate the protein was unstable and undergoing denaturation.

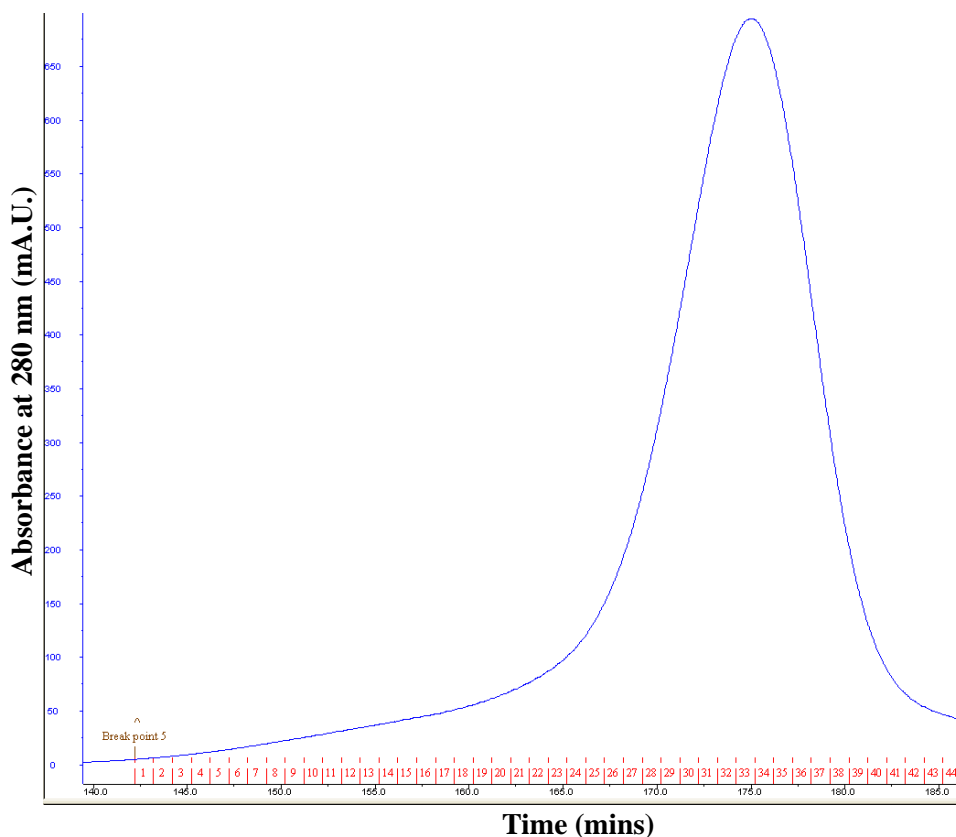


Figure 3-9: Chromatogram from the SEC purification of the LH2 complex from *Mcr. purpuratum*. A single monodisperse peak can clearly be seen eluting over time. The fraction numbers can be seen in red. These collected 0.5 ml of the eluted protein each. In this example the fractions from 27-39 were tested for $OR_{830:280} > 2.2$.

During purification of the LH2 complex the absorbance at 280 nm, where aromatic residues of protein absorb, decreases as protein contaminants are reduced. This allows an optical ratio (OR) of the LH2 peak (830 nm) to protein (280 nm) content to increase, which can be used as a purity guide. LH2 complexes with an $OR_{830:280\text{ nm}} > 2.2$ were pooled and concentrated to either OD₈₃₀ 50, 100 or 150 using Vivaspin2 Centricons with a 50 kDa molecular weight cut-off. The absorption spectra after each purification step, from membranes all the way through to after SEC, is shown in Figure 3-10. This is a very good representation of the decrease observed in the 280 nm peak throughout the purification process. The steady-state absorption spectrum of fully purified *Mcr. purpuratum* LH2 complex can be seen in Figure 3-11. The OR of this purified sample is ~2.3.

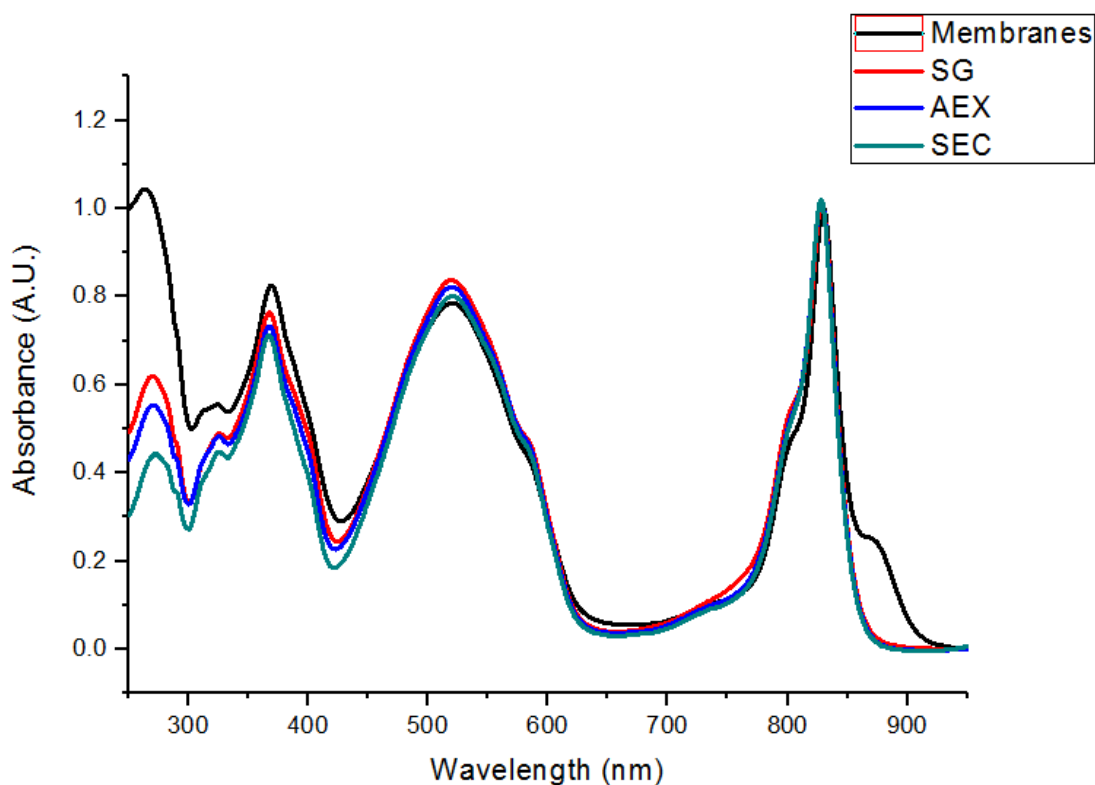


Figure 3-10: Absorption spectra recorded throughout the purification of the LH2 complex. The starting material is membranes, seen as the black line with the LH1-RC shoulder still present at 875 nm. The red line shows the LH2 complex after the SDG step. The LH1-RC shoulder is gone and there has been a huge decrease in the 280 nm, from ~1.0 down to ~0.6. The next purification step was the AEX, seen as a blue line, with another decrease in the 280 nm peak to ~0.5. Finally, the teal line shows the absorption after SEC and a decrease of the 280 nm peak to ~0.4.

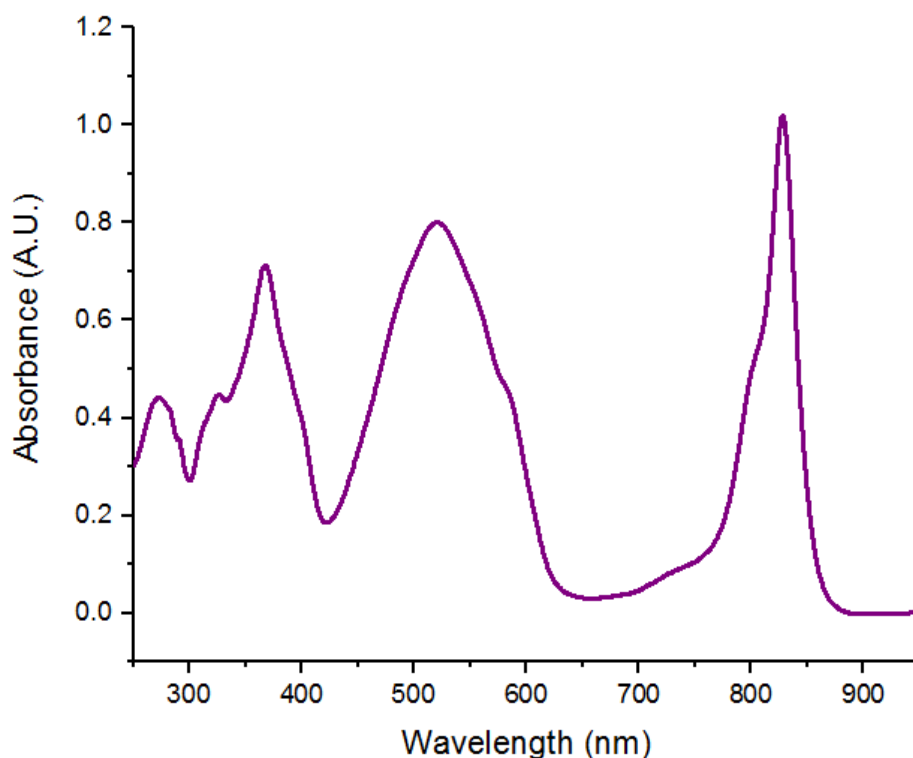


Figure 3-11: Absorption spectrum of the fully purified LH2 complex from *Mcr. purpuratum* at room temperature. This measurement was taken after the fractions from the SEC had been pooled together. It can be clearly seen that the 830 nm equals 1 whilst the 280 nm peak equals 0.4. This results in an OR of ~2.3.

3.1.5. SDS-PAGE of Membranes, Crude LH2 Extracts and Purified LH2 Complex from *Mcr. purpuratum*.

Purified LH2 complexes were also analysed using SDS-polyacrylamide gel electrophoresis (Figure 3-12). Samples were taken at various stages of the LH2 purification protocol (membranes, after SG, after AEX and after SEC (or gel filtration/ GF) and at different concentrations were run on a denaturing SDS-PAGE gel. From this SDS-PAGE, it can be seen at each purification stage the number of contaminating bands decrease. From the lanes loaded with GF (SEC) sample, only the α and β polypeptide components of the LH2 complex remain. These lie between 3.5KDa and 10KDa, which is to be expected from previous LH apoprotein data. In the GF2 and GF3 lanes, there are multiple protein bands present for the α and β polypeptides. This indicates that there may be more than one of each type of polypeptide present in this LH2 complex. There seems to be at least three α polypeptides and three β polypeptides. Previous work (Cheryl A Kerfeld, Yeates, and Thornber 1994) revealed 6 total bands seen, so the results seen here are consistent with that work. Further work was done to identify these in Chapter 4.

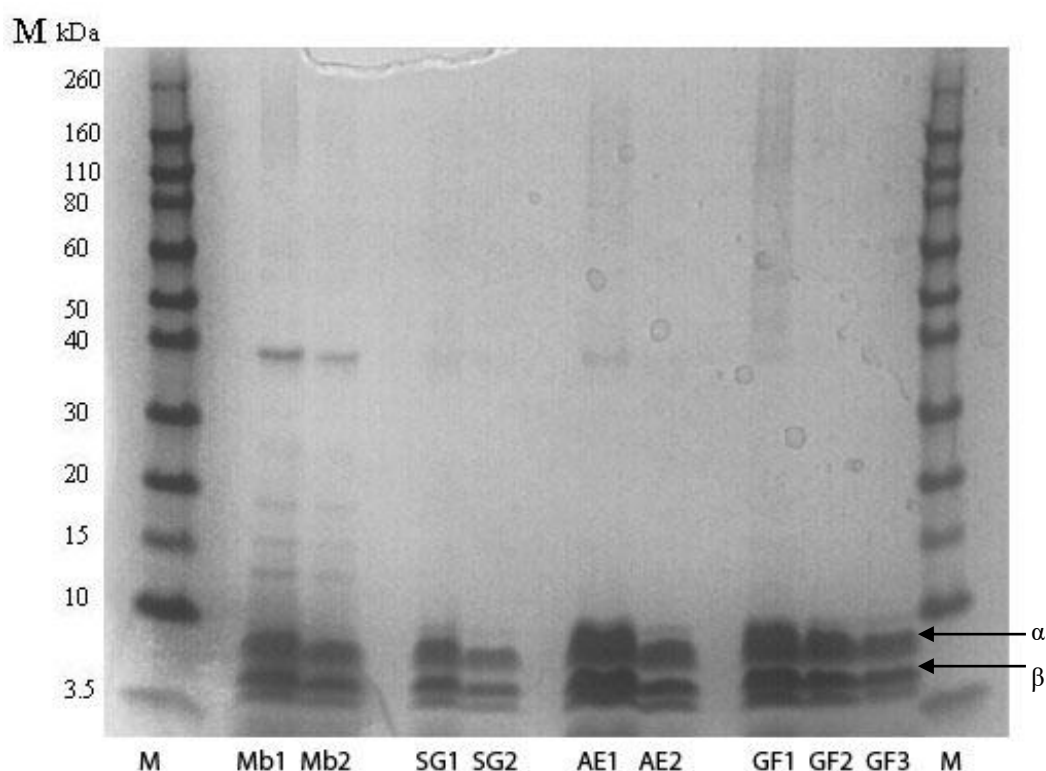


Figure 3-12: SDS-PAGE gel of samples taken at various points along the LH2 purification protocol. M=Marker, Mb1=*Chr. purpuratum* membranes OD 10 and Mb2=OD 5, SG1=LH2 taken from the Sucrose gradient at OD 10 and SG2=OD5, AE1=After Anion Exchange OD 10 and AE2=OD5 and finally GF=after the Gel filtration step where the protein is at its purest GF1=OD 10 GF2=OD 5 and GF3=OD 2. The α and β polypeptides can be seen between molecular weight marker 3.5 and 10.

3.2. Electron Micrograph Images of *Mcr. purpuratum* Whole Cells

To obtain information about the internal organisation of *Mcr. purpuratum*, culture sections of whole cells were imaged under an electron microscope (EM). These images were obtained by Dr Pu Qian, University of Sheffield.

Once the *Mcr. purpuratum* cells had been sectioned, they were viewed under an electron microscope and photographed. Figure 3-13 shows that clear, clean sections of the *Mcr. purpuratum* were obtained.

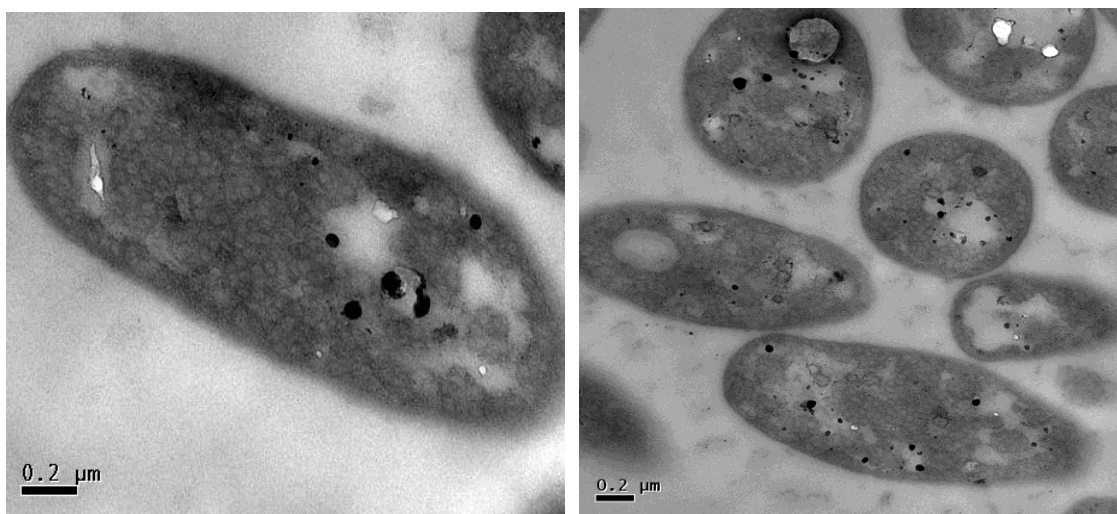


Figure 3-13: EM image of a thin section of *Mcr. purpuratum* whole cells. The average diameter of the spherical membrane is 37nm.

In the thin whole cell sections of *Mcr. purpuratum* presented in Figure 3-13 the ICM is present as vesicles. These are very tiny vesicles in comparison to those seen in other photosynthetic bacteria, approximately 37 nm in diameter. Vesicular ICM are present in many species of purple bacteria, including *Rba. sphaeroides* and *Rsp. rubrum*, and the size of these vesicles in *Rba. sphaeroides* is 200 nm. The large "white" structures are empty sulphur granules. They are empty because the process used to produce the thin section dissolves away all of the sulphur in the granule. The structure and arrangement of the ICM can vary. There are three types of ICMs present in purple bacteria called tubular, vesicular and lamella. Before the development of 16S tRNA sequencing, this phenotype was often used as an identifying feature for classifying a bacterium within a particular genus (Stolz 1990).

3.3. Lipid Reconstitution of the LH2 Complex

If LH complexes are reconstituted into flat lipid membranes, then Atomic Force Microscopy (AFM) could be utilised to view the ring size and structure. This was done to obtain two-dimensional (2-D) crystals for cryo-EM. This technique has been successful in obtaining

details on the organisation of the individual complexes within the functioning photosynthetic membrane (Miller 1982, Stark, Kuhlbrandt et al. 1984, Walz and Ghosh 1997, Siebert, Qian et al. 2004, Gonçalves, Busselez et al. 2005, Qian, Neil Hunter et al. 2005). This work was done in collaboration with Dr Pu Qian at the University of Sheffield. Before the purified complex was reconstituted into lipid, it was negatively stained and images were taken with an Electron microscope (EM). This was to ensure that the sample was monodisperse, had not denatured and contained no contaminants. The image in Figure 3-14 shows tiny circular structures, which are the LH2 complexes from *Mcr. purpuratum*. They are monodispersed, with no aggregates.

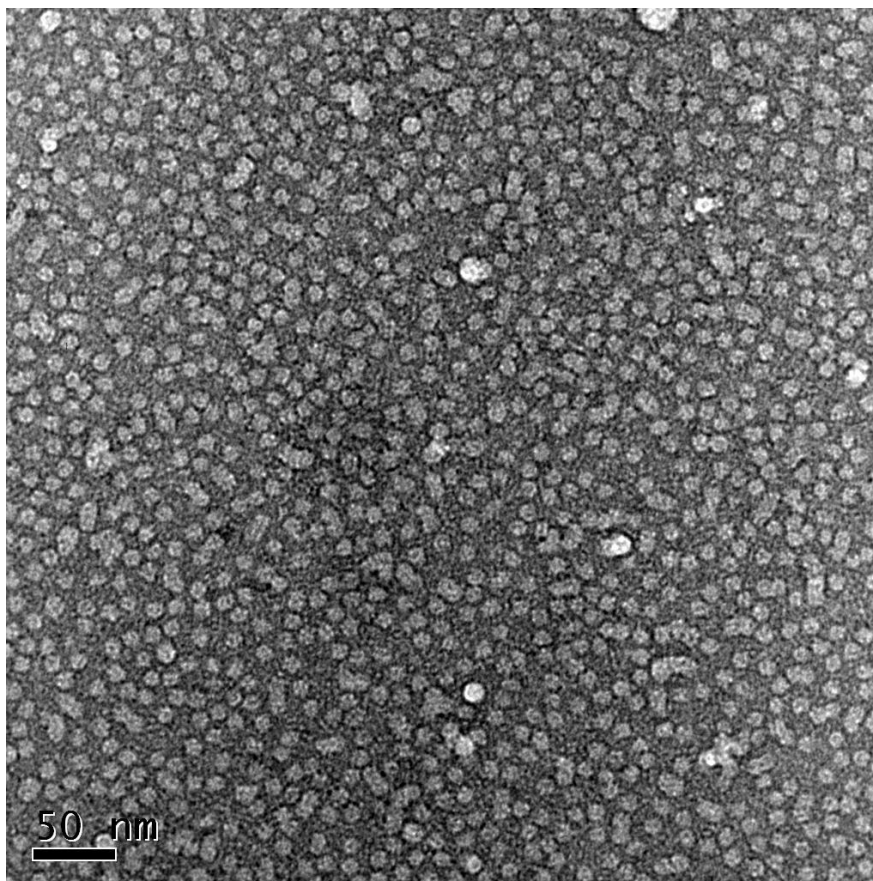


Figure 3-14 -Negative stained EM image of fully purified, monodisperse LH2. The approximate diameter of an LH2, according to this image, is 10 nm.

The LH2 protein was then reconstituted into four separate lipids, each with a different head group, at different [Lipid]/[Protein] ratios. The solution was dialysed to remove the detergent and therefore allow the LH2 complex to be reconstituted into the lipid bilayer. Interestingly, the LH2 complex did not form 2-D crystals sheets but instead formed tight nanoballs, or proteoliposomes, for all the lipids tested and every ratio. The images collected can be seen in Figure 3-16. This is a very unique and fascinating result as it reveals a trait about this LH2 that is not present in any other LH2 so far studied (Stamouli, Kafi et al. , Savage, Cyrklaff et al. 1996, Gonçalves, Busselez et al. 2005). As shown previously in this chapter, the natural ICM of *Mcr purpuratum* is vesicular. It is possible that this LH2 complex induces curvature of the membrane. The proteoliposome diameter is equal to the size of the ICM vesicles. As mentioned in previously, *Rba. sphaeroides* also has a

vesicular ICM. The vesicular structures need to be flattened for AFM analysis (Bahatyrova, Frese et al. 2004, Scheuring and Sturgis 2009). An explanation for this strange behaviour of the LH2 complex from *Mcr. purpuratum* could be due to its shape. The complex may have a smaller diameter towards the C-terminal side compared to the N-terminal side. The C-terminal and N-terminal side are found on the cytoplasmic and periplasmic side of the membrane, respectively. This would cause the complexes to align at an angle to each other, which would result in a curve. A graphic to help illustrate this point can be seen in Figure 3-15. This result is not fully understood at this point and is still under investigation.

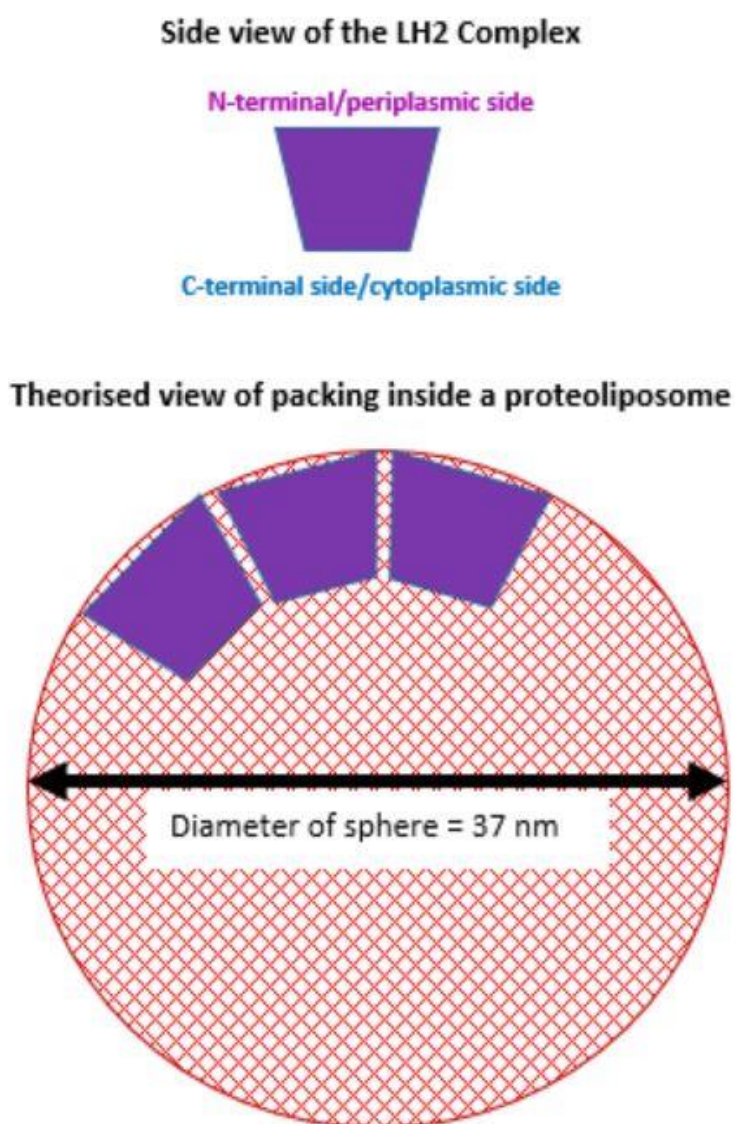


Figure 3-15: Theorised view of the formation of the proteoliposomes from the *Mcr. purpuratum* LH2 complex. A graphic showing the side view of the LH2 complex can be seen in purple. The C-terminal /cytoplasmic side is thought to be narrower than the N-terminal /periplasmic side. This could be a reason for the molecules form these proteoliposomes. Red sphere depicts a proteoliposome sphere and the diameter was taken from the diameter recorded in the EM images, which can be seen in Figure 3-16

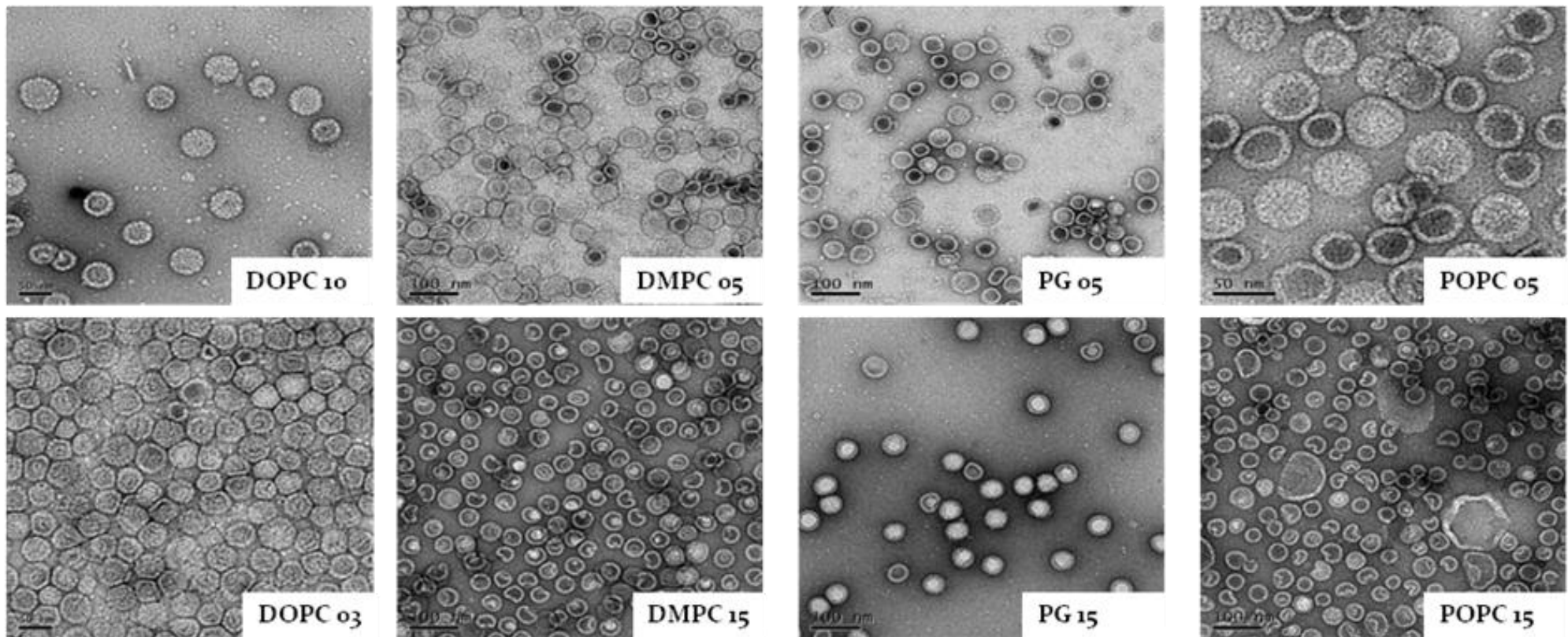


Figure 3-16: Electron micrograph (EM) images of *Mcr. purpuratum* LH2 reconstituted into different lipids. (1,2-Dioleoyl-*sn*-glycero-3-phosphocholine (DOPC), 1,2-Dihexanoyl-*sn*-Glycero-3-Phosphocholine (DMPC) L- α -phosphatidylglycerol (PG), 1-palmitoyl-2-oleoyl-*sn*-glycero-3-phosphocholine (POPC)). The numbers following the detergent name refer to the lipid-protein ration that was used. The scale for DMPC 05, DMPC 15, PG 05, PG 15 and POPC is 100 nm. The scale for DOPC 10, DOPC 03 and POPC 05 is 50 nm. The proteoliposomes formed for every lipid that was used in this experiment. The diameter of the proteoliposomes varies slightly but it is approximately equal to the diameter of the vesicular ICM for the thin whole cell section of *Mcr. purpuratum* – ~37 nm. The proteoliposomes are uniform in all of the lipids, except POPC. They are larger, ~50 nm and have a more irregular, non-circular shape.

3.4. Crystallisation of the LH2 Complex from *Mcr. purpuratum*

Purified LH2 from *Mcr. purpuratum* was used for crystallisation trials to find a condition that would yield high resolution, diffracting crystals. These would lead to the determination of a high-resolution structure of this LH2 complex. The initial screening had to take place to locate promising conditions that could be optimised. 96-well plates were used for this stage because they use a small volume and lots of conditions can be quickly screened. Crystallisation was performed by the vapour-diffusion method in HT 96-well plates using the Cartesian HoneyBee 8+1 nanovolume robot. The vapour diffusion technique is the most commonly used method for initial crystal screening (Kimber, Vallee et al. 2003, Page and Stevens 2004). Sitting drops were prepared by dispensing 0.5 µl of the reservoir solution into the well, followed by 0.5 µl of purified protein in 20 mM Tris-HCl pH 9.0 with 0.15% DM, and equilibrated against 50 µl reservoir solution at 20 °C. The plates were sealed, stored in a Rhombix Plate Hotel and periodically scanned using a Rhombix Imager (Thermo Fisher Scientific). The initial sparse-matrix screens chosen were MemGold and MemStart/MemSys crystallisation screens (Molecular Dimensions). MemStart/MemSys is a good starting point for screening and optimising crystallisation conditions for transmembrane proteins (Iwata 2003). MemGold was designed for use with α -helical membrane proteins (Newstead, Ferrandon et al. 2008).

This initial screen of conditions produced several hits from the sparse matrix screens. Many of the conditions resulted in phase separation and amorphous precipitation. Some conditions also denatured the complex, which was easy to identify due to the change in the bright purple colour to a muddy brown. Several crystals were seen that were not of favourable morphology or size. Most of the crystals were small, very flat, diamond shaped and very delicate or thin needles.

Deep purple, square-bipyramidal crystals appeared after six weeks from condition E11 of the MemGold screen. This condition, consists of 33% (v/v) PEG 300, 0.1 M sodium phosphate pH 7.0 and 0.1 M sodium chloride. The crystals grew to their final size (approximately 200 µm) within the next two weeks (Figure 3-17).

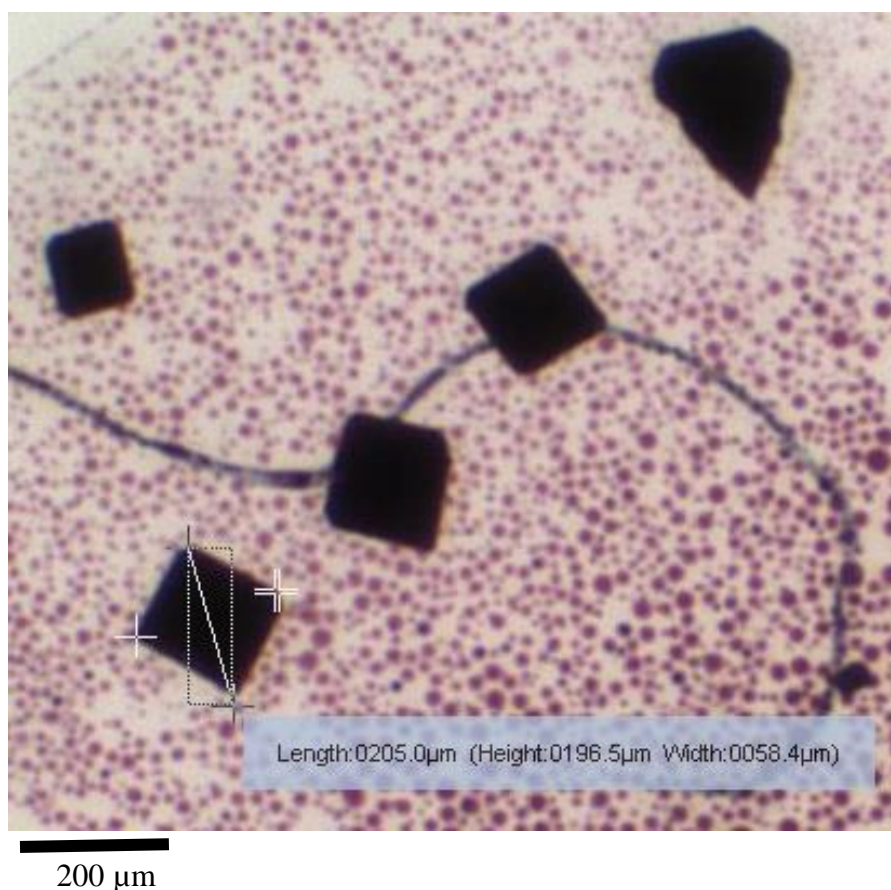


Figure 3-17: Crystals of the LH2 complex from *Mcr. purpuratum* from initial 96-well screens. The complex was crystallised in the buffer 20mM Tris-HCl pH 9.0 with 0.15% DM. The conditions in the reservoir are; 0.1M Sodium phosphate at pH 7.0, 0.1M Sodium chloride and 33% PEG 300. The droplet is a 50:50 mix of the protein solution with the reservoir solution. The crystals were grown at 20°C in the Plate Hotel. The photograph was taken by an automated imaging device, which served as part of the Hotel. Some phase separation can also be seen in the well

Optimisations around the initial conditions were performed using 24-well plates by varying the reservoir conditions. This included the salt concentrations, the pH of the buffer and the percentage of PEG 300. When setting up the 24-well crystal plates, to begin with, a 50:50 mix of the protein drop and reservoir solution was used. This was then changed later in the optimisation process so that the droplet solution was always the same, meaning that each condition had the same starting conditions. This was always the condition, which gave the original crystal hit. So, when optimising the conditions in Figure 3-17, the droplet was always a 50:50 mix of LH2 protein in 20mM Tris-HCl pH 9.0:0.1M Sodium phosphate at pH 7.0, 0.1M Sodium chloride and 33% PEG 300. The surrounding reservoir solution was altered by changing only one condition gradually at any given time. An example of this can be seen in Figure 3-18. All the optimisations were duplicated with LH2 OD_{830 nm} of 100 and OD_{830 nm} of 50.

Many of the optimisation conditions resulted in phase separation and amorphous precipitation. Some also denatured the complex, which was easy to identify due to the change in the bright purple colour to a muddy brown. The series of crystals seen were not of favourable morphology or size, a selection of images can be viewed in Figure 3-19. Most of the crystals were small, very flat,

diamond shaped and very delicate. Smaller thinner needle crystals were also common as well as larger variations.

Increasing PEG 300%					
Increasing [NaCl]	31% PEG 300	32% PEG 300	33% PEG 300	34% PEG 300	35% PEG 300
	0.05 M NaCl	0.05M NaCl	0.05M NaCl	0.05M NaCl	0.05M NaCl
	31% PEG 300	32% PEG 300	33% PEG 300	34% PEG 300	35% PEG 300
	0.075 M NaCl	0.075 M NaCl	0.075 M NaCl	0.075 M NaCl	0.075 M NaCl
	31% PEG 300	32% PEG 300	33% PEG 300	34% PEG 300	35% PEG 300
	0.1 M NaCl	0.1 M NaCl	0.1 M NaCl	0.1 M NaCl	0.1 M NaCl
	31% PEG 300	32% PEG 300	33% PEG 300	34% PEG 300	35% PEG 300
	0.125 M NaCl	0.125 M NaCl	0.125 M NaCl	0.125 M NaCl	0.125 M NaCl

Figure 3-18: Examples of optimising a crystal hit in a 24 well plate (6x4).

Crystal condition: 0.1M Sodium Phosphate at pH 7.0, 0.1 M NaCl and 33 % PEG 300. The buffer 0.1M Sodium Phosphate at pH 7.0 is not changed at all and is the same in every well. The purple square marks the original crystal hit condition. Sitting drops were prepared by mixing 10 μ l of the purified protein at OD_{830 nm} of 100 with 10 μ l of the reservoir solution from the highlighted purple well. This droplet was equilibrated against the 1 ml reservoir solution. This exact optimisation was duplicated for protein at OD_{830 nm} of 50.

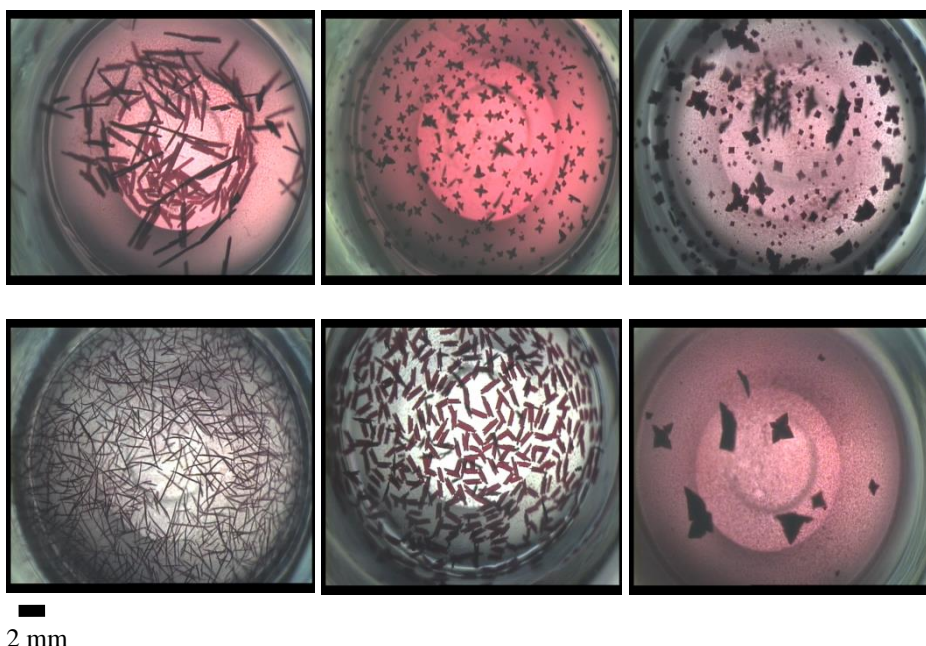


Figure 3-19: A collection of images of crystals obtained from the initial optimisation 24 well screens.

These were optimisation around the crystal condition: 0.1M Sodium Phosphate at pH 7.0, 0.1 M NaCl and 33 % PEG 300. The crystals are all very thin and flat, with not much three-dimensional shape. The solution surrounding the crystals is still very pigmented indicating there is still LH2 protein present.

During these optimisation screens, it became apparent that crystals were not forming in the original initial crystal hit conditions at all. This suggests batch-to-batch differences in the purified proteins quality or the possibility of other minor changes interfering with stopping crystallisation of the protein. This could be small temperature fluctuations or humidity problems when the screens

were being set up. One of the most likely explanations would be the increase in volumes used for the setup and the solutions used. The 96-well screens were premade solutions used at very tiny volumes. The 24-well screens use correspondingly larger volumes of both crystallisation solutions and the LH2 complex. Upscaling from smaller to larger volumes has an impact on the surface-to-volume ratio and further optimisation is often required to achieve similar results to those obtained in the 96 well screens. Where possible, the solutions used were purchased from Molecular Dimensions, the company that manufactured the sparse matrix screens. All precautions were taken to maintain a pure solution, such as filtering, but there still appears to be an unknown factor regarding the preparation of the solutions.

To ensure that the original crystal hits were reproducible additional MemGold screens were set up but only using the larger 24 well plates. The trays were kept at a constant temperature of 16 °C. It was found that crystals did not form in the conditions that produced the initial promising hit. However, three more promising crystal hits were seen after 2 weeks of growth (Figure 3-20).

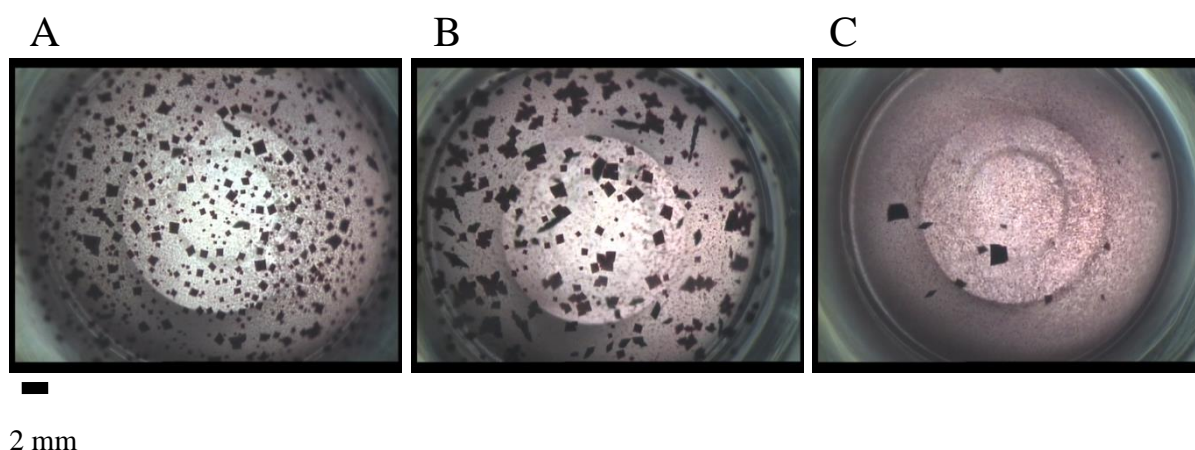


Figure 3-20: Promising crystal hits seen in the MemGold 24-well screen. Crystals are nice regular shapes with sharp edges in all cases. It can also be seen that most of the protein has been used since the surrounding solution is only slightly purple tinted. Crystals in condition C appear the most promising in shape and size, even with traces of some precipitation in the well. The precipitation is of non-denatured protein, which is a good sign that the conditions are not harmful to the protein. Since the protein has remained in its native conformation this precipitation can be stopped by decreasing the protein and/or precipitant concentrations.

A	B	C
0.1M Tris	0.1M MES	0.1M Na HEPES
pH 8.5	pH 6.5	pH 7.5
0.1M Sodium Chloride	0.1M Sodium Chloride	0.1M Magnesium Chloride
0.1M Magnesium Chloride	0.1M Magnesium Chloride	30% PEG 400
33% PEG 400	30% PEG 400	

These conditions are similar, all using PEG 400 as the precipitant and all contain the salt MgCl_2 . All the buffers have a different pH, indicating that this is not an important factor in the crystallisation of this protein. The first optimisation of these conditions occurred by varying the concentration of PEG 400 present in the reservoir solution. Photos of the results can be seen in Figure 3-21. Unfortunately, both the MES and NaHEPES based conditions did not produce crystals

with improved size or quality. The crystals were 2-dimensional and clustered together, similar to those seen in the initial 96-well screen conditions. However, the Tris based condition looked very promising. Crystals were seen in 5 out of the 6 wells conditions and were all cubic shaped with nice sharp, defined edges. They were also much larger, the crystals seen in image 3 of the Tris row in Figure 3-21 are approximately double the size of those seen in the initial hit. This indicated that the optimisation of the condition had improved on the original.

Several more optimisations of these three conditions were attempted. These include varying the salt concentration, changing the buffer pH and adding additional salt to the buffer and using different concentrations of protein at OD_{830 nm} 100, 50 and also 80.

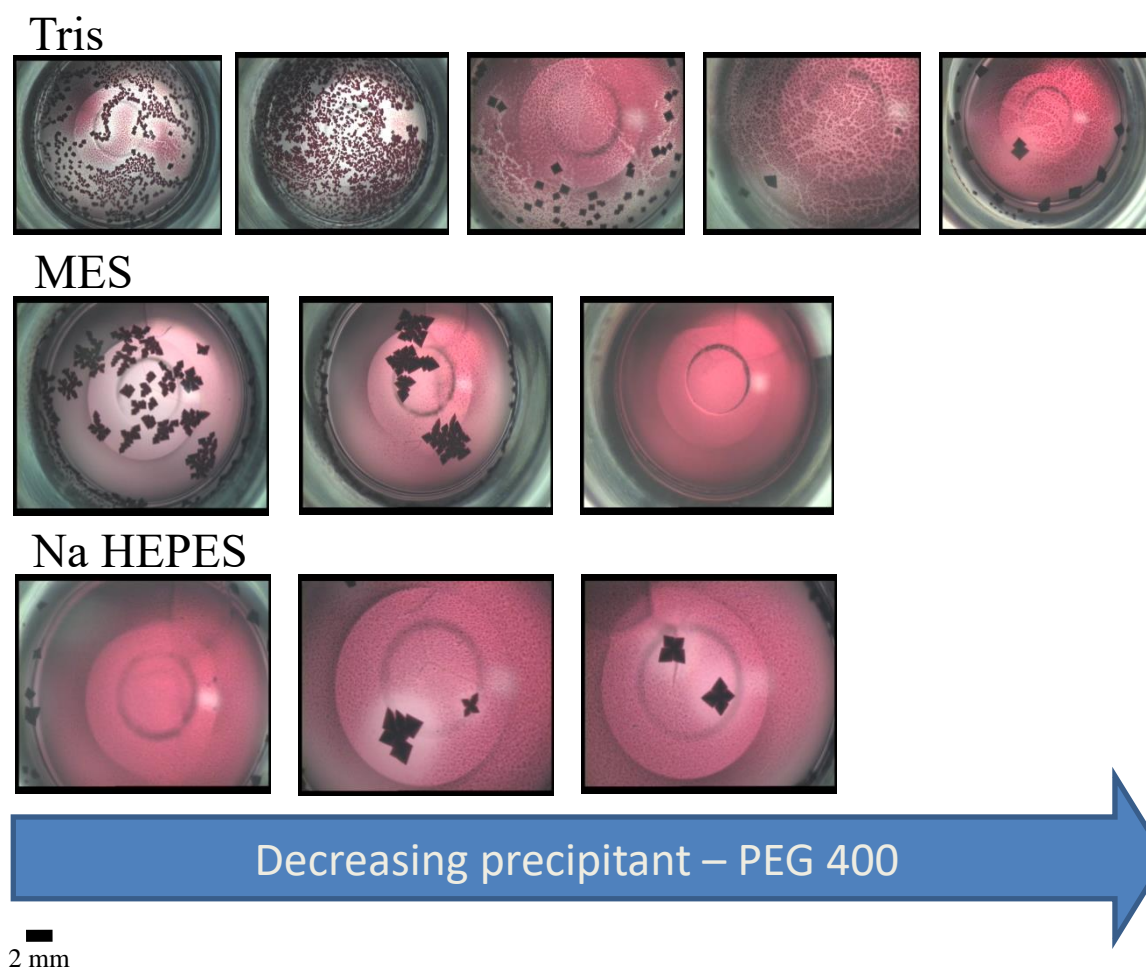


Figure 3-21: Optimisation of the crystal hits seen in the MemGold 24-well screen (Figure 3-20). The images show the wells that produced crystals in relation to the change in the concentration of the precipitant, PEG 400. Tris = condition A in Figure 3-20 and all droplets were mixed 50:50 with this condition and the protein in buffer solution. At the highest concentration of PEG 400, the crystals formed are very tiny. As the concentration of PEG 400 decreased the crystals increased in size, but precipitation is also observed in the well. In the lowest concentration of PEG 400, the precipitation has decreased and large sharp edged crystals are seen. MES = condition B in Figure 3-20 and all droplets were mixed 50:50 with this condition and the protein in buffer solution. It can be seen at the lowest concentration of PEG 400 that no crystals formed in this condition. The conditions at higher PEG 400 concentrations formed irregular, stacked, flat crystals. Na HEPES = condition C Figure 3-20 and all droplets were mixed 50:50 with this condition and the protein in buffer solution. The crystals seen here are similar to those seen in the MES conditions, they are flat and irregular shaped. In the highest concentration of PEG 400 they crystals look more ordered, but they have only formed along the outside of the well and are small. All other conditions were kept the same as the initial

condition hits for their respective buffer. The optimisations were done at OD₈₃₀ 100, 50 and 80. These results are from the OD₈₃₀ 80.

Seeding trials were attempted using the Tris-HCl pH 8.5 condition (Figure 3-20A). Small crystals were picked and placed in 100 µl of the new reservoir solution; 0.1 M Tris-HCl pH 8.5, 0.1 M Sodium chloride, 0.1 M Magnesium chloride and 30 % PEG 400. This was homogenised by vortexing. This was the seed stock and from it, six 1:3 serial dilutions were made. Once the crystal trays were set up 1 µl of this seed stock was added to 9 µl of the reservoir and 10 µl of LH2 protein at OD_{830 nm} 80. Four trays were made in total varying PEG 400 concentration downwards, seed stock dilution across and buffer NaCl concentration. An Additive Screen (Hampton) was also attempted using the same conditions (Figure 3-20A). Neither of these optimisation strategies significantly improved the crystal quality and mostly led to denaturation of the LH2 protein.

At this stage in the project, time constraints became a factor and crystallisation trials had to be halted. Over the course of this project over 5000 different crystallisation conditions were set up. It took a full week of laboratory work to get from *Mcr. purpuratum* cell culture to purified LH2 complex. The yield from a normal prep of 50 mls of OD₈₃₀ 50 membranes produced ~1 ml of OD₈₃₀ 100 LH2 complex at OR of >2.2. This was enough to set up four 24 well optimisation trays. After all the different trials and optimisations - no crystal hits were observed that were as promising as the initial condition E11 (See appendices) of the MemGold screen (Figure 3-17). This consisted of 33%, PEG 300, 0.1 M sodium phosphate pH 7.0, 0.1 M sodium chloride. These crystals were tested for diffraction.

3.5. X-ray data collection and processing

Crystals of approximately 200 × 200 × 100 µm in size were scooped up from the droplet using LithoLoops (Molecular Dimensions). They were then cryo-cooled for protection in a nitrogen gas stream at 100 °K. This was done directly due to the high content of PEG 400 in the crystal condition. Figure 3-22 shows the crystal inside the loop.

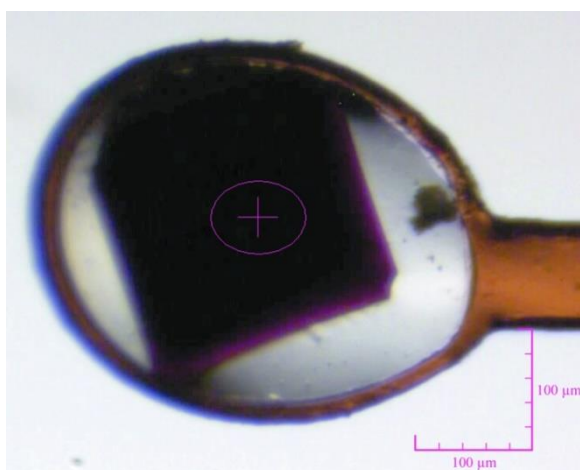


Figure 3-22: Crystal of the *Mcr. purpuratum* LH2 complex shown inside the LithoLoop (Molecular Dimensions). This is the crystal that was used for data collection.

X-ray data were collected from a single crystal at a temperature of 100 °K on the I02 beamline at the Diamond Light Source (DLS) equipped with an ADSC Quantum 315r detector. 180 images were collected at a wavelength of 0.9795 Å using 1.0° rotations (Figure 3-23). These crystals diffracted to 6.7 Å. All the data collection, processing, phasing and refinement were done in collaboration with Dr Aleksander Roszak. More details of this section and the data processing can be read in the published paper (Cranston, Roszak et al. 2014).

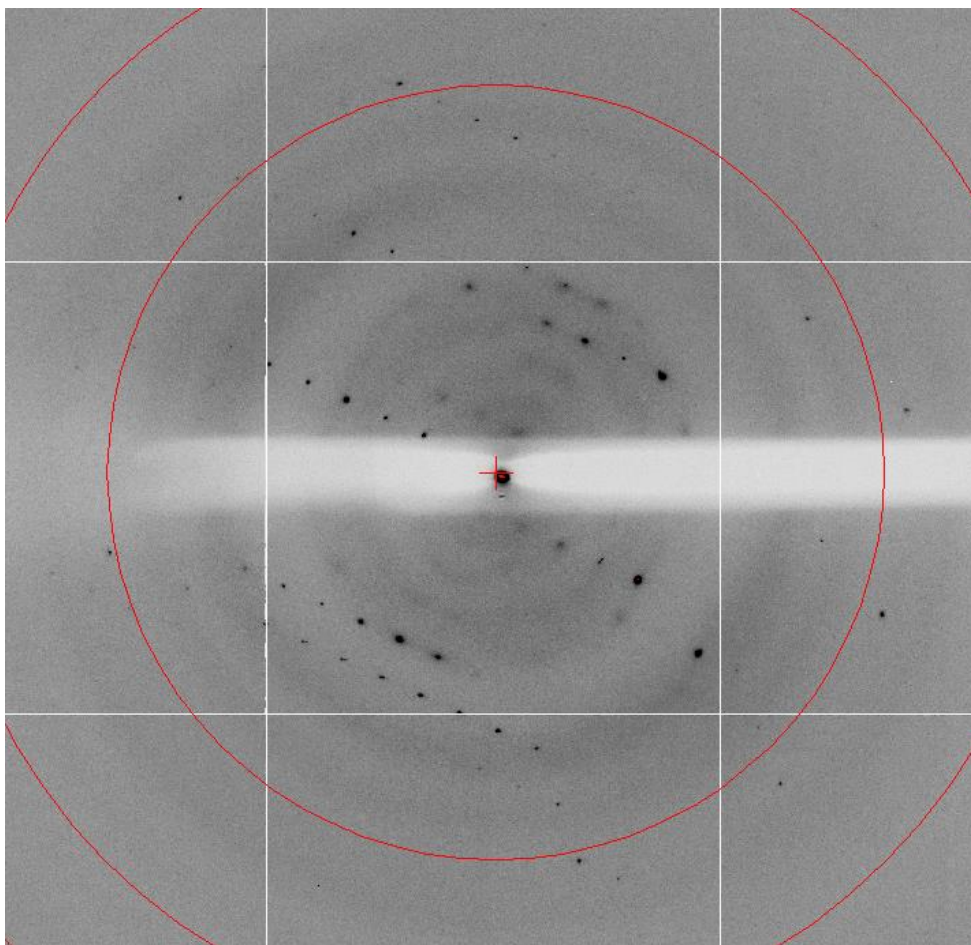


Figure 3-23: Diffraction pattern from the *Mcr. purpuratum* LH2 crystal. The diffraction shows well-defined lunes with diffraction spots extending to 6 Å resolution.

In the absence of a high resolution and a heavy atom derivative, the molecular replacement (MR) method was used. The software used to perform MR was *Phaser* (McCoy et al. 2007). As mentioned in the introduction, there are currently two different ring structures for the LH2 complex, the nonamer from *Rps. acidophila* (Papiz, Prince et al. 2003) and the octamer from *Phs. molischianum* (Koepeke, Hu et al. 1996). A comparison of the sequences of the α/β -apoproteins of the LH2 complex from *Mcr. purpuratum* with those of the LH2 complexes from *Rps. acidophila* and *Ph. molischianum* shows a high degree of sequence similarity (Henry and Cogdell 2013) (More detail in Chapter 4). It is, therefore, to be expected that the basic structure of the *Mcr. purpuratum*

LH2 complex will also have a similar ring-like oligomeric structure. The LH2 from *Rps. acidophila* and *Phs. molischianum* were tested as search models in MR attempts to obtain phase information for diffraction data for *Mcr. purpuratum* LH2. A series of different models were tried, including the mentioned nonmer and octamer. A ten heterodimer model was also generated.

The crystals diffracted to a resolution of 6.7 Å using synchrotron radiation and belonged to the tetragonal space group *I*4, with unit-cell parameters $a = b = 109.36$, $c = 80.45$ Å. The data appeared to be twinned, producing apparent diffraction symmetry *I*422. This space group has higher symmetry than that *I*4. This tetragonal symmetry of the unit cell from this species revealed that this complex is an octamer (Figure 3-24), having 8 $\alpha\beta$ apoprotein heterodimers present in the ring structure.

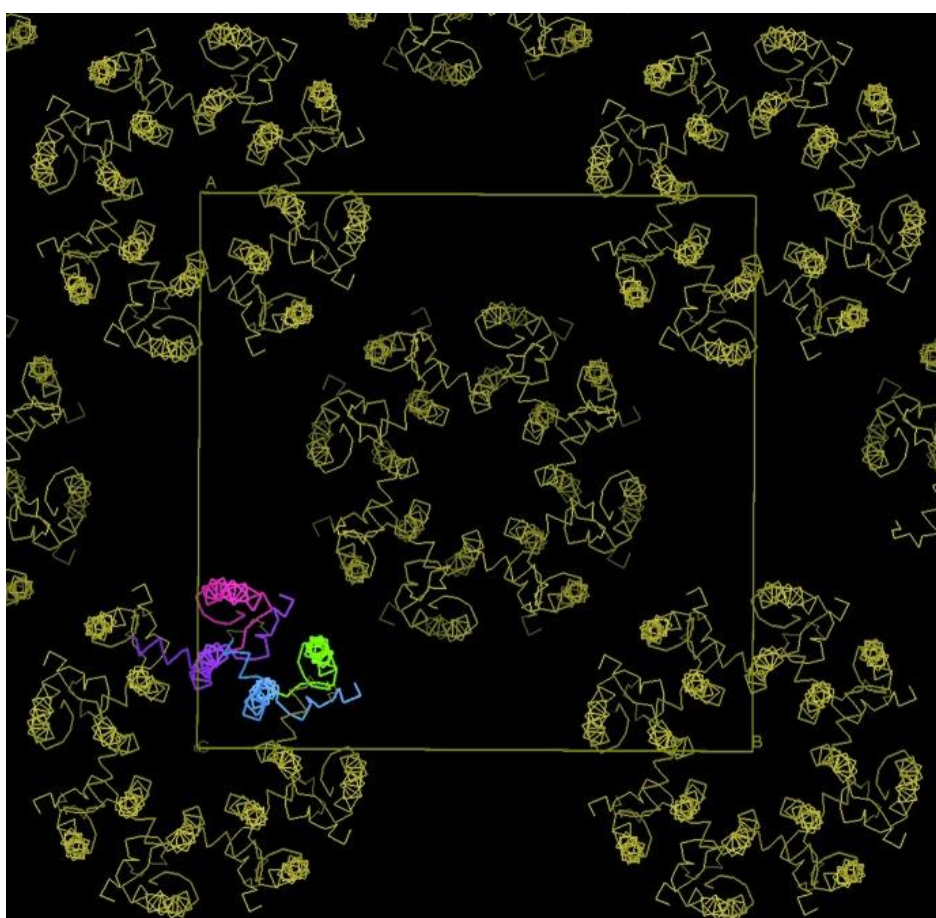


Figure 3-24: Crystal packing for the successful Molecular Replacement (MR) solution in space group *I*4, which forms the octameric *Mcr. Purpuratum* LH2 ring around the fourfold axis, viewed along this axis. A *Rps. acidophila* LH2 dimer of α/β -heterodimers (represented as C $^{\alpha}$ backbones in blue/green and purple/magenta colours) was used as the MR model; the associated Bchl *a* cofactors were included in the model but are omitted here for clarity. This figure was generated in the macromolecular graphics program *Coot* (Emsley, Lohkamp et al. 2010)

3.6. Summary and Analysis

The LH2 complex from *Mcr. purpuratum* was successfully grown and purified. No major changes were made to the growth conditions or cell media when compared to the original literature (Cogdell et al. 1990; Cheryl A Kerfeld, Yeates, and Thornber 1994). An attempt was made to grow the bacteria under low light conditions. It was interesting to note that this bacteria species only produced one type of LH2 complex under differing growth conditions, unlike other relatives such as *Alc. vinosum*. There are as many species of photosynthetic bacteria that do not produce different LH2 complexes under different growth conditions as those that do. One related species which also does not modify the absorbance of its LH2 complex in response to environmental conditions is *Tcr. Tepidum*. The absorption spectra of the whole cells and chromatophores taken at room temperature are the same as seen previously. The single strong absorption peak at 830 nm, with pronounced shoulders at 800 nm of the LH2 complex can be clearly seen in the NIR region. Another shoulder at 875 nm can also be identified as the LH1-RC complex. In the visible region, the Bchl *a* Soret band can be seen between 360-370 nm and the major carotenoid component, okenone, between 450 nm and 600 nm. These distinct features of the absorption spectra remain as the LH2 complex is purified, with the LH1-RC shoulder being removed and a reduction in the 280 nm protein peak being observed. The purification method was optimised to find the detergent best for the extraction of the complex from the lipid membrane and the stability. LDAO was used to solubilise the ICM but was found to denature the LH1-RC complex. This is not untypical as LDAO has denatured the LH2 complex previously (Cogdell et al. 1990) as well as other LH complexes (source communication within the lab team). Therefore, the LH2 complex was detergent exchanged into DM during anion exchange purification. This ensures that a strong detergent is used to solubilize the membrane, hence fully extracting the complex with minimum lipid contamination (Joanne Lemieux, Reithmeier et al. 2002, Guan, Smirnova et al. 2006, Sonoda, Newstead et al. 2011) but ensuring that the complex remains stable for as long as possible in a comparatively gentle detergent.

SDS-PAGE revealed that this single LH2 complex was comprised of multiple β and α polypeptides. This indicates that the LH2 complex from *Mcr. purpuratum* is heterogeneous. Unfortunately, the resolution of this technique is not very high and it is unclear how many of each peptide is present. It has been shown previously that the different β and α polypeptides expressed both within a single photosynthetic bacteria and between photosynthetic bacteria species are very homogenous (Henry and Cogdell 2013). The difference in size between two α polypeptides could as small as 1-50 Da, which, makes them too similar in size to be separated. An increased gradient in the polyacrylamide gel towards the 0-10 kDa region would help but investigation using another technique with high resolution would be better. An in-depth study of the polypeptides occurs in chapter 4. The clear information that we can take away from the SDS-PAGE is the increased purity of the LH2 complex after each purification stage. A distinct decrease in extra protein bands are seen after each step, finally disappearing after the SEC method (GF).

Sparse matrix crystallisation screens were tested initially during the crystallisation trials. These are popular due to their ability and efficiency to screen many crystal conditions. Even though the screens have been designed specifically with membrane proteins in mind, this, as mentioned in the introduction is a tiny area of protein crystallography. The MemGold screen, specifically designed for crystallisation of α -helical membrane proteins, produced the most promising crystal hits. Crystals from the condition 0.1M sodium phosphate at pH 7.0, 0.1M sodium chloride and 33% PEG 300 diffracted to 6.7 Å. These conditions could not be improved on within the time frame of this project. The use of the sparse matrix screens was efficient but also bias. Nature is not comprehensive and what works for some membrane proteins will not work for others. Screening for the best conditions must be widened, but this takes increased time, effort and protein. Several other promising crystal conditions were tested and optimised but did not yield better diffracting crystals. Over the course of this project over 5000 different crystallisation conditions tested with data ranging from 14 Å down to the 6.7 Å. This is an improvement on the previously published crystallisation, which only managed weak diffracting crystals (C A Kerfeld, Thornber et al. 1993). This improvement in diffraction appears to be due to the changes in the purification method and choice of detergent for solubilisation and crystallisation. However, some similar problems were encountered as the previous attempts, such as excessive nucleation during crystallisation. Further optimisation should be more focused on reducing the speed at which nucleation point form. The 6.7 Å data was high enough to obtain a structure model using MR from *Rps. acidophila* and *Phs. molischianum*. The crystals belonged to the tetragonal space group *I*4 and the higher symmetry space group, *I*422. The tetragonal symmetry of the unit cell from this species reveals that this complex is an octamer, having 8 $\alpha\beta$ apoprotein heterodimers present in the ring structure. The data produced good statistics that suggested the solution was correct. However, higher diffracting crystals are needed to resolve the details of the structure. This data was received for publication in (Cranston, Roszak et al. 2014)

The LH2 complex from *Mcr. purpuratum* was reconstituted into lipid to obtain two-dimensional (2-D) crystals for cryo-EM. AFM could be utilised to view the ring size and structure of the *Mcr. purpuratum* LH2. However, instead of forming the flat sheets as was typical, LH2 proteoliposomes were observed. This is a fascinating phenomenon that has not been observed before. As such, it can only be speculated why these proteoliposomes formed. It is suggested that it is due to the shape of the LH2 complex (Figure 3-15) as vesicular ICM are witnessed in whole cell sections. The proteoliposomes were similar in size to the ICM vesicles. It is also possible that the LH2 complex induced curvature of the membrane. The biosynthetic processes that initiate the curvature of the cellular membrane and subsequent budding to produce intracytoplasmic structures are currently not known. There has been a study which suggested that the asymmetry of the proteins present within the ICM can act as a determinant of shape (Law and Cogdell 2007).

Chapter 4 - Analysis of the LH2 Polypeptides from *Mcr. purpuratum*

The LH complexes are heterodimers made up of small hydrophobic α and β apoproteins: the $\alpha\beta$ -subunit, which aggregate to form the LH2 ring structure. As mentioned in section 1.5 of the Introduction, the $\alpha\beta$ -subunits are encoded by the *puc* operon (Kiley and Kaplan 1987, Lee, Wang et al. 1993). The *puc* operon contains *pucBA*, which encodes the β and α apoproteins respectively. Some purple bacteria are known to have multiple β and α polypeptides that are encoded by multiple *puc* operons. Some examples, that are close relatives to *Mcr. purpuratum*, include *Tcr. tepidum* and *Alc. vinosum* (Weissgerber, Zigann et al. 2011, Sekine, Horiguchi et al. 2012, Carey, Hacking et al. 2014). These contain multiple *pucBA* gene pairs, which allows different genes to be switched on and off to produce different α and β heterodimers (Gardiner, Cogdell et al. 1993, Brotosudarmo, Collins et al. 2011, Niedzwiedzki, Bina et al. 2012). The expression of different *pucBA* genes can be regulated by light intensity, temperature, or nutrients (Gardiner, Cogdell et al. 1993). Several examples were explained in the Introduction, they will be summarised here.

- Multiple *pucBA* genes - only one gene is ever expressed under any conditions. Resulting in a homogenous ring.
- Multiple *pucBA* genes – different genes are expressed individually under different growth conditions. Resulting in a homogeneous ring.
- Multiple *pucBA* genes - multiple genes are expressed under different growth conditions at the same time. Resulting in a heterogeneous ring.

The β and α polypeptides essentially ‘tune’ the BChl absorption. This chapter will investigate the β and α polypeptides that are expressed in the B800-B830 of *Mcr. purpuratum* and explore what influence they have on its unusual NIR absorption maxima.

4.1. Locating the *Mcr. purpuratum* *puc* Operons

The genome of *Mcr. purpuratum* strain 984 was sequenced during the duration of this project however it was only partially annotated, thus requiring manual checking of each uploaded contig to locate the *puc* operon. It was sequenced by Professor Donald A. Bryant under the U.S. Department of Energy Joint Genome Institute (Nordberg, Cantor et al. 2014). The *puc* operon was located manually using Uniprot, PATRIC, NCBI Blast searches to check each individual uploaded contig. Fourteen potential *puc* operons were located on contig 82. The annotated contig can be seen in Figure 4-1.

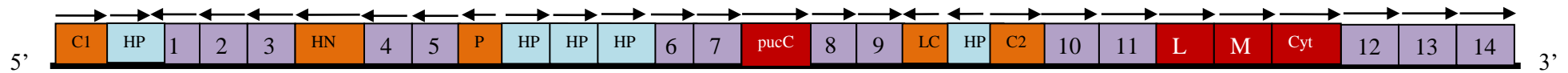


Figure 4-1: Contig 82 of the *Mcr. purpuratum* genome. Numbers 1-14 correspond to the theoretical *puc/puf* genes that have been identified through NCBI, UniProt and PATRIC. The sequences of these can be seen in Table 1. The rest of the key can be seen below, arrows correspond to the direction in which the gene is transcribed. C1: phytoene dehydrogenase, phytoene synthase, and Geranylgeranyl pyrophosphate synthetase. HN: Hydroxyneurosporene methyltransferase. HP: hypothetical protein. P: Phytoene desaturase. LC: Lycopene cyclise. C2: Methoxyneurosporene dehydrogenase, Hydroxyneurosporene synthase, 2-desacetyl-2-hydroxyethyl bacteriochlorophyllide A dehydrogenase BchC, Chlorophyllide reductase subunit BchX, Chlorophyllide reductase subunit BchY, Chlorophyllide reductase subunit BchZ. L: Light chain of the RC. M: Medium chain of the RC. Cyt: Cytochrome c.

The possible *pucBA* are seen in purple, numbered 1-14. Their gene sequences were translated into the predicted peptide amino acid sequence, using the program BioEdit (Hall 1999). From the amino acid sequence, the predicted mass of the peptide could be calculated. Table 4-1 shows the translated amino acid sequence and the calculated mass for that peptide. Some of the calculated masses were very similar – with only 10 Da of a difference. Therefore, this explains why it was difficult to achieve high separation of the peptides on an SDS-PAGE gel. Loading a very small concentration of protein on the gel still resulted in an unclear amount of bands, as seen in Chapter 3.1.3 Figure 3.12. It was suggested from this data, it would indicate that there were multiple β polypeptides and multiple α polypeptides.

<i>Puc gene</i>	Amino Acid sequence translated from DNA	Calculated mass (Average/Da)
1	MHKVWMMFNPPLILASLLGGLFLLALFIHFVLLSTAEFNWLTGA	4975.075 (av.)
2	MANEKQLAGLTDEEAQEFNGFFMQGMSAFIGVAAFAHLLAWFW RPWL	5379.155 (av.)
3	MANEKSVTGLTDEEAQEFHGFQMGMFIGVAAFAHLLAWFW RPWL	5363.112 (av.)
4	MQVPVMMGDPNAKLNHPEDDWKIWTVINPATWMVPFFGILFVQ MWMHISYALSLPGYGFKDSVRVAQPAAVVAPAPEFK	8932.500 (av.)
5	MANLSGLTDA QAKEFHEHWK HGVWSWVMIA SAVHVVTWVY QPWF	5181.904 (av.)
6	MADPKAANLS GLTDAQAKEF HEHWKHGVWS WVMIA SAVHV VTWIYQPWF	5678.467 (av.)
7	MQVPVLLADKDVKLNHPEDDWKIWTVINPATWMVPFFGILFVQ MWMHISYALSLPGYGFKDSVRVAQPAAVVAPAPEFK	8970.549 (av.)
8	MAESKNLSGLSDEQAKEFHEHWKHGVWSWVMIA SAVHVVTWI YQPWF	5584.308 (av.)
9	MKVPVMMADESIATINHPEDDWKIWTVINPATWMVPFFGILFVQ MWLIHSYALSLPGYGFKDSVRVAQPAAVVAPAPEFK	9019.597 (av.)
10	MADNPSLSGLTEQEAQEFHGIFVQSMAFFGIVVVAHILAWLWR PWL	5375.251 (av.)
11	MFPTETMWKIWMLIDPRRVLIAIFALLVLALAIHMILLSTTEFNW LEDGIPASPVQQVTPVVPQNQ	7706.233 (av.)
12	MAHENRSMGLTEDEAREFHGIFVSSFAFTGIVVVAHILVWLW RPWL	5543.387 (av.)
13	MHKIWQIFDPRRTLVALLGFLFVLALLIHFILLSSPAFNWVSGA	5053.110 (av.)
14	MNKIWQIWQIVDPRMIIIAVVGFSFATCALVFHLLLSVPDYSWFK GEAIGYSAVGDMSPPLTLR	7180.544 (av.)

Table 4-1: The amino acid sequences of the *Mcr. purpuratum puc* genes numbered for the order they appear on contig 82. Protein sequence was determined from the gene sequence using BioEdit (Hall 1999) and the monoisotopic (mono.) and average (av.) mass of the peptide chain calculated.

The LH1 and LH2 β and α polypeptides are similar, meaning that the genes identified may be either a *puf* or *puc* operon. Information available on the genome (and other photosynthetic bacteria genome) was used to eliminate some. The *puf* operon encodes the pigment-binding proteins of the RC and the LH1. Generally, the *puf* operon has similar genes in the same order in many photosynthetic bacteria. This includes the *pufBA*, the Light (L) and Medium (M) chain that make up the RC, cytochrome *c* and, in some cases, PufX (or Protein W) (Donohue, Kiley et al. 1988, Kortlüke, Breese et al. 1997). It is presumed that the genes numbers 10 and 11 code for the β

and α polypeptides of the LH1 of *Mcr. purpuratum* due to their position beside the RC genes. It is also unlikely that genes 12-14 are LH2 coding genes due to their position next to the RC genes on the *puf* operon. It is possible one of these codes for *Mcr. purpuratum* PufX protein (or Protein W) (Codgell, Southall et al. 2006). Many of the genes listed produce enzymes, which synthesise the pigments that are found in the LH complexes and are coloured orange. Many also remain unidentified and are coloured blue, it is possible these are non-coding regions or their function is currently unknown.

4.2. Mass Spectrometry

As mentioned earlier, SDS-PAGE was insufficient in resolving the different peptides so experiments with higher accuracy and sensitivity were looked to. One of these techniques was mass spectrometry. Matrix-assisted laser desorption/ionisation time of flight mass spectroscopy (MALDI-TOF) was employed to determine the masses of the *Mcr. purpuratum* LH2 β and α polypeptides. LH2 complexes were purified, and the β and α peptides extracted as outlined in the Methods and Materials section 2.12.2. Figures 4-2 and 4-3 show examples of chromatograms, which were obtained from the MALDI-TOF experiments. The peaks of interest are labelled with the mass/charge (m/z). The masses of the fragments detected are shown in Table 4-2. The detected masses were compared to the *puc* genes amino acid sequences (whose average masses had been calculated (Table 4-1)). Multiple peaks were seen over multiple experiments, a peak at 8086.933 in one run could shift to 8084.013 for another run. Due to this, an error range of ± 5.0 was used for the TOF/MS detected masses. This allowed much easier assignment of potential β and α peptides peaks.

Two different samples were run on the MALDI-TOF. The first was the extracted peptides with pigments (ExPP) and the second was the extracted peptides without pigments (ExP). The best results were seen from the ExP sample. Much fewer peaks were seen, which were much more easily identified. There were peaks, such as the 5052.679, that were not visible during the experiment using the ExPP and only when the ExP sample was used.

Detected Mass m/z	<i>Puc</i>	<i>puc</i> Amino Acid Sequence	<i>puc</i> Calculated (Av.) Mass Da	<i>puc</i> Amino Acid Sequence with Modifications	<i>Puc</i> Calculated Mass (Av.) with modifications Da
4014.786	-	-	-	-	-
4817.555	-	-	-	-	-
5052.679	5	MANLSGLTDAQAKEFH EHWKHGVWSWVMIA AVHVVTWVYQPWF	5181.904	(-M) ANLSGLTDAQAKE FHEHWKHGVWSWVMIA AVHVVTWVYQPWF	5050.708
5466.775	8	MAESKNLSGLSDEQAKE FHEHWKHGVWSWVMI ASAVHVVTWIYQPWF	5584.308	(-M)AESKNLSGLSD EQAKEFHEHWKHGVWS WVMIAHAVHVVTWIYQ PWF (+Methylation or +oxidation)	5453.111 (+14.015 or +15.994)
5561.155	6	MADPKAANLSGLTDAQ AKEFHEHWKHGVWSW VMIAHAVHVVTWIYQP WF	5678.467	(-M) ADPKAANLSGLTD AQAKEFHEHWKHGVWS WVMIAHAVHVVTWIY QPWF (+Methylation or +oxidation)	5547.271 (+14.015 or +15.994)
7995.224	4	MQVPVMMGDPNAKLN HPEDDWKIWTVINPAT WMVPFFGILFVQMWM HSYALSLPGYGFKDSVR VAQPAAVVAPAEFK	8932.5	MQVPVMMGDPNAKLN HPEDDWKIWTVINPAT WMVPFFGILFVQMWM HSYALSLPGYGFKDSVR VAQPAA (-VVAPAEFK)	7993.38
8033.697	7	MQVPVLLADKDVKLNH PEDDWKIWTVINPATW MVPFFGILFVQMWM HSYALSLPGYGFKDSVR VAQPAAVVAPAEFK	8970.549	MQVPVLLADKDVKLNH PEDDWKIWTVINPATW MVPFFGILFVQMWM HSYALSLPGYGFKDSVR VAQPAA (-VVAPAEFK)	8031.429
8086.933	9	MKVPVMMADESIATIN HPEDDWKIWTVINPAT WMVPFFGILFVQM WLIHSYALSLPGYGFKDSVR VAQPAAVVAPAEFK	9019.597	MKVPVMMADESIATIN HPEDDWKIWTVINPAT WMVPFFGILFVQM WLIHSYALSLPGYGFKDSVR VAQPAA (-VVAPAEFK)	8080.477

Table 4-2: A list of masses detected by MALDI-TOF from the LH2 complex of *Mcr. purpuratum* and the *puc* amino acid sequence they correspond to. These results were obtained from the ExP sample. The detected masses, seen in the first column were matched to the calculated average (av.) mass of the different β and α polypeptides. Some undergo N or C terminus post-translational modifications.

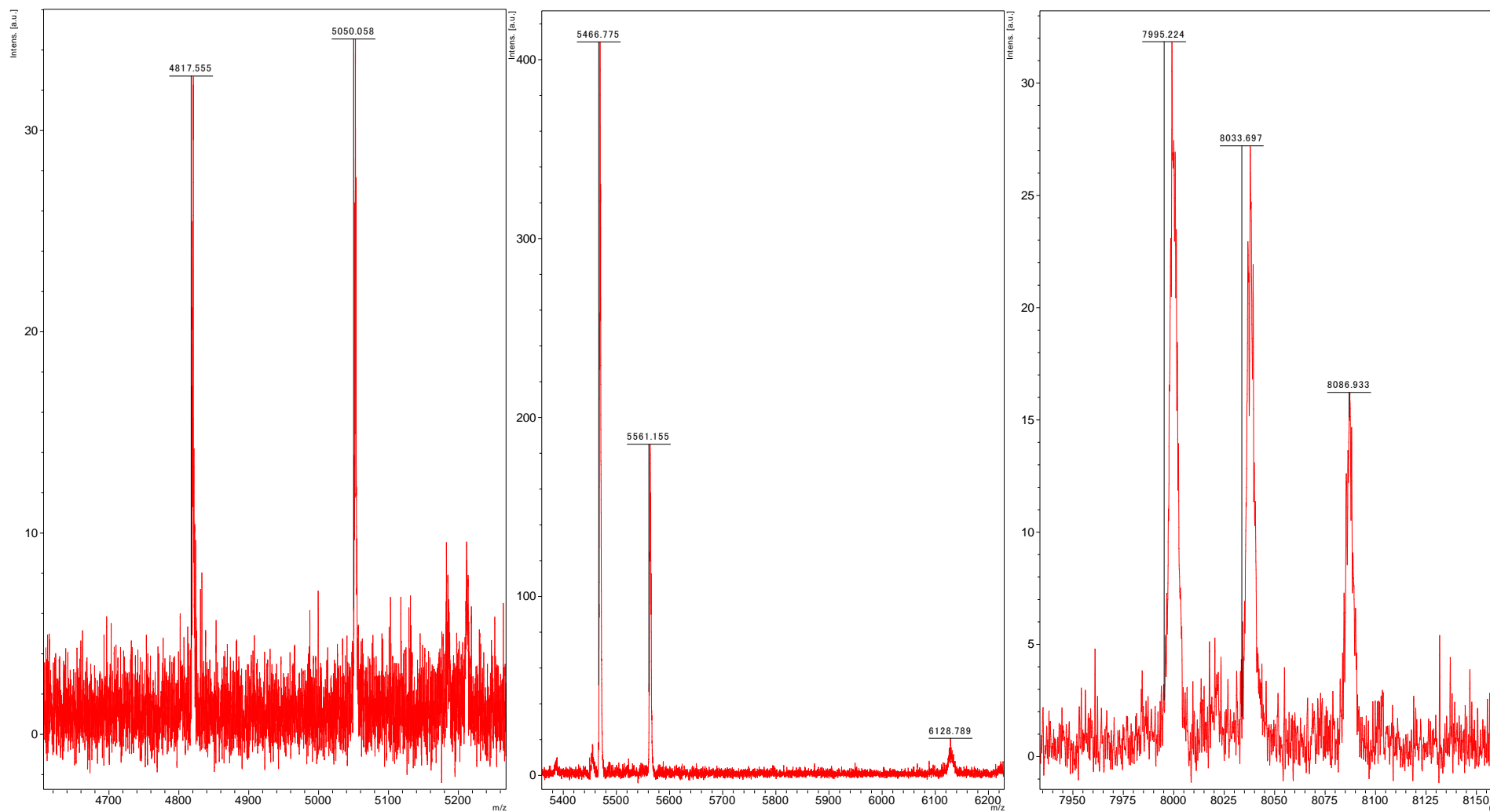


Figure 4-2: Mass Spectrometry Chromatograms for the ExP sample from purified LH2 complexes from *Mcr. purpuratum*. These are more focused on the peaks of interest. The α polypeptides can be seen at the higher m/z end (7000-9000) and the β polypeptides at the lower end (5000-6000). Table 4-2 lists all of the detected masses.

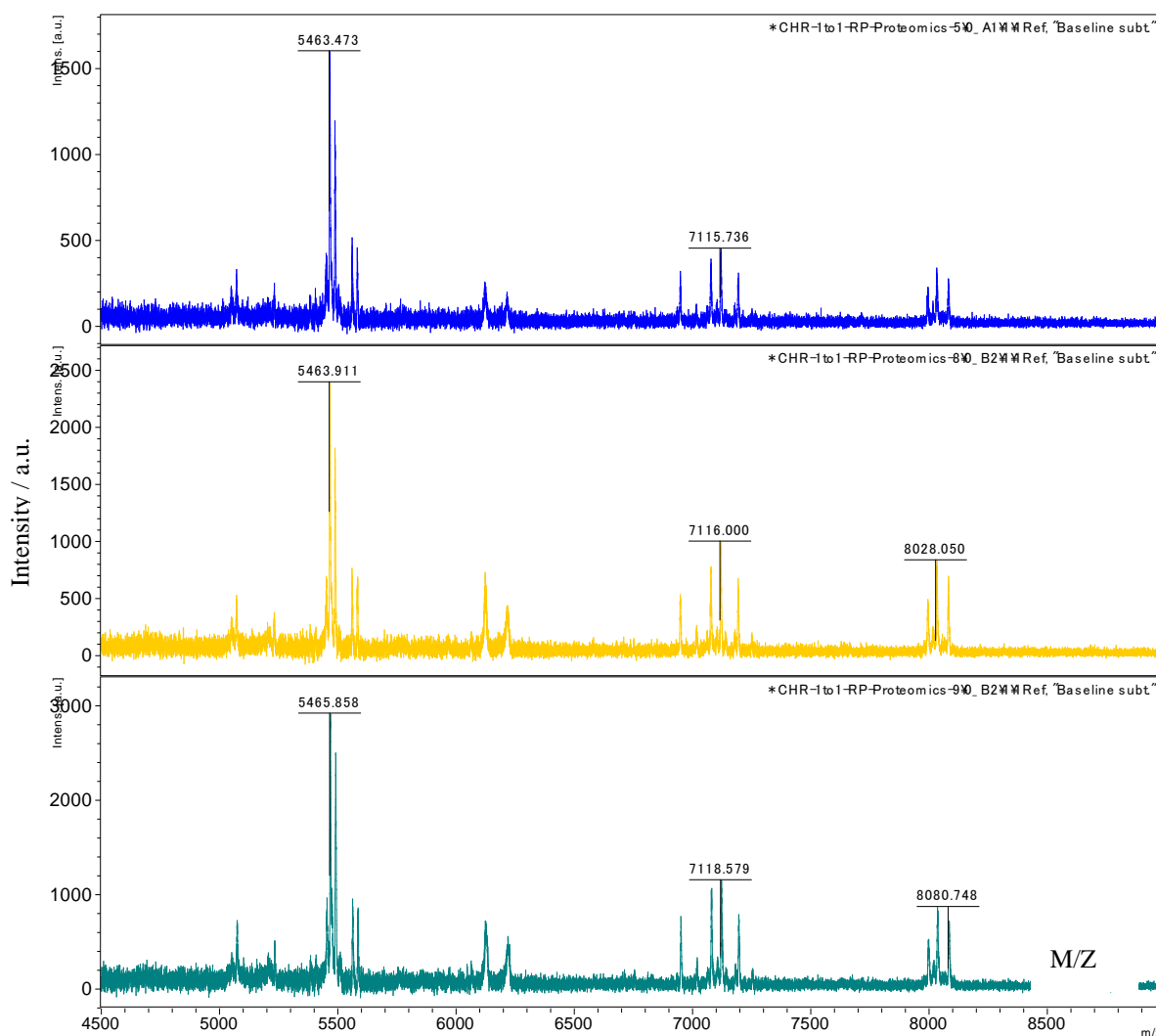


Figure 4-3: A-Overview of the MALDI-TOF results from the ExP sample from *Mcr. purpuratum* LH2. The same sample is shown in all 3 chromatograms and different peaks have been highlighted

From the masses detected a table was created of the suspected *puc* genes, which can be seen in Table 4-2. In order for this to be done, the average possible mass for each translated *puc* gene was calculated. They were then modified individually, by removing 1 amino acid at a time using a peptide mass calculator, from the C-terminus or N-terminus until a matching mass was located.

There is evidence from other LH2 complexes that the peptide chain undergoes post-translational processing, especially sequences that have a number of repeating prolines, alanines and valines at the C-terminus (Gardiner, MacKenzie et al. 1996). Examples of this can be seen in *Mcr. purpuratum* *puc* 4, 7 and 9 in Table 4-2. *puc* 4, 7 and 9 are speculated to be alpha polypeptides. Following the amino acid sequence of PAA, a cleavage appears to occur. The sequence of VVAPAEFK is removed from the C-terminus of each. This could be a targeting sequence for proteases, though the mechanism for this has not yet been characterised.

In some bacteria, such as *Phs. molischianum*, the N-terminal methionine residue can be cleaved off in both the α and β peptides. Due to this N-terminal modification and shorter length of

the amino acid chain the *puc* 5, 6 and 8 are the suspected β polypeptides. Other modifications such as the addition of methyl groups to methionine residues can also occur and oxidation (Silva, Vitorino et al. 2013, Doll and Burlingame 2015). These can either occur post-translational or can be an effect of the solvents used to dissolve and extract the peptides. All of these possible changes were taken into consideration when comparing the masses detected in the experiment and the calculated theoretical masses. Some of the masses remain unassigned and more investigation would need to occur to identify them. It is possible they are contaminants, or smaller fragments of the peptides already detected, which have been modified. In the case of the mass detected mass 4014.786, it's possible this is +2 charge of detected mass 8033.697. However, the masses that have been detected have been matched closely to some translated *puc* genes. This includes *puc* 4,6,5,7,8 and 9.

Information from other photosynthetic bacteria has shown that *puc* genes are most commonly located in pairs, which are transcribed together (Alberti, Burke et al. 2004) however, this is not always the case (Carey, Hacking et al. 2014). Figure 4-1 was created using the information available on the *Mcr. purpuratum* genome from NCBI, UniProt and PATRIC. This figure shows contig 82 of *Mcr. purpuratum* from 226794 bp to 258614 bp, the location of many of the major photosynthetic genes. At this stage, it is thought that the *pucBA* pairs are as follows: 5 and 4, 6 and 7 and finally 8 and 9. As mentioned earlier 10 and 11 are most probably *puf* genes, encoding for the LH1. However, this is theoretical and more experiments are planned to confirm if this assignment is accurate. In conclusion 4, 7 and 9 have been labelled as alpha polypeptides and 5, 6 and 8 as beta polypeptides

4.2.1. Tandem MS-MS

To further try to elucidate and confirm the different polypeptides of the B830 complex of *Mcr. purpuratum* the complex was purified and peptides extracted and sent to Dr Bill Mullen for Tandem MS-MS (Methods and Materials section 2.12.5). Electron-Transfer Dissociation (ETD) was the fragmentation method used and only one result hit was seen. The raw data can be seen in Figure 4-4. The hit that was seen was listed on the website Uniprot (UniProt: the universal protein knowledgebase 2017) as F9TXE3 (F9TXE3_MARPU) with the sequence:

MANLSGLTDAQAKEFHEHWKHGVWSWVMIASAVHVVTWVYQPWF

This matches the polypeptide sequence of *puc* 5 listed in table 4-2 above. The major reason only one hit was seen with this method is due to the unannotated genome. MS and MS/MS data files were searched against UniProt *Mcr. purpuratum* database using SEQUEST (by using Thermo Proteome Discoverer), with no enzyme specified. However, since the genome had only just been sequenced and was not annotated, only a single peptide match could be seen and was then extracted using high peptide confidence and top one peptide rank filters. It would be interesting to revisit this method after the genome has been fully annotated and the *puc* genes confirmed.

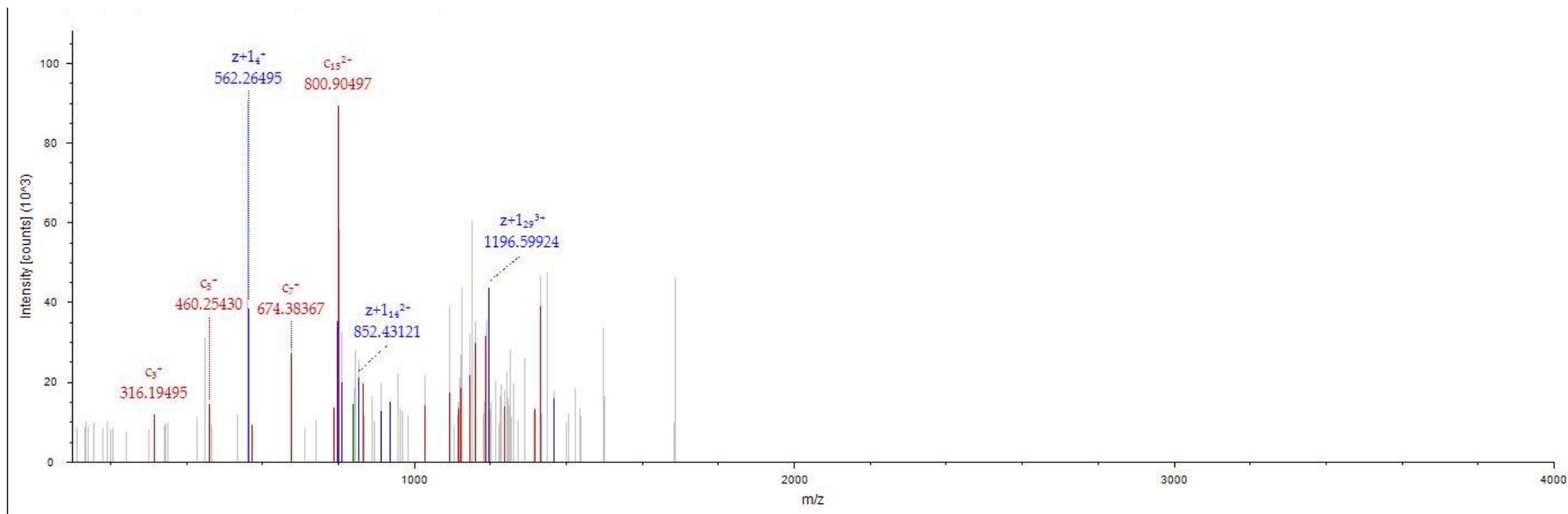


Figure 4-4: Raw Tandem MS-MS data from the LH2 complex from *Mcr. purpuratum*. The fragmentation method used was Electron-transfer dissociation (ETD) The peptide that was fragmented was *puc* 5, a suspected β polypeptide with the sequence. MANLSGLTDAQAKEFHEHWKHGVWSWVMIASAVHVVTWVYQPWF. The charge on this molecule was +6 and the mono m/z mass is 842.25336 Da with the mother ion having a mass of 5048.48376 Da. The data strongly indicated that the primary methionine (M) residue was removed. This confirmed what was suspected from the MALDI data.

4.3. Peptide Sequences and Alignment

The expressed *puc* genes had been identified with the aid of MALDI-TOF. They were given more accurate nomenclature to reflect that they had been identified:

pucBA1 codes for β -1 and α -1 (*puc* 5 and 4).

pucBA2 codes for β -2 and α -2 (*puc* 6 and 7).

pucBA3 codes for β -3 and α -3 (*puc* 8 and 9).

The *puc* gene sequence and number can be seen alongside the final modified expressed β or α polypeptide in Figure 4-5. They can be seen alone in Figure 4-6, which highlights the sequence similarity. The α polypeptides have incredible sequence identity. Only the N-terminus ends differ and the amino acid sequence is identical from the first conserved asparagine (N) residue. The same can be said of the β polypeptides, the amino acid sequence is identical from the first conserved histidine residue.


```

4 Mcr. purpuratum      ~~~~MQVPVMMGDPNAKLNHPEDDDWKIWTVINPATWMVPFFGILFVQMWWMIHSYALSLPGYGFKDSVRVAQPAAVVAPAPEFK
Mcr. purpuratum alpha-1 ~~~~MQVPVMMGDPNAKLNHPEDDDWKIWTVINPATWMVPFFGILFVQMWWMIHSYALSLPGYGFKDSVRVAQPAA
5 Mcr. purpuratum      ~~~~MANLSGLTDAQAKEFHHEHWKHGVWSWVMIASAVHVVVTWVYQPF
Mcr. purpuratum beta-1  ~~~~ANLSGLTDAQAKEFHHEHWKHGVWSWVMIASAVHVVVTWVYQPF

7 Mcr. purpuratum      ~~~~MQVPVLLADKDVKLNHPEDDDWKIWTVINPATWMVPFFGILFVQMWWMIHSYALSLPGYGFKDSVRVAQPAAVVAPAPEFK
Mcr. purpuratum alpha-2 ~~~~MQVPVLLADKDVKLNHPEDDDWKIWTVINPATWMVPFFGILFVQMWWMIHSYALSLPGYGFKDSVRVAQPAA
6 Mcr. purpuratum      ~~~~MADPKAANLSGLTDAQAKEFHHEHWKHGVWSWVMIASAVHVVVTWIYQPF
Mcr. purpuratum beta-2  ~~~~ADPKAANLSGLTDAQAKEFHHEHWKHGVWSWVMIASAVHVVVTWIYQPF

9 Mcr. purpuratum      ~~~~MKVPVMMADESIATINHPEDDDWKIWTVINPATWMVPFFGILFVQMWLIHSYALSLPGYGFKDSVRVAQPAAVVAPAPEFK
Mcr. purpuratum alpha-3 ~~~~MKVPVMMADESIATINHPEDDDWKIWTVINPATWMVPFFGILFVQMWLIHSYALSLPGYGFKDSVRVAQPAA
8 Mcr. purpuratum      ~~~~MAESKNLSGLSDEQAKEFHHEHWKHGVWSWVMIASAVHVVVTWIYQPF
Mcr. purpuratum beta-3  ~~~~AESKNLSGLSDEQAKEFHHEHWKHGVWSWVMIASAVHVVVTWIYQPF

```

Figure 4-5: Alignment of the final modified expressed β and α LH2 polypeptides of *Mcr. purpuratum* alongside the original *puc* gene sequence. The post-translational modifications that occur on all can be seen. The loss of the VVAPAPEFK tail on all of the α polypeptides and the N-terminus removal of the methionine (M) Alignments were made to the conserved histidine (H) on both the α and β polypeptides (pink H). Alignments were created using BioEdit (Hall 1999)

```

Mcr. purpuratum alpha 1 ~~~~MQVPVMMGDPNAKLNHPEDDDWKIWTVINPATWMVPFFGILFVQMWWMIHSYALSLPGYGFKDSVRVAQPAA
Mcr. purpuratum alpha-2 ~~~~MQVPVLLADKDVKLNHPEDDDWKIWTVINPATWMVPFFGILFVQMWWMIHSYALSLPGYGFKDSVRVAQPAA
Mcr. purpuratum alpha-3 ~~~~MKVPVMMADESIATINHPEDDDWKIWTVINPATWMVPFFGILFVQMWLIHSYALSLPGYGFKDSVRVAQPAA
Mcr. purpuratum beta-1  ~~~~ANLSGLTDAQAKEFHHEHWKHGVWSWVMIASAVHVVVTWVYQPF
Mcr. purpuratum beta-2  ~~~~ADPKAANLSGLTDAQAKEFHHEHWKHGVWSWVMIASAVHVVVTWIYQPF
Mcr. purpuratum beta-3  ~~~~AESKNLSGLSDEQAKEFHHEHWKHGVWSWVMIASAVHVVVTWIYQPF

```

Figure 4-6: Alignment of the final expressed β and α LH2 polypeptides of *Mcr. purpuratum*. The high sequence similarity can clearly be seen. Alignments were made to the conserved B850 coordinating histidine (H) on both the α and β polypeptides (pink H). Alignments were created using BioEdit (Hall 1999)

Using these protein sequences of the potential different peptides from *Mcr. purpuratum*, which were extrapolated from the identified *puc* genes, they were compared to peptides from other LH2 complexes (Figure 4-7). As mentioned in the Introduction 1.4, there are several reasons for a change in the NIR Q_y absorption band of the BChl *a* of an LH2 complex. This includes a change in the site energy of the Bchl *a* binding pocket. This site energy is controlled by the amino acid sequence of the polypeptide chains. Different hydrogen bonds (H-bonds) donor residues are found on the α peptide, and sometimes on the β as seen in *Phs. molischianum*. There are regions of conserved amino acids found in the binding pocket. In the case of *Rps. acidophila* strain 10050, the B800 Bchl *a*s are stabilised by coordination between the Mg^{2+} of the Bchl *a* and COO- α -methionine1, and an H-bond between the acetyl group of Bchl *a* and the guanidinium group of β -arginine20 (Papiz, Prince et al. 2003). The B850 Bchl of *Rps. acidophila* are coordinated through their central Mg^{2+} ions to the imidazole ring side chain of the conserved histidine residues, α -histidine31 and β -histidine30. The Bchl *a* forms hydrogen bond to α -tyrosine44 (Y) and α -tryptophan45 (W) (at position 62 and 63 in the Figure 4-7 alignment). These conserved histidine residues are also seen in both the α and β of all the *Mcr. purpuratum* peptides. All the alignments were made to these conserved histidine residues. A good example of this is seen with the change in site energy between the B800-B820 and B800-850 of *Rps. acidophila*. Both of these crystal structures have been determined and the reason for the change in the NIR absorption band of the BChl *a* is understood (McLuskey, Prince et al. 2001, Papiz, Prince et al. 2003). There is a hydrogen bond, which forms between the acetyl group on the bacteriochlorin rings of the B850 Bchl *a* and the α -tyrosine44 and α -tryptophan45. This hydrogen bond is not present with the B820 Bchl *a*. The crystal structure of the B800–820 form of the *Rps. acidophila* strain 7050 shows the loss of the hydrogen bonding due to the acetyl groups rotated out of the plane (McLuskey, Prince et al. 2001). It can be seen in the α polypeptide sequence of *Rps. acidophila* strain 7050 that, instead of α -tyrosine44 and α -tryptophan45, there is α -phenylalanine44 (F) and α -leucine45 (L). Instead, it is a single tyrosine at position α -41 (position 59 in Figure 4-7) that forms an H-bond with the B820 BChl *a* and locks the acetyl group out of the plane. When the Bchl *a* acetyl group is in plane the Q_y transition is red shifted due to inclusion of a double bond in the conjugated system, increasing the absorption from B820 to B850.

The *Phs. molischianum* B800-B850 complex has also had the structure determined by X-ray crystallography and the expressed α and β polypeptides are known. These are also seen in the multiple alignments in Figure 4-7. The structure of the B800-850 LH2 from *Phs. molischianum* is known to differ in the binding of the B800 from the B800-850 from *Rps. acidophila*. There is also evidence of a B800-B820 species of *Phs. molischianum* though there is no crystal structure at this moment (Sauer, Lottspeich et al. 1996, Mascle-Allemand, Duquesne et al. 2010). However, the α and β polypeptide sequences are known. This means that a comparison between the α peptides of the two LH2 complex types from *Phs. molischianum* may indicate the structural basis of the shift in absorption from B850 to B820. These can be compared to the α polypeptides of the B820 and

B850 of *Rps. acidophila*. Interesting enough, residue α -45 of *Phs. molischianum* B800-B850 is also a tryptophan, as seen in *Rps. acidophila* B800-B850. This α -tryptophan45 bind the B850 Bchl *a* as well as a tryptophan residue located on the β polypeptide chain at residue 44 (β -tryptophan44).

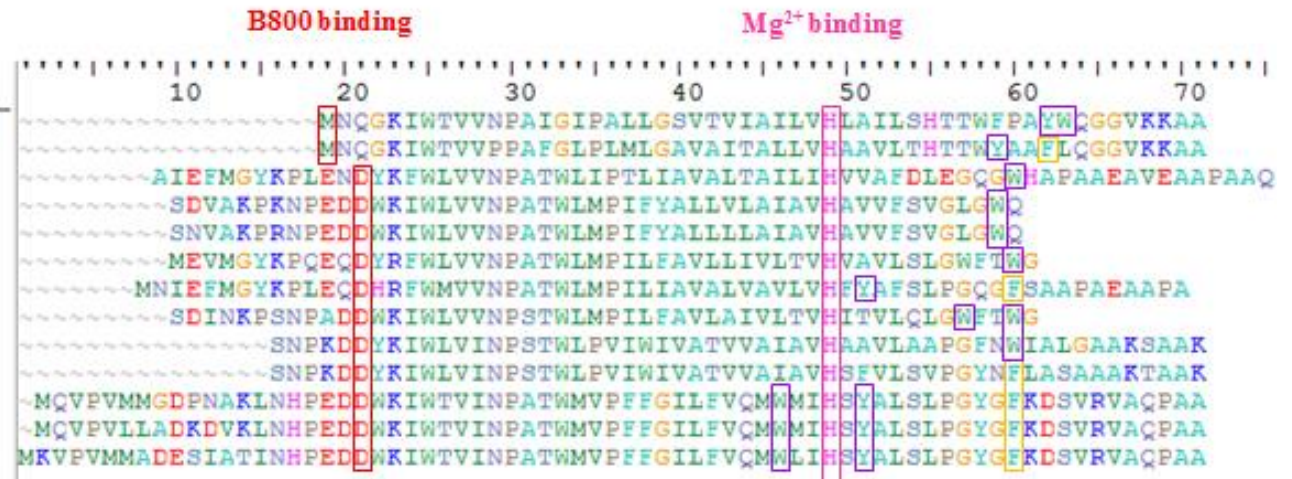
As mentioned earlier, the LH2 complexes from *Phs. molischianum* are known to bind the B800 BChl with different residues on the alpha peptide in comparison to the LH2 complexes from *Rps. acidophila*. The LH2 complex from *Phs. molischianum* binds the B800 BChl via an aspartic acid (D) residue at position 6. Other related species of purple photosynthetic bacteria have recently had more study than *Mcr. purpuratum*. This includes *Alc. vinosum*, which has three spectral forms of LH2 that have been isolated and characterised (Carey, Hacking et al. 2014). These have been named the B800-850, B800-840 and B800-820 LH2 complex types. In *Alc. vinosum*, a close relative of *Mcr. purpuratum*, are six different *puc* genes, coding for a potential 6 α polypeptides and 6 β polypeptides (Weissgerber, Zigann et al. 2011). There is no structure yet but the polypeptide sequences and which LH2 complex types they are found in have been identified. Examination of the B800 BChl *a* binding site in *Alc. vinosum* and *Mcr. purpuratum* indicates a similar B800 binding, due to a conserved aspartic acid residue. Though they are not all in the position 6, they are aligned and at equidistance from the conserved histidine residue. Binding of the *Mcr. purpuratum* B800 Bchl *a* by coordination between the Mg^{2+} of the Bchl *a* and the conserved aspartic acid residue, as seen in *Phs. molischianum*, seems likely.

The single conserved histidine on the α and the second conserved histidine on the β that coordinates with the central Mg^{2+} ion of the dimerised BChl is observed in all the residues aligned. It has already been discussed for *Rps. acidophila* how amino acid residues near to this histidine help to alter the Q_y absorption from B850 to B820. Since the NIR absorption of the *Mcr. purpuratum* is B800-B830, the binding site of the of the B830 is where we would expect to see a difference in the amino acid residues in comparison to those from B850 and B820 species. The hydrogen bonding of *Phs. molischianum* B800-B850 is also known and has been discussed. The binding of the B800-820 is still under speculation (Sauer, Lottspeich et al. 1996) This is also the case for the B800-850, B800-840 and B800-820 of *Alc. vinosum*. The suspected tryptophan residues that may be involved in the hydrogen bonding are marked in Figure 4-7 in purple. There is very high sequence similarity between the β polypeptides of *Phs. molischianum*, *Alc. vinosum* and *Mcr. purpuratum*. As mentioned earlier, the *Phs. molischianum* B800-B850 binds via the β -tryptophan44 and is “tuned” by this hydrogen bonding. This tryptophan is a highly conserved residue present in all of the β polypeptides examined. This indicates that all of the β peptides are able to form an H-bond with the B850 BChl. Looking at the α polypeptides, it can be seen that *Phs. molischianum* B800-B820 α - tryptophan45 has changed to a phenylalanine (F). In the case of *Mcr. purpuratum* the α are longer length peptide chains, so the 44 and 45 amino acids become 61 and 62 and an aspartic acid (D) residue is seen at position 61, α - aspartic acid61, and a serine (S), α -serine62. These are conserved throughout the three alphas. The amino acid residue seen at position

α 45 for both α -1 and α -2 is tryptophan, and at α 46 for α -3, which is a slightly longer peptide by one amino acid. These appear in the sequence before the dimerised Bchl *a* coordinating histidine (position 46 in Figure 4-7). It is possible that these tryptophan residues are involved with hydrogen bonding, as they are in very close proximity to the Mg² binding histidine – only 2 amino acid residues apart on the N-terminal side. This is something that is not seen in any of the other species examined. *Mcr. purpuratum* has a unique B800-B830 complex, so it would make sense that it has a unique way of binding the dimerised Bchl *a*. The α phenylalanine⁴⁵ residue from *Phs. molischianum* B800-B820 appears to be conserved between the three α polypeptides of *Mcr. purpuratum*. The α -5 of *Alc. vinosum* also has this phenylalanine residue and it was recently shown that this peptide is a major component of the B820 complex (Carey, Hacking et al. 2014). It is also interesting to note that instead of α -tyrosine⁴⁴, as seen in the B850 complex of *Rps. acidophila*, the B820 has α -phenylalanine⁴⁴ -though it is not in perfect alignment, and at the same distance from the conserved histidine. This residue in the B820 of *Rps. acidophila* does not form hydrogen bonds. There is also a tyrosine residue (Y), which is conserved in all the α peptides of *Mcr. purpuratum* and α -5 of *Alc. vinosum* (position 51 in Figure 4-7). As stated previously, α -5 of *Alc. vinosum* is a major component of the B820 complex. This tyrosine residue is also a possible hydrogen bonding site of the B830. Without a high-resolution crystal structure of the LH2 complex, it is difficult to preliminarily determine where the hydrogen bonding takes place.

Alpha polypeptides

Rps. acidophila 10050 B800-850 LH2 alpha
 Rps. acidophila 7050 B800-820 alpha
 Alc. vinosum alpha-1
 Alc. vinosum alpha-2
 Alc. vinosum alpha-3
 Alc. vinosum 0708 (alpha-4)
 Alc. vinosum alpha-5
 Alc. vinosum alpha-6
 Phs. molischianum B800-850 alpha
 Phs. molischianum B800-820 alpha
 Mcr. purpuratum alpha 1
 Mcr. purpuratum alpha-2
 Mcr. purpuratum alpha-3



Beta polypeptides

Rps. acidophila 10050 B800-850 beta
 Rps. acidophila 7050 B800-820 beta
 Alc. vinosum beta-1
 Alc. vinosum beta-2
 Alc. vinosum beta-3
 Alc. vinosum 0709 (beta-4)
 Alc. vinosum beta-5
 Alc. vinosum beta-6
 Phs. molischianum B800-850 beta
 Phs. molischianum B800-820 beta
 Mcr. purpuratum beta-1
 Mcr. purpuratum beta-2
 Mcr. purpuratum beta-3



Figure 4-7: The six potential α and β peptides from *Mcr. purpuratum* aligned to the BChl a coordinating histidine of the twelve potential α and β peptides of *Alc. vinosum* and the B800-850 and B800-820 α and β from *Rps. acidophila*, and *Phs. molischianum*. Sequences from *Ph. molischianum* and *Rps. acidophila* 10050 and 7050 come from their crystal structures and are the final expressed proteins in the complex (McLuskey, Prince et al. 2001, Papiz, Prince et al. 2003). Sequences *Alc. vinosum* are from the published work (Carey, Hacking et al. 2014). The α and β 4 of *Alc. vinosum* have not been found to be expressed and are named with their *puc* gene identity. Alignments were made to the conserved B850 coordinating histidine (H) on both the α and β polypeptides (pink H) in BioEdit (Hall 1999).

4.4. High Pressure Liquid Chromatography (HPLC)

Reversed phase HPLC (RP-HPLC) was used to separate out the different α and β 1 peptides that were found in the *Mcr. purpuratum* LH2 complex. RP-HPLC utilises hydrophobic interactions by an immobilised n-alkyl hydrocarbon. The α and β polypeptides are highly hydrophobic, which suit a separation system like this. RP-HPLC has been used successfully before to separate α and β peptides (Tharia, Nightingale et al. 1999, Wang, Shimonaga et al. 2003, Carey, Hacking et al. 2014). A Waters Alliance RP-HPLC system with an e2695 solvent module and UV detector was used for the measurements. The method was developed with the help of Dr Anne-Marie Carey. The HPLC elution profiles for the peptide extracts obtained from the purified *Mcr. purpuratum* LH2 complexes are shown in Figure 4-8. The β polypeptides eluted first, followed by the α . These elution patterns are similar to those of the LH1 and LH2 polypeptides from other purple bacteria (Miller, Hinchigeri et al. 1987, Wang, Shimonaga et al. 2003, Sekine, Horiguchi et al. 2012, Carey, Hacking et al. 2014). The MALDI-TOF experiments gave an indication of how many different peptides to expect. The sequences and masses can be seen in Table 4-2. The B800-830 of *Mcr. purpuratum* has six different polypeptides. These are α 1, α 2, α 3 and β 1, β 2, and β 3.

The peak seen at 10 mins is formic acid. The *Mcr. purpuratum* LH2 complex shows five major peaks in the HPLC trace. It would most likely seem that β 1, β 2 and β 3 have separated and are responsible for the first three peaks seen at the 45 mins point. There is a high sequence identity between the β polypeptides. β 2 and β 3, also have similar mass, 5561.155 and 5466.775 respectively. β 1 has a shorter amino acid chain and a significantly lower mass, 5052.679. This indicates that the first peak eluted is the β 1. The next peptide is then β 3, followed by β 2 due to their respective hydrophobicity. The α polypeptides all have very similar mass, α 1, α 2 and α 3 equal 7995.224, 8033.697 and 8086.933 respectively. They also have a very similar amino acid sequences, with α 3 containing one more residue in comparison to the α 1 and α 2 (Figure 4-5). α 1 and α 2 are very similar and, therefore, cannot be separated completely so they elute together. A small shoulder can be seen at the beginning of the α 1 and α 2 peak, which may equal one of these α peptides. Several methods were tried to fully separate the peptides as much as possible, but they remained unsuccessful. At this stage the results are unclear, these were preliminary experiments. In order to investigate the peptides in more detail, the eluate should be collected for each individual peak and sent back for MALDI-TOF to confirm their suspected identities.

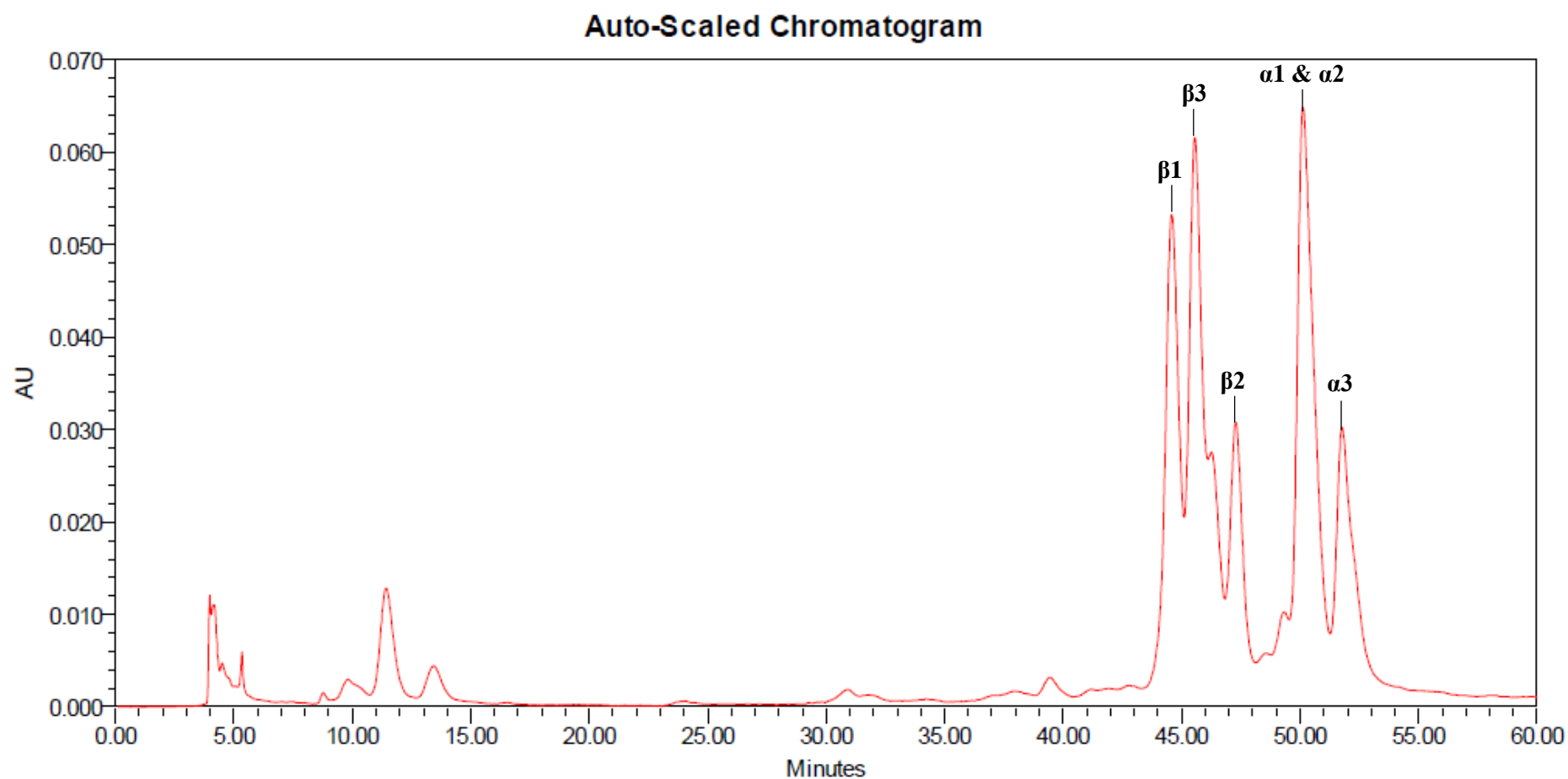


Figure 4-8: HPLC chromatograms for the peptide extracts from purified LH2 complexes from *Mcr. purpuratum*. Five distinct peptide peaks can be seen.

4.5. *puc Knock out*

The data obtained by the MALDI-TOF experiments had shown that multiple $\alpha\beta$ polypeptides were expressed in *Mcr. purpuratum*. The next step was to attempt to delete one of the three *pucBA* genes to see if the removal would have any effect on the Q_y peak. It was also possible the LH2 complex would not be able to be produced at all. The first knock out was selected as *pucBA2*, which transcribes the β_2 and α_2 polypeptides.

Mcr. purpuratum genomic DNA was prepared as described in the Methods and Materials chapter 2.10.1. The first stage was to design primers that would amplify up an upstream fragment and a downstream fragment surrounding the *pucBA2* gene. The method used was the splice-overlap extension (SOE) (Horton, Hunt et al. 1989). This required flanking primers and internal primers to be designed and a restriction enzyme site to be introduced into the flanking primers. A schematic of these primers and their respective positions can be seen in Figure 4-9. Primers 3 and 4 incorporated the start codon of the *pucBA* gene in their sequences as well as the stop codon. This ensures they would share an overlap, which could be used to anneal them together.

The primers were used to amplify the upstream (US) and downstream (DS) region. The upstream fragment's length was calculated to be 398 bp and the downstream fragment was 567 bp. The PCR product was run on an agarose gel and the 2 bands, 1 from the upstream and 1 from the downstream were cut out. The DNA gel can be seen in Figure 4-10. The US and DS DNA was spliced together and then amplified into one continuous stand, omitting the gene. The *pucBA2* KO was cloned into pJET1.2/blunt and was ready to be digested with BamHI and HindIII. The *pucBA2* KO insert can be seen in pJET1.2/blunt in Figure 4-11. It was then to be cloned into suicide vector *pK18mobsacB*. However, after digesting pJET1.2/blunt multiple times, the fragment sizes were inconsistent. The time allocated for this study ran out.

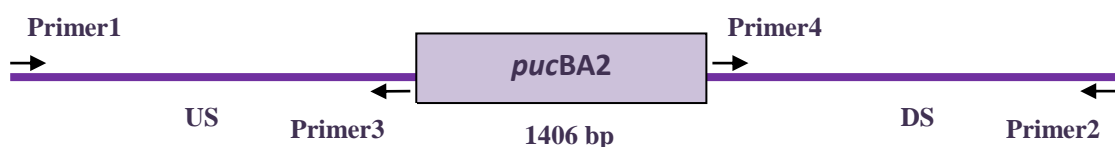


Figure 4-9: Diagram showing the location of the primers used to knock out the *pucBA2* gene. The numbers correspond to the names of the primers used. The sequences for these can be viewed in the Materials and Methods chapter 2.13.7. 1406 bp is the length of the entire *pucBA2* gene. The upstream fragment's length was calculated to be 398 bp and the downstream fragment was 567 bp. US- Upstream, DS- Downstream.

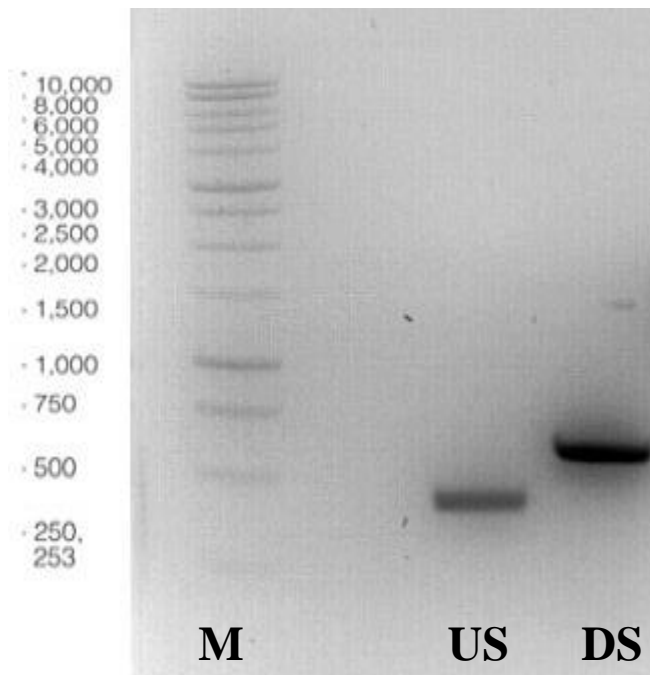


Figure 4-10: Agarose DNA gel of the amplified upstream (UP) and Downstream (DN) fragments for the *pucBA2 KO*. The correct upstream fragment's length of 398 bp and the correct downstream fragment length of 567 can be seen.

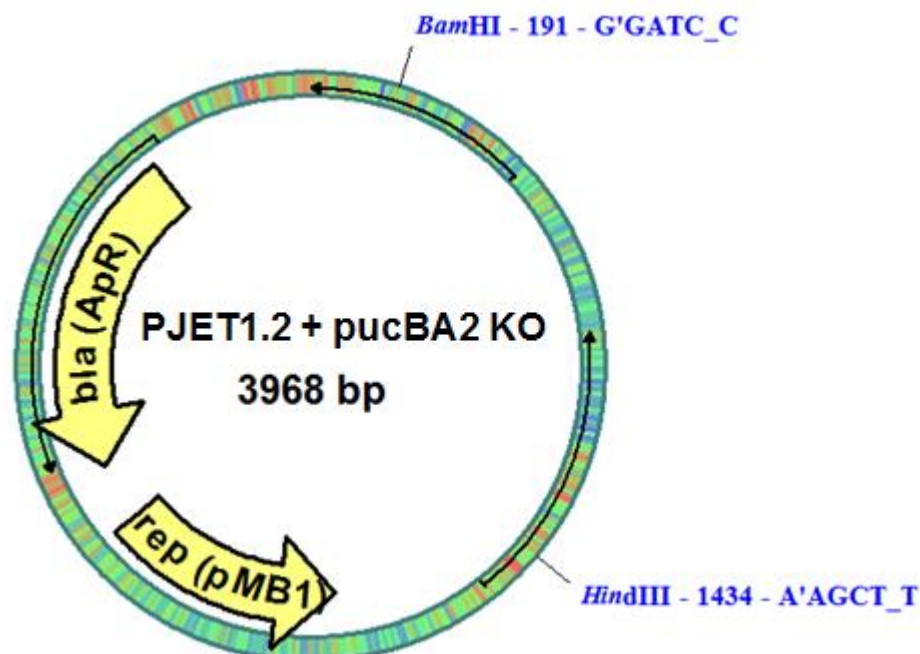


Figure 4-11: Diagram showing the PJET 1.2 vector with the *pucBA KO* insert. The features of the PJET vector include the *bla* (ApR) = β -lactamase gene conferring resistance to ampicillin and used for selection of the recombinant, *rep* (pMB1) = Replicon from the pMB1 plasmid, which is responsible for replication of the plasmid. Not shown is the *eco47IR* gene that has been split and rendered unfunctional by the inclusion of the *pucBA2 KO*. It is a lethal gene, which enables positive selection of the recombinants. The restriction enzyme sites of the insert, BamHI and HindIII can also be seen clearly.

4.6. Summary and Analysis

The *Mcr. purpuratum* genome was examined to locate potential *pucBA* operons to determine how many α and β polypeptides were transcribed and expressed in the B800-B830 LH2 complex. The $\alpha\beta$ polypeptides were identified using MALDI-TOF and RP-HPLC. There was found to be three *pucBA* operons, which coded for three β polypeptides and three α polypeptides, respectively. This agreed with the previous work (Cheryl A Kerfeld, Yeates et al. 1994). These *pucBA* operons were named *pucBA1*, *pucBA2* and *pucBA3*. The expression of multiple $\alpha\beta$ polypeptides confirmed the heterogeneity of this LH2 complex. The α peptides all had very similar sequence identity to each other and had the same the post-translational modification – the removal of the C-terminal sequence –VVAPAEFK. The β peptides also had high sequence similarity and had their N-terminal methionine removed.

Many α and β polypeptides from photosynthetic bacteria have been sequenced and they have several structural features that are conserved. They consist of a single transmembrane α helical domain with an N-terminal cytoplasmic and C-terminal periplasmic domain (Tadros et al. 1987). Within the transmembrane α helical domain of these polypeptides, conserved histidine residues are located that bind the Bchl *a*. Due to this highly conserved primary structure feature, it is possible to assign a peptide as an α or β and align them with other photosynthetic bacteria. Figure 4 7 shows the sequences of the six *Mcr. purpuratum* LH2 polypeptides and their alignment with published antenna sequences to try and determine the B800 and B830 binding sites and hydrogen bonding. The first key similarity was the conserved histidine residues on the α and the β that coordinates with the central Mg^{2+} ion of the dimerised BChl *a*. The presence of an aspartic acid residue indicates the B800 BChl *a* binding site is most probably similar to that in *Phs. molischianum* as opposed to that of *Rps. acidophila*. There is a tryptophan residue at the C-terminus end of the β peptide, which is conserved throughout all the beta peptides of *Alc. vinosum* and *Mcr. purpuratum*. This residue is also conserved in *Phs. molischianum* and has been shown to participate in hydrogen bonding of the Bchl *a*.

Mcr. purpuratum has a unique B800-B830 complex, so it would make sense that it has a unique way of binding the dimerised Bchl *a*. There is a phenylalanine residue which, is seen in the *Phs. molischianum* B800-B820 is conserved between the three α polypeptides of *Mcr. purpuratum* and the α -5 of *Alc. vinosum* (a major component of the B820 complex) (Carey, Hacking et al. 2014). There is also a tyrosine residue, which is conserved in all the α peptides of *Mcr. purpuratum* and α -5 of *Alc. vinosum*. This tyrosine residue is also a possible hydrogen bonding site of the B830. The final amino acid residue that may take part in hydrogen bonding is a tryptophan, seen in all α polypeptides of *Mcr. purpuratum*. Tryptophan has been shown to form hydrogen bonds, which help “tune” the Qy absorption band of the dimeric BChl *a* in both *Phs. molischianum* and *Rps. acidophila* B850 complexes. Without a high-resolution crystal structure of the LH2 complex, it is difficult to preliminarily determine where the hydrogen bonding takes place.

Further work includes the use of the RP-HPLC to attempt to further separate α and β polypeptides and then run them separately on the MALDI-TOF. Fragmentation experiments can also be used to identify the peptides. The *pucBA2* KO should also be continued. By deleting any of the *pucBA* operons an obvious change to the absorption spectra should be visible. This will further confirm if these genes are expressed in the LH2.

Chapter 5 - Investigating whether the LH2 complex from *Mcr. purpuratum* can be synthesised in the absence of carotenoid

The aims of this chapter were to investigate the carotenoids from the LH2 complex from *Mcr. purpuratum*. The major aim was to create an LH2 complex without carotenoid by means of chemical inhibition and by genetic knock out. Studying LH2 complexes in the absence of carotenoids can be useful for energy transfer studies. The major carotenoid in *Mcr. purpuratum* is okenone, which has a very broad absorption peak. Carotenoidless mutant strains have been identified and isolated in several PNSB species (Sistrom and Clayton 1964, Davidson and Cogdell 1981, Ghosh, Hauser et al. 1988, Bartley and Scolnik 1989). It was established that the LH2 complexes are not assembled in the cells of carotenoidless mutants of these PNSB. There is some contradiction on the investigation of carotenoid biosynthesis and LH2 complex assembly in cells of purple bacteria. In the case of *Rps. acidophila* it is accepted that carotenoids play an important role both in assembly and in structure stabilisation of the LH2 complex (Papiz, Prince et al. 2003, Gall, Henry et al. 2005). On the other hand, there is work that supports that PSB can still form LH2 complexes in the absence or inhibition of carotenoid synthesis. This is seen with *Alc. vinosum* (Bril 1963, Hacking 2015) and with *Alc. minutissimum* (Makhneva, Bolshakov et al. 2008, Moskalenko and Makhneva 2012). This indicates that carotenoid functions have different weightings in different LH2 complexes. Not all LH2 are the same and understanding the differences is key for understanding how the system has adapted. As *Mcr. purpuratum* is a PSB and closely related to *Alc. vinosum* and *Alc. minutissimum*, there is a good promise that a stable LH2 complex can be produced without carotenoids.

5.1. Inhibition of Carotenoid Biosynthesis by Diphenylamine

Diphenylamine (DPA) inhibits the activity of the enzyme phytoene desaturase, (CrtI). This enzyme performs the progressive desaturation of phytoene to lycopene, preventing the early desaturation steps that create the conjugated double bond system (Young and Britton 2012). Inhibiting it causes a build-up of phytoene and related precursors (Jensen, Cohen-Bazire et al. 1958). The pathway can be viewed in the Introduction section 1.7.3. DPA also disrupts the biogenesis pathway that produces ubiquinol, making it toxic at high concentrations. This experiment was chosen due to the effects that were seen in many other photosynthetic bacteria (Cohen-Bazire and Stanier 1958, Moskalenko, Makhneva et al. 2005, Toropygina, Makhneva et al. 2005, Moskalenko and Makhneva 2012). This will provide information on the effect of the carotenoid okenone on the stability of the LH complexes. It is possible that *Mcr. purpuratum* could produce a carotenoidless LH2 complex or at least a carotenoidless LH1 complex.

5.1.1. Determining the effective DPA concentration

Initial small-scale experiments were designed to help narrow down the range of DPA concentrations to use before moving up to a larger scale. This was to ensure the most effective concentration would be used, that bacterium wasn't killed and that the carotenoid biosynthesis pathway was fully inhibited allowing the production of carotenoidless LH complexes. The concentration of DPA in other photosynthetic bacteria varied from 50 μM to 80 μM (Gall, Henry et al. 2005, Makhneva, Bolshakov et al. 2008, Hacking 2015).

DPA was added to the growth medium of *Mcr. purpuratum* to inhibit the carotenoid biosynthesis, as described in the Methods and Materials section 2.11. It can be seen in Figure 5-1 the colour of the cells varies depends on the different concentrations of DPA in 100 ml flat bottles. The contrast between the different treatments in comparison with the control can be seen. 20 μM and 40 μM are similar in colour, if only slightly paler. At 60 μM an orange tinge can now be seen in the culture, a sign that the DPA is affecting the carotenoid content of the cells. The carotenoids that are being produced and incorporated into the light-harvesting machinery have shorter conjugation lengths due to the inhibition of the phytoene desaturase enzyme. This makes them appear more orange during the visual assessment. The most distinctive change can be seen between 60 μM and 70 μM of DPA, where the culture is only very slightly pink tinged compared to its usual vibrant purple of the control. This indicates the cells are growing very poorly.



Figure 5-1: *Mcr. purpuratum* culture grown in the presence of DPA between 0 μM and 100 μM . The control culture (C) grew and produced the usual purple pigmented cells. There is no change in the appearance of the culture until 60 μM of DPA. In the presence of 60 μM DPA the culture produced begins to change the pink colour to orange. At 70 μM and 100 μM DPA the culture appears to have lost all but a very faint colour.

Absorption spectra of DPA treated and untreated whole cells were recorded to preliminarily confirm the presence of the light-harvesting complexes and carotenoids (Figure 5-2) *Mcr. purpuratum* has an absorption of 830 nm, which corresponds to the dimeric BChl *a* of the LH2 complex. The shoulder at 870 nm is associated with the LH1- RC complex and the broad peak at ~500 nm is the carotenoid okenone. This was shown in the introductions chapter of this work

and in the LH2 purification results chapter. These can be seen in the absorption spectra of the control culture (Figure 5-2). In cells grown under the same growth conditions but in the presence of different concentrations of DPA changes in the okenone, the dimeric BChl *a* of the LH2 and the LH1-RC peaks are observed. After growth in the presence of 70 μM of DPA, the broad okenone peak at $\sim 500\text{ nm}$ has been flattened. This indicates that the carotenoid biosynthesis pathway has been strongly inhibited. The peaks seem to be blue shifted, which is expected due to a reduction in the number of conjugated double bonds. The spectra in Figure 5-2 have been normalised at 830 nm, the Q_y absorption, and because of this, it can be clearly seen that the highest concentration of DPA, 100 μM , has a negative effect on both the 830 nm peak of the LH2 and the 875 nm of the LH1. This could be due to the toxicity of DPA at higher concentrations or the lack of formation of the LH complexes due to the lack of carotenoid present in them. The spectra seen in Figure 5-2 reflect the colour differences observed in Figure 5-1. The control, 20 μM and 40 μM all have a similar absorption with a high 830 nm peak, 875 nm shoulder and broad okenone peak at $\sim 500\text{ nm}$. At 100 μM there is a very small 830 nm peak and no 875 nm shoulder anymore, indicating the LH1 complex is not forming. This is unusual as it should be stable in the absence of O_2 . The DPA had a very negative effect on the culture, causing poor growth due to the toxicity.

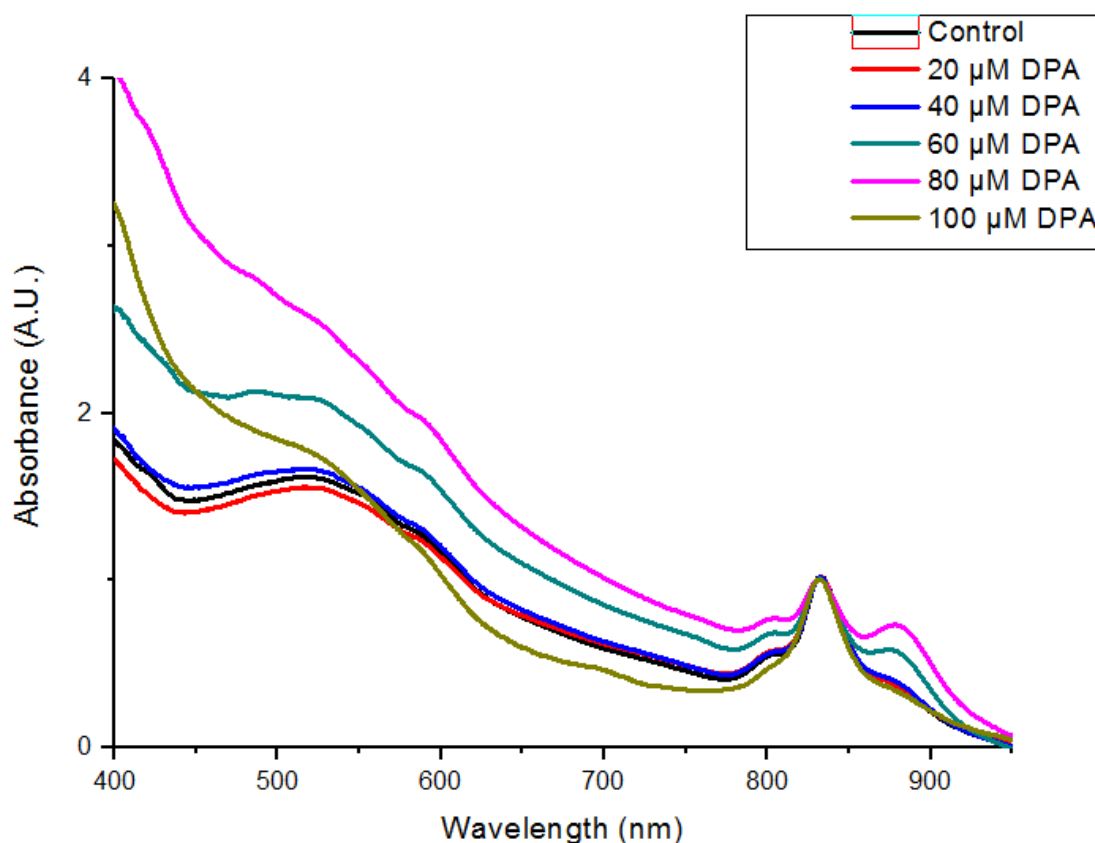


Figure 5-2: The absorption spectra normalised at the Q_y 830 nm showing the effect of different concentrations of DPA on *Mcr. purpuratum* for the small scale test. The carotenoid peak of okenone can be seen in the region between 450 nm and 550nm. The Q_y of the LH2, seen at 830 nm, decreases in intensity as the concentration of DPA increases. The LH1-RC shoulder at 875 nm, disappears entirely at 100 μM . It can be seen with the spectra normalised at 830 nm that the amount of LH1 to LH2 increases.

5.1.2. Large scale production of DPA treated cells

The next stage was to scale up to 500 ml growth bottle and purify the LH complexes. This meant that the individual spectra and carotenoid content of the LH2 and LH1 could be examined. The concentrations of DPA used were 0 μM (control), 40 μM , 60 μM and 80 μM , as the small scale tests indicated that this was a good range. Photographs of the whole cells can be seen in Figure 5-3. As previously shown in the small-scale experiments, the control culture grew and produced pigmented cells that were the typical purple colour known to *Mcr. purpuratum*. This was also the case for the 40 μM DPA culture. In the presence of 60 μM DPA the colour of the culture appears to change to a more orange, as it had with the small scale tests. At 80 μM the culture appears to have lost all but a faint pink colour, which has a grey tint to it. This indicates very poor growth and the grey/blue tint may be BChl *a* or phytoene. In the range of DPA concentrations between 60-80 μM the level of inhibition can be easily assayed by eye. These cells were then harvested and the membranes prepared. The absorption spectrum of the membranes can be seen in Figure 5-4. The difference in the colour of the culture, seen in Figure 5-3, is reflected in the absorption spectra of the membranes. It can be seen at 60 μM and 80 μM of DPA there is a strong reduction in the intensity of the LH2 830 nm peak and a flattening of the Okenone peak at ~500 nm. This agrees with the smaller scale experiments that between 60 μM to 80 μM of DPA that phytoene desaturase is being inhibited and therefore the production of okenone. However, the carotenoid inhibition is affecting the LH2 complexes produced. This may be either directly through unknown effects on the polypeptide production or due to the stability of the LH2 complex. This means that the *Mcr. purpuratum* LH2 complex may not be stable enough to exist without carotenoids present.

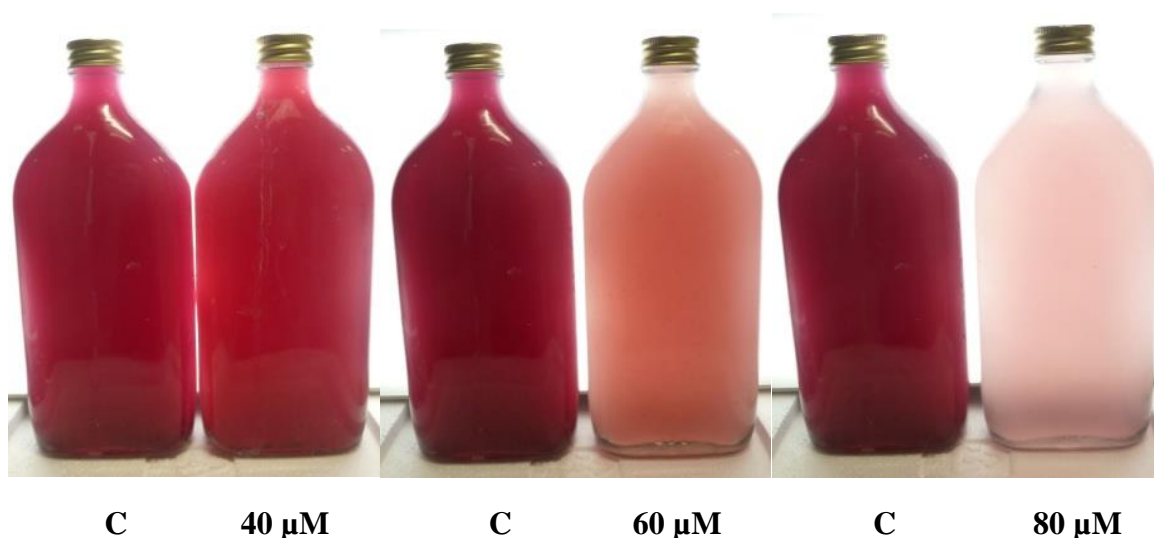


Figure 5-3: *Mcr. purpuratum* culture grown in the presence of DPA at 0 μM (C), 40 μM , 60 μM and 80 μM . The control culture grew and produced pigmented cells that were the typical purple colour. There is no noticeable difference observed at 40 μM DPA. In the presence of 60 μM DPA the colour of the culture appears to change to a more orange. At 80 μM the culture appears to have lost all but a faint colour, which has a grey tint to it. This indicated that there is a very low to negligible level of carotenoids.

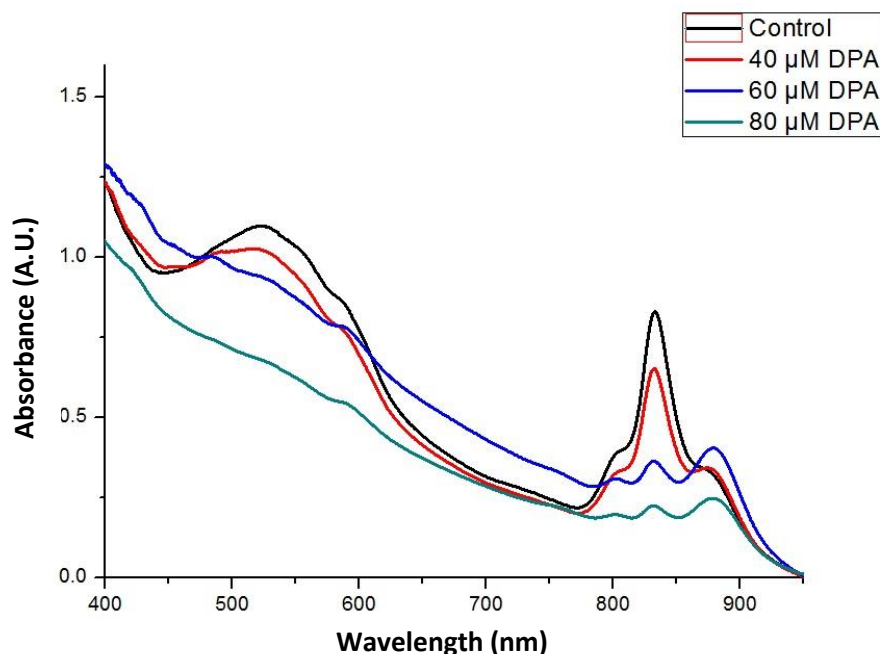


Figure 5-4: The absorption spectra of *Mcr. purpuratum* membranes grown in the presence of DPA at 0 μM (Control), 40 μM , 60 μM and 80 μM . A strong decrease in the 830 nm peak of the LH2 complex can be seen as the concentration of DPA is increased, as well as the ~500 nm peak of the carotenoid okenone. The LH1-RC appears to go from a shoulder to a peak at 875 nm at 60 μM of DPA.

In order to determine if there is preferential incorporation of carotenoid into one LH over the other, the membranes must be solubilised and the LH complexes separated using SDG centrifugation. It has been shown previously in this study that the LH1-RC complex of *Mcr. purpuratum* is unstable in the detergent LDAO so DM was used to solubilize the membranes. The light-harvesting complexes were separated by overnight SDG centrifugation. Figure 5-5 shows the visual distinctions between the SDG for each concentration of DPA used and the separation of the LH complexes. The LH2 complex is the upper coloured band, which can be clearly seen to be purple/pink coloured in the control and 40 μM . The purple colour is completely gone from 60 μM and 80 μM . At 60 μM the LH1-RC band is much stronger, whilst the LH2 band no longer appears as a tight pink band, but as an orange dispersed one. This is similar in appearance to the free pigment band, which is sometimes seen in SDG above where the LH2 band is normally seen. This implies that in the absence of the LH2 complex the LH1-RC is produced in much higher concentrations. At 80 μM the LH1-RC has shifted away from an orange colour to a brown. It still appears quite concentrated but is no longer a tight band of colour as seen in the lower concentrations of DPA. This implies that 80 μM of DPA is harmful to LH1-RC and is causing it to begin to breakdown.

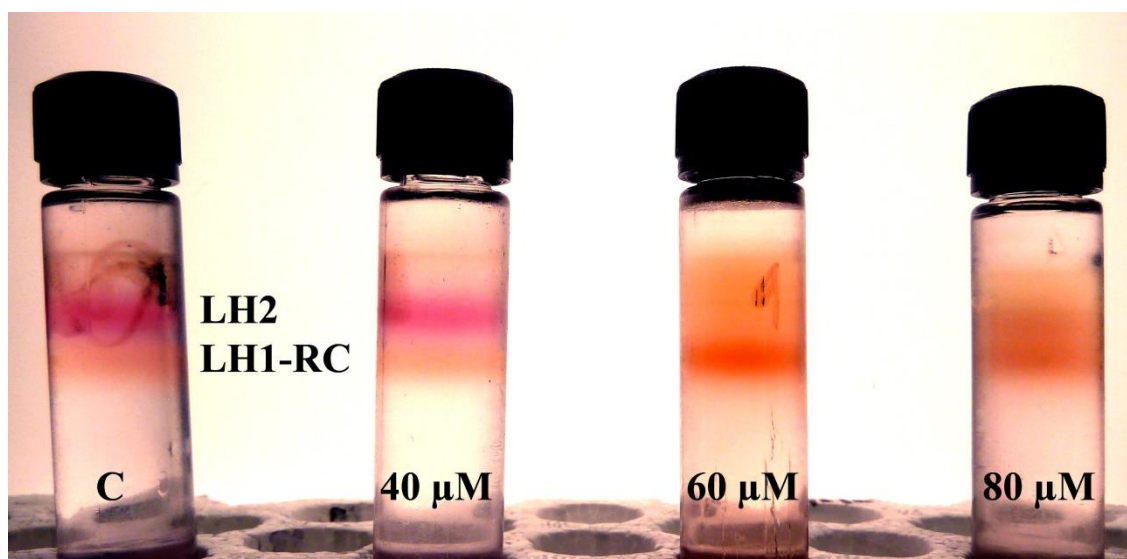


Figure 5-5: *Mcr. purpuratum* LH complexes grown in the presence of DPA at 0 μM (Control), 40 μM , 60 μM and 80 μM . *Mcr. purpuratum* membranes were solubilized in DM and separated by SDG centrifugation. The loss of the pink colour in the LH2 complex can be seen at 60 μM and 80 μM , whilst the orange band of the LH1-RC is strongest at 60 μM

The LH2 and LH1-RC were removed and the individual absorption spectrum for each of the LH complexes at the different DPA concentrations was recorded. It can be seen when looking at the spectrum of the LH2 complex in Figure 5-6A that the 830 nm peak has completely degraded. This information combined with that images from the SDG imply that the LH2 complex of *Mcr. purpuratum* is unable to form in the absence of carotenoid. The LH2 complex doesn't form carotenoid, and the cytotoxic effects would kill the cell, not just the LH2. The LH1-RC, on the other hand, seems not to be as affected by the presence of the DPA. The LH1-RC starts to be affected by the toxicity of the DPA at high concentrations of 80 μM , but it is also possible that it is not able to form without carotenoid either. There is still a lot of carotenoid present in the LH1-RC clearly showing that the carotenoid is being preferentially incorporated into the LH. It may indicate that the LH1 still needs carotenoids present to form. There is still strong orange pigment shown in the SDG bands and the absorption spectrum shows peaks in the 450-550 carotenoid range in all crude fractions, which indicates poor or incomplete carotenoid biosynthesis inhibition.

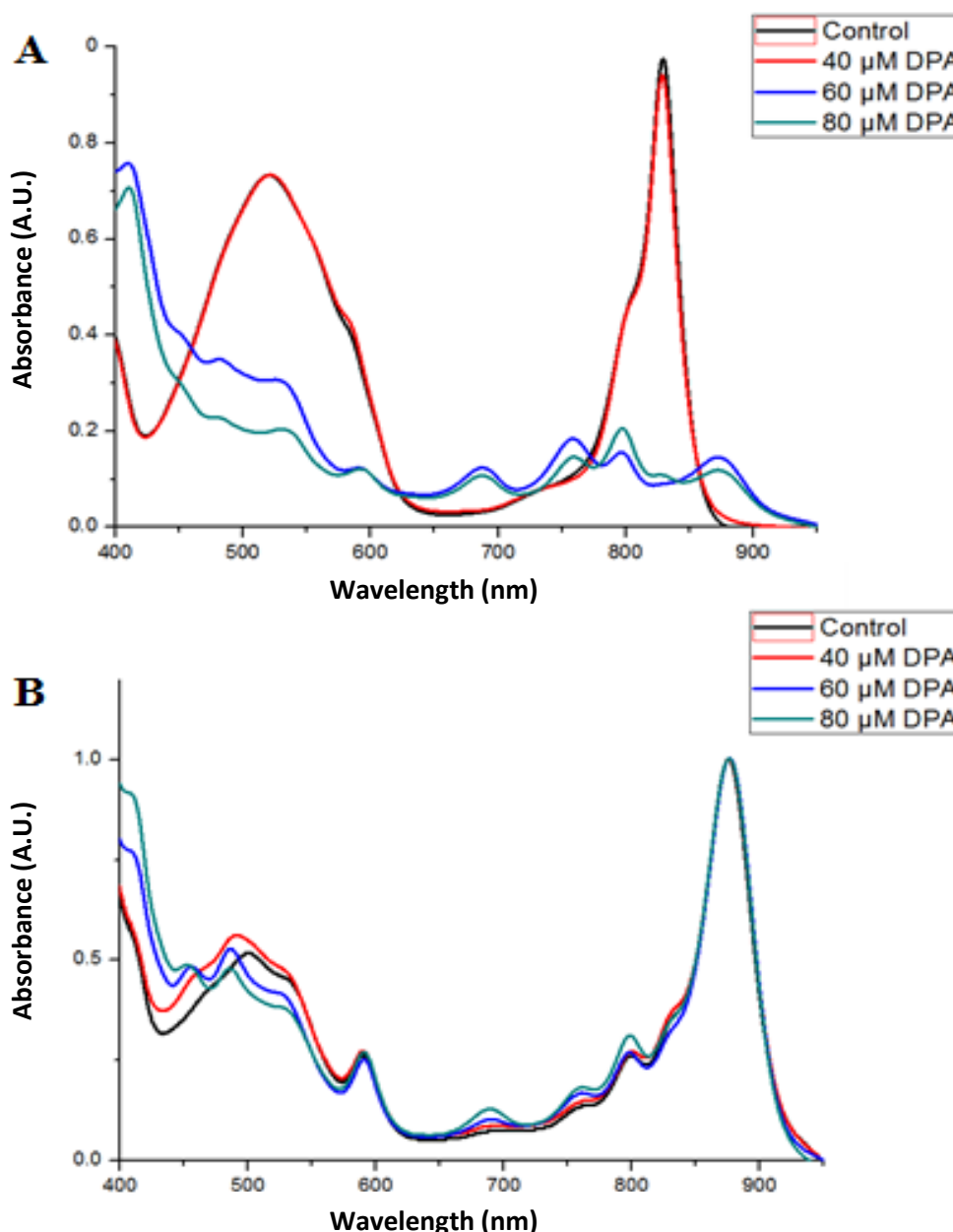


Figure 5-6: Absorption spectrum showing the effect of different concentrations of DPA on the LH complexes of *Mcr. purpuratum*. A) LH2 complex. The peak at 830 nm completely disappears at 60 μ M. The peaks at 450-550 nm carotenoid also decrease with increased DPA concentration but they do not flatten completely. This indicates that as the DPA prevents the carotenoid from being synthesised, the LH2 is prevented from forming. B) LH1-RC. The 875 nm peak of the LH1-RC appears to be unaffected by the increased concentrations of the DPA. However, there are still clear signs that there is carotenoid present by the peaks at 450 – 550 nm.

These results are interesting because they imply that *Mcr. purpuratum*, which is a PSB, is unable to form a stable LH2 complex in the absence of carotenoid. As mentioned in the introduction of this chapter, other PSB have been shown to be able to form LH2 without carotenoid (Bril 1963, Makhneva, Bolshakov et al. 2008, Moskalenko and Makhneva 2012). These seem to be exceptions to the rule, as most purple photosynthetic bacteria cannot form LH2 complexes without carotenoid. *Mcr. purpuratum* appears to be in this same category.

At this stage, it is suggested that the LH1-RC can exist without carotenoid. However, higher concentrations of DPA are cytotoxic to the cell cultures, resulting in their death. Most LH1

complexes are able to form in the absence of carotenoid. The investigation was decided to be continued using another method.

5.2. Trials to Grow *Mcr. purpuratum* on Agar Plates and Antibiotic Resistance

The availability of the complete genome sequences of *Mcr. purpuratum* is a crucial requirement for a detailed analysis of their physiological and ecological properties. It allows suitable methods allowing easy and efficient genetic manipulation of the genome. However, in order to perform this genetic manipulation *Mcr. purpuratum* culture had to be grown on 1.5% agar plates. This had not been attempted previously and so several different variations of media were attempted. The liquid media recipe is complex with a total of six different solutions, of which three cannot be autoclaved (see appendix). LB, modified LB with extra salt, and LB with sulphur were tried but failed to produce any colonies. It was found to grow on plates made from a modified version of the *Mcr. purpuratum* liquid media recipe. Solution 1 was prepared and autoclaved as normal with the addition of 1.5 % agar (w/v). The other solutions were filtered and sterilised as normal and added to the agar/solution 1 mix when it had cooled (just before the agar set). Total volumes of all solutions used for 50 ml agar plates can be seen in the appendix. Figure 5-7 shows dilutions of OD₈₃₀1 culture, from neat to 10⁻⁵ adding 100 µl in total to the plate. Single colonies can clearly be seen at the highest dilution of 10⁻⁵.

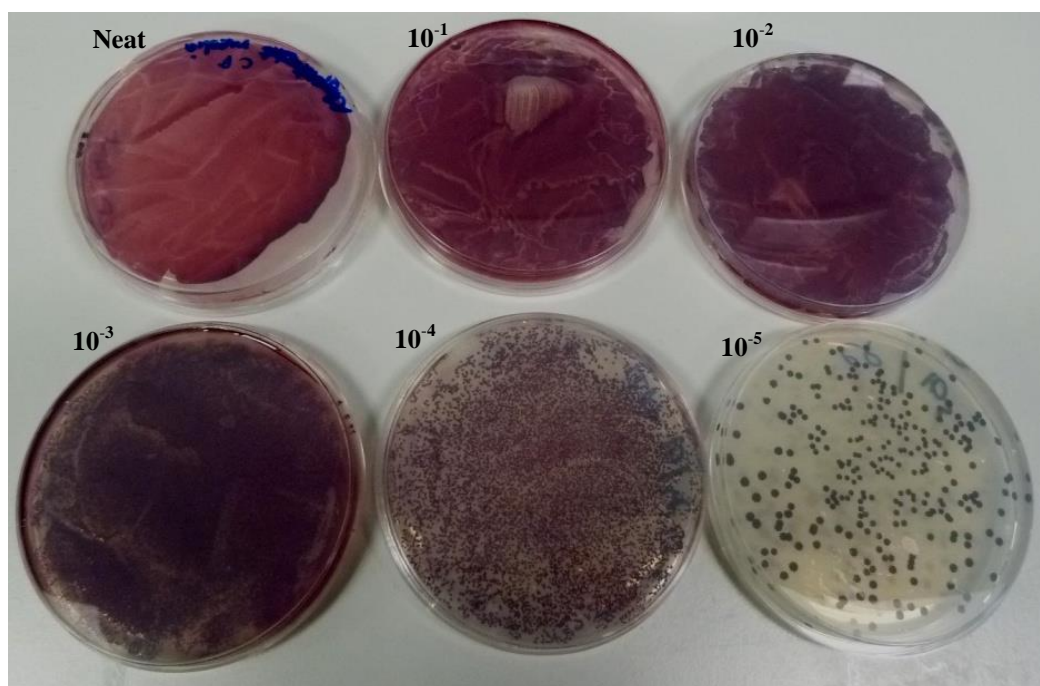


Figure 5-7: *Mcr. purpuratum* growing on 1.5% agar plates in a series of culture dilutions. Labels correspond to the serial dilutions investigated with Neat = OD 1 of undiluted culture.

The antibiotic susceptibility of *Mcr. purpuratum* species was then investigated to identify useful selective markers. This would be needed for experiments that required mutants to be created.

For the antibiotic trials, three different concentrations of ampicillin, kanamycin, chloramphenicol, tetracycline and streptomycin were set up on the *Mcr. purpuratum* media agar plates. The results can be seen in Figure 5-8.



Figure 5-8: Antibiotic trials of *Mcr. purpuratum*. It is clear where the growth of the bacteria is prevented when the antibiotic plates are viewed alongside the control plate. Growth is completely halted in the presence of all antibiotics apart from ampicillin where some growth is still observed at 100 µg/ml. Kanamycin and chloramphenicol completely kill the bacteria at their lowest concentrations, 10 µg/ml and 100 µg/ml respectively.

Though affected by ampicillin, *Mcr. purpuratum* can still manage to grow in its presence, even at the highest concentration of 100 µg/ml. Growth on tetracycline and streptomycin plates is halted at higher concentrations; 75 µg/ml and 50 µg/ml respectively. However, growth on the kanamycin and chloramphenicol plates is prevented at the lowest concentrations. It has been reported that several antibiotics, including tetracycline, can be affected by their chemistry by high salt concentrations (Lambs, Venturini et al. 1988). It is not the stability of the antibiotic that is affected but a decrease the membrane permeability of a cell and the bioavailability of this antibiotic (Loftin, Adams et al. 2008). This is a possibility here due to the high salt concentration of the *Mcr. purpuratum* media. These results mean that in later experiments plasmids with kanamycin and chloramphenicol antibiotic resistant cassettes can be used for cloning.

5.3. Deletion of the phytoene desaturase (CrtI) gene

New information has been made available with the elucidation of the pathway for Okenone (Vogl and Bryant 2011), which can be seen in the Introduction chapter. With this information and the sequencing of the *Mcr. purpuratum* genome (Grigoriev, Nordberg et al. 2011) it was possible to genetically knock out carotenoid synthesis genes. The *CrtI* gene encodes for the enzyme phytoene desaturase, the same enzyme that DPA inhibits.

The removal of the *CrtI* gene would result in the build-up of phytoene, stopping the synthesis of okenone and therefore the loss of the deep purple colour of the *Mcr. purpuratum* culture. This part of the study is a compliment to the DPA trials described in this report and to attempt to overcome some of the limitations that were implemented. The creation of a carotenoid mutant through DNA ‘knock-out’ would remove these limitations and produce fully carotenoidless LH2 and LH1-RC complexes. As mentioned in the DPA section it was unclear whether either of the LH complexes from *Mcr. purpuratum* would be able to form at all in the absence of carotenoid.

5.3.1. Primer design and creation of the CrtI KO insert

Mcr. purpuratum genomic DNA was extracted as outlined in the Materials and Methods section 2.10.2. As with the *pucBA2* KO, the first stage was to design primers that would amplify up an upstream fragment and a downstream fragment surrounding the *CrtI* gene. A summary of the location of these primers in relation to the *CrtI* gene can be seen in Figure 5-9. A restriction enzyme site, Eco R I and a Hind III was designed into primers 1 and 4, respectively. This was vital for later on in the cloning process. Primers 3 and 4 incorporated the start codon of the *CrtI* gene in their sequences as well as the stop codon. This ensured that they would share an overlap of 18 base pairs, which would be used to anneal them together. The upstream fragment’s length was calculated to be 500 bp and the downstream fragment was 630 bp.

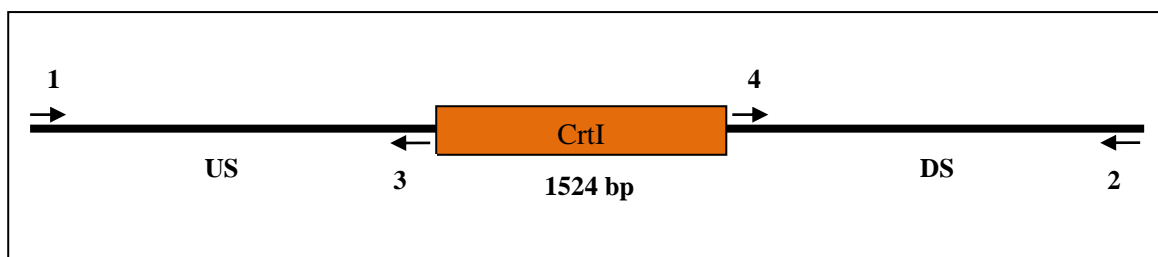


Figure 5-9: Diagram showing the location of the primers used to knock out the *CrtI* gene. The numbers correspond to the names of the primers in Table 2-3 on the Methods and Materials chapter. US- Upstream, DS- Downstream

The first stage in the knock out of the *CrtI* was the amplifying of DNA fragments upstream and downstream of the gene. Phusion PCR program was created on a C-1000 thermal Cycler from Bio-Rad. The method for this can be read in the Materials and Methods, section 2.11.2.1. The results of this Phusion PCR can be seen on the agarose gel in Figure 5-10. Both the upstream fragment and the downstream fragment can be seen at the predicted calculated sizes, 500 bp and 630 bp respectively.

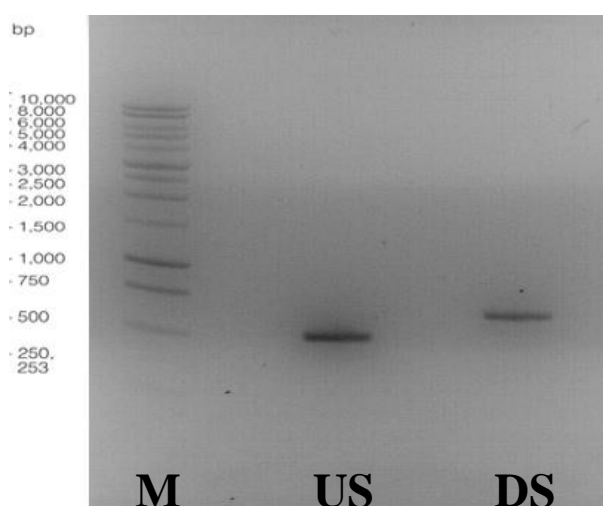


Figure 5-10: Agarose gel of the amplified upstream (UP) and Downstream (DN) DNA fragments for the *CrtI* KO M= Molecular marker, US fragment was amplified using Primers 1 and 3 and downstream fragment was amplified using primers 2 and 4. Both the upstream fragment and the downstream fragment can be seen at the predicted calculated sizes, 500 bp and 630 bp respectively.

The DNA extracted from these fragments was amalgamated into a full *CrtI* KO insert through the use of the SOE method followed by another Phusion PCR. This series of programs took advantage of the overlap in both fragments to join them together to form one continuous strand, which did not contain the *CrtI* gene. The PCR product was run on an agarose gel and the results can be seen in Figure 5-11. The fragment appears at approximately 1100 bp, equalling the predicted size of the upstream and downstream fragments joined together.

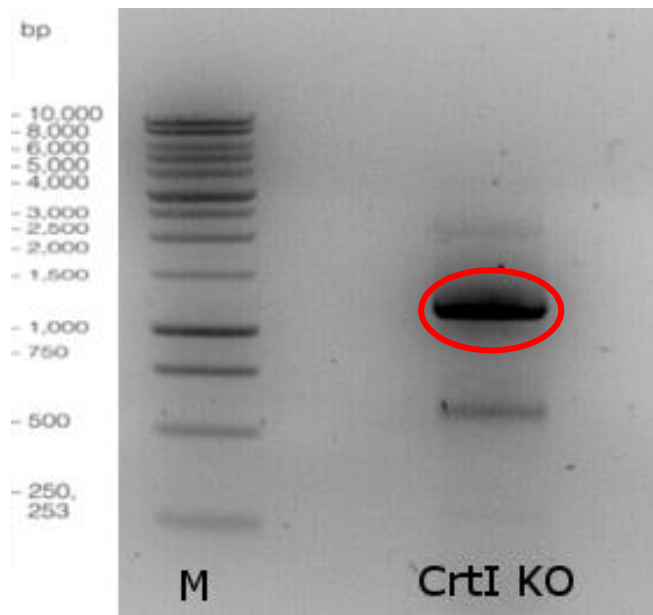


Figure 5-11: Agarose DNA gel image of the *CrtI* KO PCR. The resulted fragment circled at 1100 bp is the upstream and downstream fragment previously amplified now joined together as a single fragment.

5.3.2. Transformation into pJET 1.2/blunt

This *CrtI* KO was confirmed to be correct by sequencing. The *CrtI* KO fragment is blunt ended, so it was cloned into pJET1.2/blunt and transformed into JM 109 competent *E. coli* cells. A schematic of the *CrtI* KO--pJET1.2 can be seen in Figure 5-12.

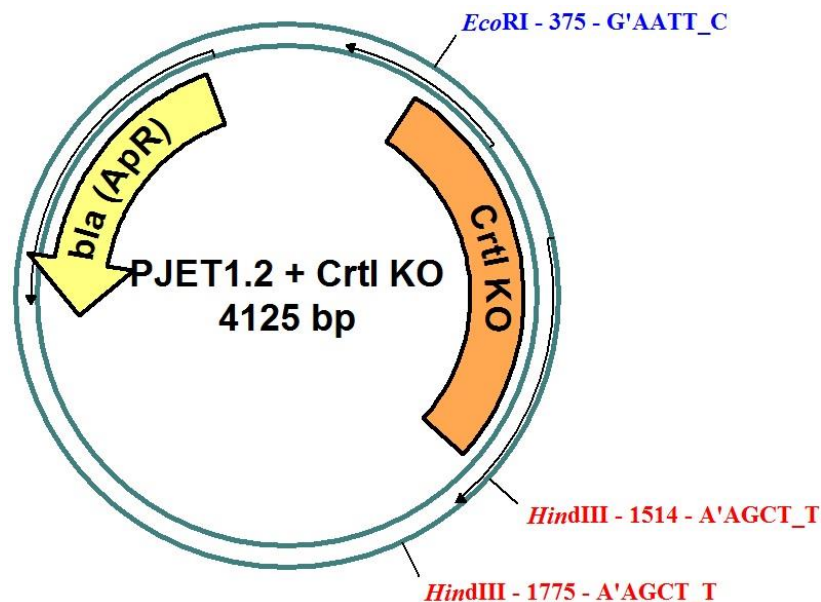


Figure 5-12: Diagram showing the pJET 1.2 vector with the *CrtI* KO insert. The features of the pJET vector include the *bla* (ApR) = β -lactamase gene conferring resistance to ampicillin and used for selection of the recombinant, rep (pMB1) = Replicon from the pMB1 plasmid, which is responsible for replication of the plasmid. Not shown is the *eco47IR* gene that has been split and rendered unfunctional by the inclusion of the *CrtI* KO. It is a lethal gene that enables positive selection of the recombinants. The restriction enzyme sites of the insert, EcoRI and HindIII can also be seen clearly.

Four colonies were successfully grown up in liquid LB and the *CrtI* KO-pJET1.2/blunt plasmid extracted. The four different plasmids were then digested separately, using Eco I and Hind

III. A small sample of the digestions was run on an agarose gel, which can be seen in Figure 5-11. Colonies 2, 3 and 4 have been digested correctly, with the Eco I and Hind III restriction enzymes cutting once each on their restriction sites. This results in the fragment size of approximately 1100 bp for the *CrtI* KO, as discussed previously, and another fragment that is approximately 3000 bp for the cut pJET1.2/blunt plasmid. Another very faint band at 200 bp can be seen, which is the result of the extra Hind III site present on the pJET1.2/blunt plasmid (Figure 5-13) also being cut. In the case of colony 1, only this extra Hind III site has been cut, resulting in a fragment size of ~1500 bp.

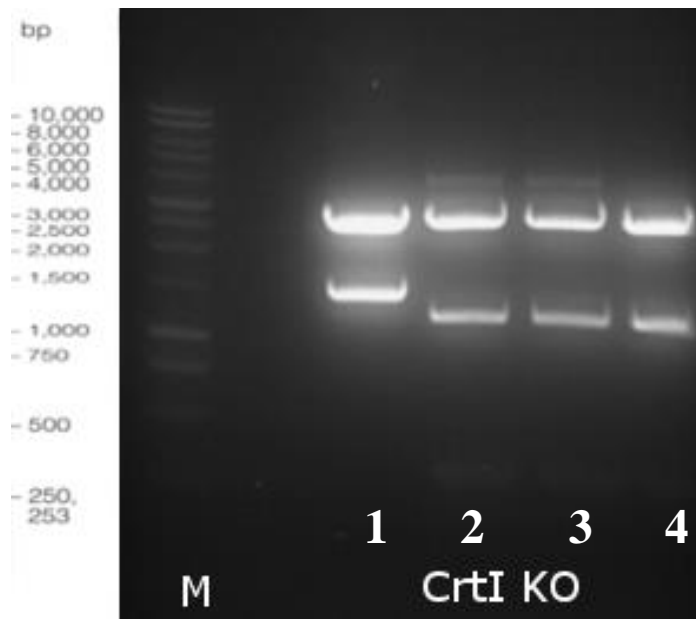


Figure 5-13: Agarose DNA gel of the Eco I and Hind III digestion of the *CrtI* KO-pJET1.2/blunt plasmid for the 4 different colonies selected. Colony 2, 3 and 4 have the correct fragment size of ~1100bp. These colonies were taken on for further process.

5.3.3. Ligation of the *CrtI* KO into Mobsac

The digestion of the *CrtI* KO-pJET1.2 by Eco I and Hind III results in 'sticky ends'. The pk18mobsacB vector also contains HindIII and EcoRI restriction sites (Figure 5-14). When this vector is digested with these same enzymes it allows easy ligation of the *CrtI* KO into the pK18mobsacB vector.

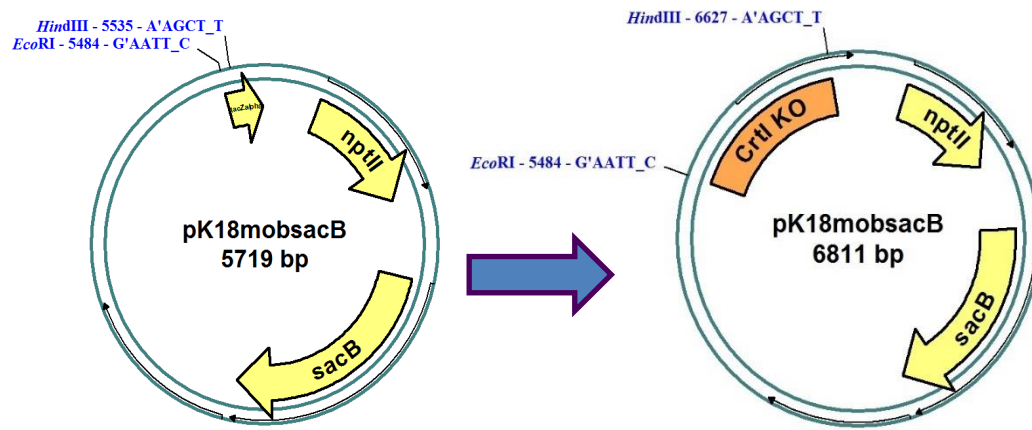


Figure 5-14: Diagram showing the pK18mobsacB vector before and after the ligation of the *CrtI* KO insert. The features of the PJET vector include the *nptII* = neomycin phosphotransferase II, which confers resistance to aminoglycoside antibiotics such as kanamycin and is used for selection of the recombinant, *SacB* = Expression from *sacB* confers sensitivity to sucrose in a wide variety of gram positive and negative bacteria and thus has been used as a negative selectable marker. *LacZalpha* - B-galactosidase. In the presence of IPTG and X-gal, colonies containing the insert will be white, and those without it will be blue. The restriction enzyme sites of the insert, *EcoRI* and *HindIII* can also be seen clearly.

pK18mobsacB + *CrtI* KO was then transformed into JM 109 strain competent *E. coli* cells. Transformed cells were then plated onto LB plates enriched with kanamycin, IPTG and XGAL to induce the lac operon, and grown overnight at 37 °C. In the presence of IPTG and X-gal, colonies containing the insert will be white, and those without it will be blue due to the *CrtI* KO insert interrupting the *LacZalpha* gene within the pK18mobsacB (Figure 5-14). The kanamycin ensures only colonies containing the pK18mobsacB vector will grow. Five colonies were picked and grown up separately in LB + kanamycin, they were then plasmid prepped and digested. A DNA gel confirmed that all of the 5 colonies had successfully incorporated the pK18mobsacB + *CrtI* KO.

5.3.4. Conjugation of the pK18mobsacB + *CrtI* KO with *Mcr. purpuratum*

Colony 5 was selected and sent for sequencing. Once this was confirmed conjugation of *Mcr. purpuratum* with the pK18mobsacB + *CrtI* KO in λ pir occurred. This strain of cells has been modified so when it is used as specific host strain into what the transposon vector DNA is transformed, the transfer occurs by biparental mating. They can utilise any gram-negative bacterium as a recipient for conjugative DNA transfer. A range of dilutions were tried as described in the Materials and Methods section 2.11.5. The results from earlier in this chapter ensured that that *Mcr. purpuratum* had no resistance to kanamycin. This meant that experiments with plasmids with kanamycin antibiotic resistant cassettes can be used for cloning, such as the pK18mobsacB. *Mcr. purpuratum* is unable to grow in the presence of kanamycin under normal conditions. If the pK18mobsacB vector was incorporated into then they would adopt kanamycin resistance. The cells were then spread on a 1.5 % LB agar plate that contained kanamycin. The plate was left to grow at 37 °C overnight and then 2 colonies were picked from the plate and each grown up separately in 5 mls of LB that contained kanamycin. Five dilutions were made using the LB culture containing the

pK18mobsacB + *CrtI* KO in λ pir cells and *Mcr. purpuratum* fresh cultures, 1:5, 1:10, 1:50, 1:100 and 1:200. Each of the conjugation dilutions was pipetted onto an LB agar plate and grown at 37 °C for 6 hours. After 6 hours had passed a scraping of each conjugation mixture was taken and resuspended in 200 μ l of *Mcr. purpuratum* media. All the dilutions were plated in duplicates, using 100 μ l per plate. The control was plated on two CP media plates, one containing kanamycin and one without. These were grown under anaerobic conditions in the light.



Figure 5-15: Conjugation of *Mcr. purpuratum* with the pK18mobsacB + *CrtI* KO in λ pir. A range of dilutions were tried as described in the methods previous. The control plate (C) is wild type (WT) *Mcr. purpuratum* grown on media containing none of the antibiotic kanamycin. The other control plate (C + kanamycin) shows WT *Mcr. purpuratum* grown on a media containing the antibiotic kanamycin. *Mcr. purpuratum* naturally has no resistance to this antibiotic, shown in previous result chapter 3. These control plates ensure there is nothing wrong with the culture that was used for the conjugations and that the results seen are correct. It can be seen that all of the different dilutions for the conjugations were successful, with purple colonies present on all.

It can be seen from the images in Figure 5-15 that all of the conjugations were successful. The control shows that wild-type (WT) *Mcr. purpuratum* was unable to grow on the media plate containing kanamycin (C + kanamycin). It grew on a media plate containing no kanamycin (C). Single colonies were then picked from these conjugation dilution plates and grown in 8 mls of CP media with kanamycin. Four dilutions of this culture were made and plated on CP media agar plates made with 10% sucrose

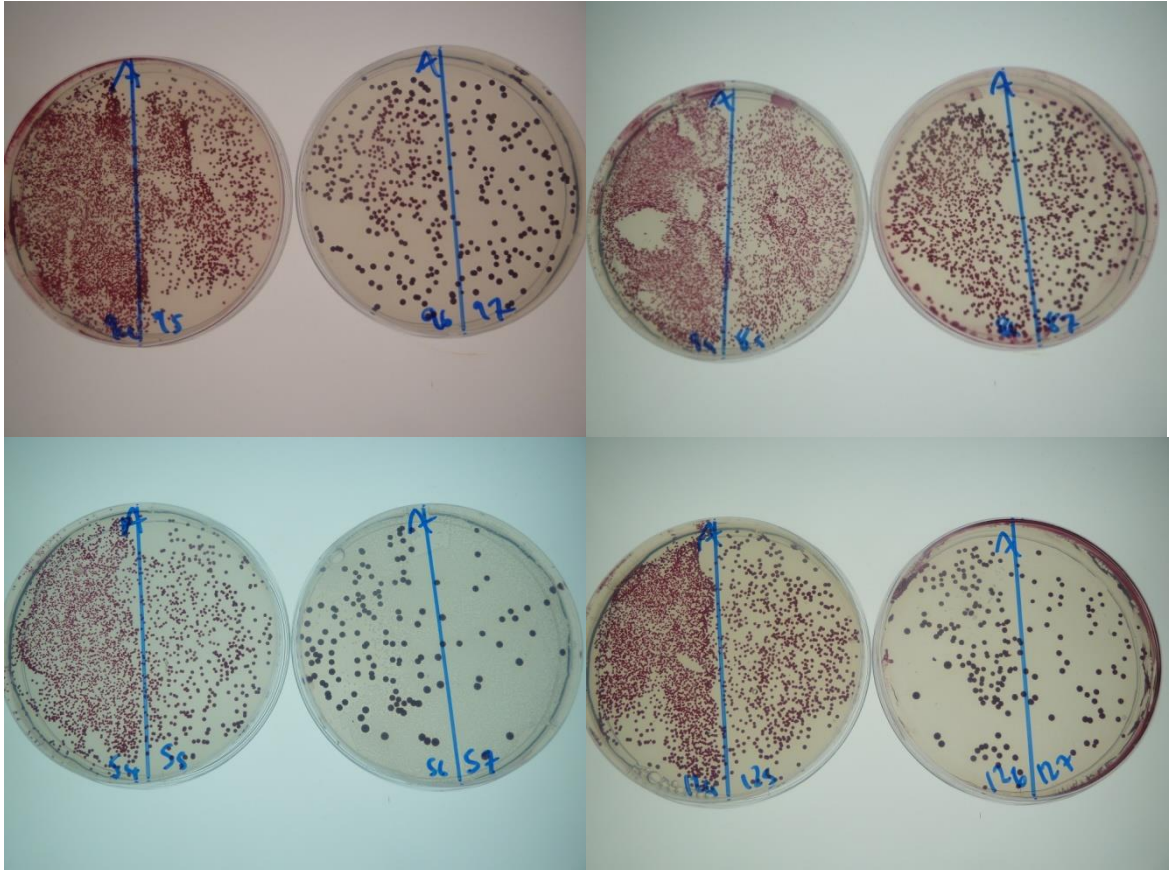


Figure 5-16: Sucrose dilutions plates of the *Mcr. purpuratum* *CrtI* KO. The *SacB* gene present in pK18mobsacB acts as a negative selectable marker. Expression from *sacB* confers sensitivity to sucrose in bacteria. 5

The *SacB* gene present in pK18mobsacB acts as a negative selectable marker. Expression from *sacB* confers sensitivity to sucrose in bacteria. This means that in the presence of sucrose the vector should fail to thrive, allowing allelic recombination to occur and the *CrtI* KO DNA fragment to become incorporated into the chromosomal DNA of the recipient *Mcr. purpuratum*. Single colonies produced were then grown on both CP media agar with kanamycin and CP media with no antibiotic present.

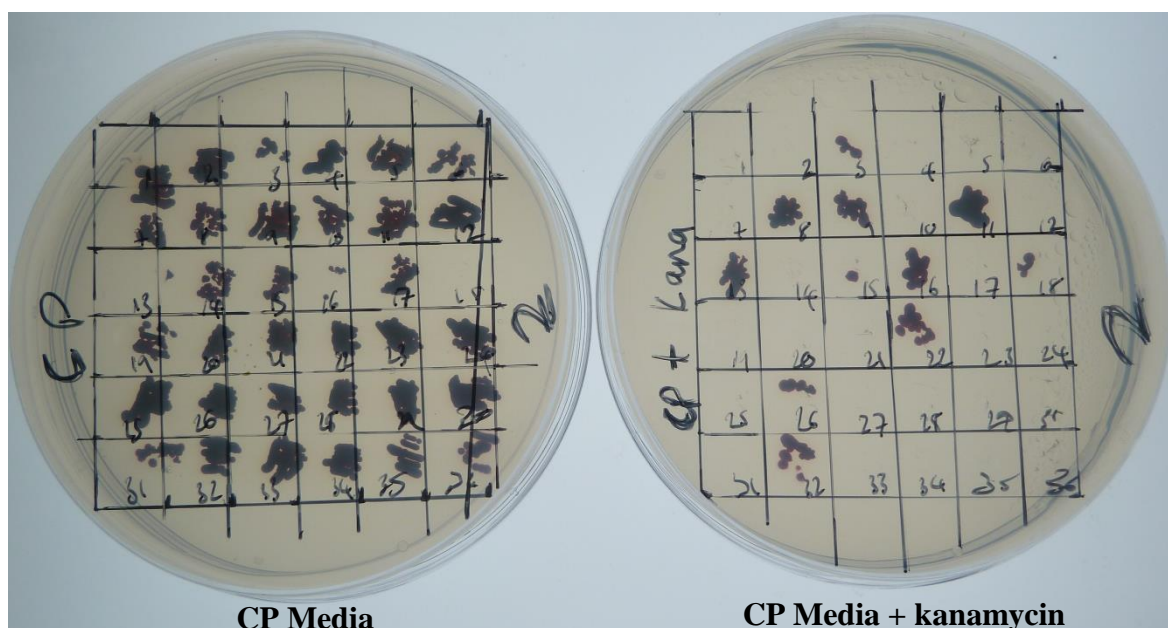


Figure 5-17: Grid plates to test for the presence of the vector pk18mobsacB. The single colonies picked from the sucrose plates were streaked onto the two agar plates, one supplemented with kanamycin as a negative control. Colonies that grew only on the agar plate with no kanamycin did not contain pk18mobsacB. *CrtI* KO mutant would be expected to have blue/grey colonies since the production of okenone has been inhibited. Only purple, wild-type colonies are seen.

If the *CrtI* KO had been incorporated into the *Mcr. purpuratum* we would expect to see blue/grey colonies. Purple colonies mean that the carotenoid okenone is still being produced via its biosynthesis pathway. Unfortunately, none of these conditions yielded blue, carotenoidless colonies for any of the conjugation colonies under any of these conditions. Different growth conditions of the sucrose plates were attempted to try and optimise the production of the *CrtI* KO mutant.

4. The plates were grown anaerobically in the dark for 24 hours before being exposed to light.
5. The plates were grown aerobically in the dark.
6. The plates were grown anaerobically in the light.

A repeat of the entire procedure from the start was attempted with the same results. There are several possible explanations for these results. The first is that something is wrong with the molecular biology method. It is possible that one, or more, of the steps involved in the creation of the *CrtI* KO, is incorrect. To solve this would involve going back to very beginning of the process. This would involve creating new primers and trying different cloning vectors.

5.4. Summary and Analysis

DPA inhibition studies indicate that *Mcr. purpuratum* cannot produce LH2 or LH1 complexes in the absence of carotenoids. It has been mentioned in the introduction of this chapter that is it uncommon for LH2 to form in the absence of carotenoid. The exceptions to this rule are seen with *Alc. vinosum* (Bril 1963, Hacking 2015) and with *Alc. minutissimum* (Makhneva, Bolshakov et al. 2008, Moskalenko and Makhneva 2012). The LH1-RC can usually form without carotenoid. This

is because carotenoids are of key importance for photo quenching and not structural stability in the LH1. However, in the LH2 complex the carotenoids have a more important role in the structural stability of the molecule (Frank and Cogdell 1996).

The more recent work on *Alc. vinosum* investigated the effect of DPA on the different LH2 complex that can be produced under differing growth conditions (Hacking 2015). The B800-B850 LH2 complex was able to form under carotenoid biosynthesis inhibiting conditions. However, the B800-B820 appears not to be structurally stable without carotenoid as it does not form in the presence of DPA. The B800-B830 LH2 of complex of *Mcr. purpuratum* may be more like this B800-B820 complex than to the B800-B850 complex.

It was shown that *Mcr. purpuratum* could be grown on 1.5% agar plates, using a modified recipe of the liquid culture. Resistance to the antibiotics ampicillin, tetracycline and streptomycin was observed, but kanamycin and chloramphenicol prevented bacterial growth strongly. These results will be useful and important for molecular biology experiments, as plasmids with kanamycin and chloramphenicol antibiotic resistant cassettes can be used for cloning. It is thought that increased resistance to kanamycin compared to the other antibiotics is due to mechanism of action. Kanamycin works by interfering with protein synthesis. It binds to the 30S subunit of the bacterial ribosome leading to incorrect alignment with the mRNA and non-functional peptide chains (Pestka 1974). In comparison, ampicillin acts as an irreversible inhibitor of an enzyme involved in the third and last stage of bacterial cell wall synthesis (Law et al. 2014). This means that the enzyme synthesis is not blocked and more can be produced, eventually out competing the antibiotic inhibitor. This is why we see decreased ampicillin resistance with increased concentration of the antibiotic.

It is currently not known at this stage if a *CrtI* KO strain of *Mcr. purpuratum* is possible. The results of the DPA trials imply that the LH2 cannot form without okenone. There is the possibility of a mistake in one of the stages of the creation of the KO. To remedy this, new primers will be designed to create a new *CrtI* KO insert. An alternative subvector can also be used to amplify the insert for incorporation into pK18mobsacB. Unfortunately, this could not be investigated further due to the time restraints of this project. However, it seems that *Mcr. purpuratum* is similar to the *Rps. acidophila* LH2 complex, which carotenoids play an important role both in assembly and in structure stabilisation (Papiz, Prince et al. 2003, Gall, Henry et al. 2005). If the *CrtI* gene had been successfully inhibited or deleted it would have stopped the carotenoid biosynthesis pathway for okenone at neurosporene. This leaves the pathway unfinished and neurosporene would be accumulated as the major carotenoid. From the configuration of carotenoids, it is found that neurosporene only has 9 conjugate double bond. In comparison, okenone has 14 conjugated double bonds, including the carbonyl group. Okenone also has an additional O-CH₂ and is the only pigment with a 2,3,4 trimethylaryl substitution pattern. Is highly studied because it is viewed as structurally unique. Other purple sulphur bacteria have acyclic carotenoid pigments like rhodopin,

lycopene and spheroidene. An experiment was done to reconstitute okenone into the LH1-RC and LH2 complex of *Alc. minutissimum* (Toropygina, Makhneva, and Moskalenko 2005). As mentioned previously, this LH2 complex has been shown to be stable without carotenoid. It was found that okenone was readily reconstituted into the LH1-RC complex, whereas the reconstitution into LH2 complex was of very low efficacy (10%). All of this information implies that the LH2 complex is structurally unique for binding the carotenoid okenone. Each $\alpha\beta$ polypeptide pair is able to specifically bind one molecule of okenone. A 3D structure of the LH2 complex would reveal exactly how the okenone binds, fits within the polypeptide subunits and stabilises them.

6. Conclusions and Outlook

The overall aim of this study was to investigate the unusual B800-B830 LH2 complex of *Mcr. purpuratum* and the structural basis for this unusual Q_y NIR absorption.

An understanding of how the Bchl in LH complexes “tune” the absorption is a step towards how to create our own artificial solar biomimetic devices with high efficiency and complete control over the wavelengths of light absorbed (Cogdell, Brotosudarmo et al. 2010). There are many different factors, which affect the position of the Q_y absorption in LH complexes (Cogdell, Howard et al. 2002). These include Bchl *a* aggregation, the site energy of the Bchl binding site and the homology or heterogeneity of the LH2 complex. We can relate each of these to the results obtained in this thesis.

Now, it is thought that *Mcr. purpuratum* produces a single type of LH2 complex that incorporates all three *pucBA* genes that were identified. This results in a complex that is formed of six different apoproteins, three α and three β , resulting in a heterogeneous complex. The presence of such heterogeneity will be a challenge for structural biology techniques, such as crystallography, which deals poorly with a mixed sample. An example of this is seen with the B800-B820 LH2 complex from *Rps. palustris* LL. This has shown to be heterogeneous (Brotosudarmo, Kunz et al. 2009), and only a low-resolution X-ray structure was obtained. Crystallisation of the LH2 complex from *Mcr. purpuratum* was accomplished. These crystals diffracted to 6.7 Å and preliminary data from this indicates that the *Mcr. purpuratum* LH2 complex is an octamer, having 8 $\alpha\beta$ apoprotein heterodimers present in its ring structure. In comparison, the LH2 from *Rps. acidophila* is a nonamer, with 9 $\alpha\beta$ apoprotein heterodimer (Papiz, Prince et al. 2003). This makes the *Mcr. purpuratum* LH2 complex more similar to that from *Phs. molischianum*, which was determined to be an octamer (Koepke, Hu et al. 1996, Mascle-Allemand, Duquesne et al. 2010). The Q_y band will be blue shifted in comparison to the B800-B850 complex of *Rps. acidophila*. This is due to the exclusion of a single Bchl *a* dimerised pair from the ring structure. This effect is seen in the *Phs. molischianum* octamer ring structure. The LH2 of *Phs. molischianum* exhibits two absorption maxima, at 800 nm and 846 nm, though it is often referred to as the B800-B850 complex. This change from 850 to 846 is due to several reasons, including the change from nine $\alpha\beta$ heterodimers to eight. Further optimisation of these crystallisation conditions and others is still required to obtain a high-resolution structure of this LH2. I believe that the field will see an increased use of the technique Lipid Cubic Phase crystallisation (Landau and Rosenbusch 1996)(Rummel et al. 1998)(Caffrey and Cherezov 2009) to successfully crystallise membrane proteins. It has already been used to crystallise photosynthetic antenna complexes with success (Prince et al. 2003)(Katona et al. 2003) and will continue to do so. The field of protein crystallisation has come incredibly far over the years and will hopefully expand to the point where the membrane protein entries in the Protein Data Bank (PDB) match those of the soluble proteins (Giegé 2013).

Mcr. purpuratum has also been shown to be heterogeneous, expressing three different α and three different β . Both *Rps. acidophila* and *Phs. molischianum* only express a single $\alpha\beta$ polypeptide pair in their determined structures. A comparison of the sequences of the α and β apoproteins of the LH2 complex from *Mcr. purpuratum* with those of the LH2 complexes from *Rps. acidophila*, *Phs. molischianum* and *Alc. vinosum* shows a high degree of homology. The most homology is seen with the B800-B820 α and β of *Phs. molischianum*, and the α and β of the from the major component of the B820 LH2 complex from *Alc. vinosum*. This makes sense, as the absorption of B820 is closer to the B830 of the *Mcr. purpuratum* LH2 than the B850 complex. It was also observed that the B800 binding site of *Mcr. purpuratum* is probably similar to that in *Phs. molischianum* and *Alc. vinosum* as opposed to that of *Rps. acidophila*. It is the presence of an aspartic acid residue toward the N-terminus of the α polypeptide, which binds the B800 BChl *a*. There is a tryptophan residue at the C-terminus end of the β peptide, which is conserved throughout all the beta peptides of *Alc. vinosum* and *Mcr. purpuratum*. This residue is also conserved in *Phs. molischianum* and has been shown to participate in hydrogen bonding of the Bchl *a*. A unique feature of the *Mcr. purpuratum* binding site is the presence of a tryptophan residue that may be involved in hydrogen bonding. This tryptophan is found three amino acid residues before the conserved histidine, which participates in the Mg^{2+} binding of the dimeric Bchl *a*, and is present in all the α peptides. There is currently no known LH2 complex, which has hydrogen bonding that occurs before this conserved histidine residue. Another possible hydrogen bonding candidate is the tyrosine residue, which is conserved throughout the *Mcr. purpuratum* α polypeptides and the B820 *Alc. vinosum* α polypeptide. Both tryptophan and tyrosine are well-known hydrogen bond donors within LH2 complexes. Mutagenic experiments targeting these two residues would confirm if they were involved in hydrogen bonding to the B830 (Fowler, Sockalingum et al. 1994). On a similar note, it would be interesting to delete the *puc* operon to see what effect it would have on the Q_y absorption of the B830.

Though three α and three β polypeptides were found to be expressed in the *Mcr. purpuratum* B830 LH2 complex, it is not known in what ratio they appear. The six different peptides cannot be incorporated equally with the predicted ring structure as an octamer. Further experiments are needed in order to determine the ratio in which these peptides exist within the LH2 complex. Nano-HPLC MS-MS, which would separate the peptides, fragment them and detect the masses, could be used. Alternatively, a high-resolution crystal structure would also show the arrangement of the α and β polypeptides in the complex. There was success with using single molecule spectroscopy to characterise the heterogeneous polypeptide composition of the LL LH2 complex from *Rps. palustris* (Brotosudarmo et al. 2009).

Mcr. purpuratum did not produce alternate LH2 complexes under different growth conditions. Several bacteria species with multiple *pucBA* genes are known to do so. This includes a close relative of *Mcr. purpuratum*, *Alc. vinosum*. However, on the other hand, *Tcr. Tepidum*, which is

another close relative, does not produce different LH2 complexes in response to changes in environmental conditions. On a similar note, different strains of *Rps. acidophila* have been shown to respond differently to the same growth conditions. *Rps. acidophila* 7050 expresses the B800-850 LH2 at HL conditions and B800-820 at LL conditions. Whilst *Rps. acidophila* strain 10050 only expresses B800-850 LH2 complexes despite containing multiple *pucBA* gene pairs. For the experiments in this research, only growth in different light conditions was investigated. In *Alc. vinosum* different LH2 complexes are seen in changing light conditions and nutrient conditions. It could be revisited by changing the thiosulphate, used in the current *Mcr. purpuratum* media, to sulphide. At this stage, I believe it is highly unlikely that another complex would be produced under different growth conditions. It is possible that *Mcr. purpuratum* has adapted to its environment via the use of its unusual B800-830 complex which has not been found in any other photosynthetic organism so far. Most species have a B800-850 and/or a B800-820 complex to access the higher and lower ends of the NIR spectrum respectively. *Mcr. purpuratum* B830 LH2, which absorbs at 830 nm, is effectively in the middle of the standard absorbance range of 820 nm and 850 nm. Therefore, it has access to both without the need to produce multiple complexes. The heterogeneous nature of this LH2 complex contribute for the lack of different complexes under different growth conditions. *Mcr. purpuratum* expresses multiple α and β polypeptides within a single complex, which modifies the spectral features of these polypeptides to compensate for changing light intensities. It is possible that this could be an evolutionary adaptation and initially the antenna complexes of *Mcr. purpuratum* began as several subunits that contributed to a single spectral form.

It was found that the LH2 complex of *Mcr. purpuratum* is not stable without carotenoid, which is a typical result. It is rare to find LH2 complexes that can assemble without the need of carotenoid. The *CrtI* knock-out strain of *Mcr. purpuratum* was not completed within the time restraints of this project due to complications at the very final stage. The creation of a carotenoidless *Mcr. purpuratum* mutant would have allowed for the production of carotenoidless LH2 complexes at large scale without the use of the toxic chemical DPA and under standard growth conditions (without the use of a red filter). It would also have allowed the LH2 to be reconstituted - the complex taken apart and put back together again with the same parts, or brand new ones. I believe this is a huge area of exploration for photosynthetic antenna complexes. It would allow individual components of the complexes to be studied and the importance of different structural elements to protein binding, complex formation and function to be determined.

It was shown through thin cell sections in Chapter 3 that *Mcr. purpuratum* contains vesicular ICMs. It was found that carotenoidless mutants exhibit membrane structure changes. The species *Rba. sphaeroides* has a carotenoidless and LH2- mutant, known as R26, which has an altered membrane structure. Instead of the vesicular ICM that are usually seen, there was both vesicular and lamella (Lommen and Takemoto 1978, Golecki, Ventura et al. 1991). Further studies would

include repeating the thin cell sections for a carotenoidless *Mcr. purpuratum* mutant. This would have been a wonderful compliment to the DPA trials and *CrtI* KO, which were carried out in this study. The vesicles of the ICM seen in the whole cell sections were very small, only 37 nm across. A very similar diameter was seen when LH2 complex from *Mcr. purpuratum* was reconstituted into lipid and proteoliposomes were observed. This is a fascinating phenomenon that has not been observed before, usually flat sheets of membranes are seen, which are then used for AFM studies. As such, it can only be speculated why these proteoliposomes formed. It is suggested that it is due to the shape of the LH2 complex, as vesicular ICM are witnessed in whole cell sections.

In conclusion, the work in this thesis has revealed new information about *Mcr. purpuratum* and the reasons for why it exhibits the Q_y absorption that it does. There is still room for more work to be done to fully understanding this unique photosynthetic bacteria. For now though, this research has contributed to several publications which take us one step closer to understanding the structural basis of the B800-830 complex from *Mcr. purpuratum* and the detailed energy transfer that occurs. (Cranston, Roszak, and Cogdell 2014) (Niedzwiedzki and Cranston 2015) (Perlík, Seibt et al. 2015).

8. Appendices

8.1. *Mcr. purpuratum* media (Pfennig's Media)

<u>Solution 1: Autoclave</u>	per 500ml	5l	10l
Distilled H ₂ O	475ml	4750ml	9500ml
Trace Elements Solution	0.5ml	5ml	10ml
Potassium di-hydrogen phosphate	0.5g	5g	10g
Ammonium chloride	0.25g	2.5g	5g
Magnesium sulphate.7H ₂ O	1.5g	15g	30g
Calcium chloride DiHydrate	25mg	0.25g	0.5g
Sodium chloride	12.5g	125g	250g
Sodium acetate	0.5g	5g	10g

<u>Solution 2: Trace Elements</u>	per litre
EDTA di-Sodium salt	5.2g
Iron (II) chloride	1.5g
Zinc (II) chloride	0.07g
Manganese (II) chloride.4H ₂ O	0.1g
Boric acid	0.062g
Cobalt (II) chloride.6H ₂ O	0.19g
Copper (II) chloride.2H ₂ O	0.017g
Nickel (I) chloride.6H ₂ O	0.024g
Na ₂ MoO ₄ .2H ₂ O	0.036g

Add these in order. Adjust the pH with 30 drops of Na₂CO₃ (4.24g/20mL)

Solution 3: Refrigerate

2mg of Vitamin B12 Cyanocobalamin in 100ml of distilled H₂O.

Filter and sterilise the stock solution. Add 1ml per litre.

The solution 3, 4, 5, and 6 are added to solution 1 after it has been autoclaved and cooled. Solution 2 is used for solution 1.

Solution 4: 5% w/v Sodium Hydrogen Carbonate in distilled water. This solution is filtered and sterilised. 40mL per l is added to the medium.

Solution 5: 15% w/v (15g in 100mL) Sodium Thiosulfate. This is filtered and sterilised. 10mL per l is added to medium.

Solution 6: Autoclaved

5% w/v yeast extract. 10mL per l of media is added.

After adding all of the solutions, mix well and adjust the pH to 7.2 with sterile 2 molar Sulphuric acid or Na₂CO₃.

Final solution volumes	For 500ml	For 10l
Solution 1 (previously autoclaved)	475ml	9500ml
Solution 3	0.5ml	10ml
Solution 4	20ml	400ml
Solution 5	5ml	100ml
Solution 6	5ml	100ml
2M Na ₂ CO ₃ (to adjust pH)	1ml	20ml

8.2. Detergent Percentages

8.2.1. Solubilisation:

DM: = 2% (w/v)

DDM = 2% (w/v)

LDAO = 1.0% (v/v)

8.2.2. Detergent concentrations in buffers:

DM: 0.15% (w/v)

DDM: 0.02% (w/v)

LDAO: 0.1% (v/v)

8.3. Sucrose gradients:

LDAO

Protein
0.2 M 5 mls
0.4 M 6 mls
0.6 M 6 mls
0.8 M 5.5 mls

DM

Protein
0.8 M 5 mls
1.0 M 6 mls
1.2 M 6 mls
1.4 M 5.5 mls

DDM

Protein
0.6 M 7 mls
0.4 M 6 mls
0.6 M 6 mls

8.4. Dialysis Buffer

20mM Tris-HCl
 150 mM NaCl
 10 mM MgCl₂
 0.10% NaN₃
 pH to 9.0
 Make up to 5L with dH₂O

8.5. Agar Plates

Media required for *Mcr. purpuratum* growth on agar plates.
per 50 ml plate:

Autoclave 50 mls media (solution 1) with 1.5% agar.
When pouring plates add:

15 % Sodium thiosulphate	500 µl
2M Na ₂ CO ₃	100 µl
Vitamin B12 (0.02mg/ml)	50 µl
5% Sodium hydrogen carbonate	2000µl
5% Yeast extract	500 µl

For use with antibiotics: 30 µg/ml kanamycin is the working concentration.

8.6. Lysis buffer

For 1ml.

10µl 1M Tris pH 8.0

200µl 500mM EDTA

50µl 10% SDS (w/v) stock in DNase & RNase free water

740µl DNase & RNase free water

8.7. LB

For 1 L

10 g Tryptone

5 g Yeast extract

5 g Sodium Chloride

8.8. Crystallisation Screens

8.8.1. MemGold

Well	Salt	Buffer	pH	Precipitant
A1	None	0.08 M sodium citrate	5.2	2.2 M ammonium sulphate
B1	None	0.01 M Tris-HCl	8.0	1.2 M tri-sodium citrate
C1	None	0.015 M tricine	8.5	24 % (w/v) PEG 4000
D1	0.36 M sodium chloride	0.015 M sodium phosphate	7.0	9.9 % (w/v) PEG 4000
	0.1 % (w/v) sodium azide			
E1	0.3 M sodium chloride	0.01 M Tris-HCl	8.0	27.5 % (w/v) PEG 4000
F1	None	0.225 M MES/bis-tris	6.6	6.6 % (w/v) PEG 6000
G1	0.1 M ammonium sulphate	0.1 M HEPES	7.5	12.0 % (w/v) PEG 4000/22 % (v/v) glycerol
H1	0.02 M calcium chloride	0.2 M MES	6.5	7.7 % (w/v) PEG 1500
	0.01 M magnesium sulphate			
	0.02 M sodium chloride			
A2	None	0.05 M HEPES	7.5	2.5 M ammonium sulphate
B2	None	0.0665 M HEPES	7.5	1.1 M tri-sodium citrate
C2	None	0.15 M potassium phosphate	6.5	3.3 M ammonium sulphate
D2	0.1 M magnesium acetate	0.1 M sodium citrate	5.8	14 % (w/v) PEG 5000 MME
E2	0.1 M sodium chloride	0.02 M sodium citrate	5.6	11 % (w/v) PEG 3350
F2	0.1 M sodium chloride	0.02 M sodium citrate	5.6	5.5 % (w/v) PEG 3350
G2	0.05 M calcium chloride	0.1 M Tris-HCl	8.2	32 % (v/v) PEG 400
	0.05 M barium chloride			
H2	0.05 M sodium chloride	0.1 M sodium phosphate	6.2	16 % (w/v) PEG 4000
A3	0.1 M magnesium chloride	0.03 M Tris-HCl	8.2	19 % (w/v) PEG 4000
B3	0.2 M sodium chloride	0.025 M HEPES	7.5	13 % (w/v) PEG 4000
C3	None	0.1 M HEPES	7.5	11 % (w/v) PEG 3350
D3	0.1 M sodium chloride	0.02 M KMES	6.7	6.6 % (w/v) PEG 4000
E3	0.1 M potassium chloride	0.02 M Tris	7.0	20 % (w/v) PEG 4000
F3	0.05 M magnesium chloride	0.1 M sodium cacodylate	6.7	6.6 % (w/v) PEG 3350
	0.1 % (w/v) sodium azide			
G3	0.2 M potassium chloride	0.1 M sodium citrate	5.5	37 % (v/v) pentaerythritol propoxylate
H3	None	0.1 M Tris-HCl	8.0	5.5 % (w/v) PEG 4000
A4	0.1 M sodium chloride	0.02 M Tris	7.0	7.7 % (w/v) PEG 4000
B4	0.1 M magnesium chloride	0.1 M Tris-HCl	7.5	22 % (v/v) PEG 400
C4	0.04 M sodium chloride	0.04 M Tris	8.0	27 % (v/v) PEG 350 MME
D4	0.05 M sodium chloride	0.1 M sodium citrate	6.0	22 % (v/v) PEG 400
	0.02 M magnesium chloride			

E4	None	0.1 M sodium acetate	5.5	8.8 % (w/v) PET 2000 MME
F4	None	0.4 M ammonium acetate	8.0	13 % (w/v) PEG 2000 MME
G4	None	0.02 M bis Tris	7.0	15 % (w/v) PEG 2000
H4	0.1 M sodium chloride	0.02 M Tris	7.5	11 % (w/v) PEG 1500
	0.1 M magnesium chloride			
A5	0.1 M sodium chloride	0.1 M HEPES	8.0	11 % (w/v) PEG 1500
	0.1 M magnesium chloride			
B5	0.2 M sodium acetate	0.1 M HEPES	7.0	22 % (w/v) PEG 3000
	0.2 M potassium chloride			
C5	0.02 M nickel sulphate	0.1 M HEPES	7.0	33 % (v/v) Jeffamine-M600
D5	0.15 M sodium chloride	0.1 M Tris-HCl	8.0	13 % (w/v) PEG 6000
E5	0.2 M calcium chloride	0.1 M HEPES	7.5	53 % (v/v) PEG 400
F5	0.05 M magnesium acetate	0.05 M sodium acetate	5.0	28 % (v/v) PEG 400
G5	None	0.05 M HEPES	7.5	22 % (v/v) PEG 4000
H5	0.2 M calcium chloride	0.1 M Tris-HCl	8.0	44 % (v/v) PEG 400
A6	0.05 M magnesium acetate	0.05 M sodium acetate	5.4	24 % (v/v) PEG 400
B6	0.2 M calcium chloride	0.1 M MES	6.5	26 % (v/v) PEG 350 MME
C6	0.1 M potassium chloride	0.1 M Tris-HCl	8.5	39 % (v/v) PEG 400
D6	0.05 M magnesium chloride	0.1 M glycine	9.0	22 % (v/v) PEG 400
E6	0.1 M ammonium sulphate	0.1 M glycine	3.8	28 % (w/v) tri-ethylene glycol
F6	0.15 M sodium formate	0.1 M HEPES	7.2	18 % (w/v) PEG 3350
G6	None	0.2 M sodium acetate	6.8	8.8 % (w/v) PEG 6000
H6	0.2 M potassium chloride	0.1 M MES	6.5	18 % (w/v) PEG 6000
A7	0.22 M sodium citrate	0.1 M Tris	8.0	35 % (v/v) PEG 400
B7	None	0.1 M sodium acetate	4.5	17 % (v/v) PEG 400
C7	None	0.02 M Tris	8.5	1.0 M lithium sulphate/ 1.8 % (w/v) PEG 8000
D7	None	0.02 M Tris	7.5	22 % (v/v) PEG 550 MME
E7	0.05 M sodium chloride	0.02 M glycine	10.0	33 % (w/v) PEG 1000
F7	0.2 M magnesium chloride	0.1 M Tris	8.5	25 % (w/v) PEG 4000
G7	0.2 M magnesium chloride	0.1 M sodium cacodylate	6.5	31 % (w/v) PEG 2000
H7	None	0.64 M sodium acetate	4.6	18 % (w/v) PEG 3350
A8	0.1 M sodium chloride	0.1 M Tris-HCl	8.0	33 % (v/v) PEG 400
	0.1 M cadmium chloride			
B8	None	0.1 M Bicine	8.9	31 % (w/v) PEG 2000
C8	0.05 M sodium sulphate	0.05 M Tris	8.5	35 % (v/v) PEG 400
	0.05 M lithium sulphate			
D8	0.1 M sodium chloride	0.05 M glycine	9.5	33 % (v/v) PEG 300
E8	0.3 M magnesium nitrate	0.1 M Tris	8.0	23 % (w/v) PEG 2000
F8	0.12 M lithium sulphate	0.02 M Tris	7.5	20 % (v/v) PEG 300

		0.1 M sodium citrate	5.0	
G8	0.1 M sodium chloride	0.12 M Tris	9.4	20 % (v/v) PEG 400
H8	0.2 M sodium chloride	0.1 M HEPES	7.0	22 % (v/v) PEG 550 MME
A9	0.1 M sodium chloride	0.1 M Tris	8.0	21 % (v/v) PEG 400
	0.325 M sodium acetate			
B9	0.02 M sodium citrate	0.08 M sodium phosphate	6.2	18 % (w/v) PEG 2000
C9	0.02 M potassium nitrate	0.03 M potassium citrate	6.5	7.7 % (w/v) PEG 4000
D9	0.1 M sodium chloride	0.1 M Tris	8.5	30 % (w/v) PEG 2000 MME
	0.005 M magnesium chloride			
E9	0.2 M calcium chloride	0.1 M HEPES	7.0	33 % (v/v) PEG 400
F9	0.1 M calcium chloride	0.1 M Tris	6.5	13 % (w/v) PEG 2000 MME
G9	0.2 M ammonium sulphate	0.02 M sodium acetate	4.0	33 % (v/v) PEG 200
	0.02 M sodium chloride			
H9	0.07 M sodium chloride	0.05 M sodium citrate	4.5	22 % (v/v) PEG 400
A10	0.2 M ammonium sulphate	0.1 M sodium acetate	4.6	28 % (v/v) PEG 550 MME
B10	None	0.05 M glycine	9.0	55 % (v/v) PEG 400
C10	0.1 M magnesium chloride	0.1 M Tris	8.5	33 % (v/v) PEG 400
	0.1 M sodium chloride			
D10	0.1 M lithium sulphate	0.05 M citric acid	Non e	19 % (w/v) PEG 1000
	0.05 M di-sodium hydrogen phosphate			
E10	0.2 M magnesium chloride	0.025 M sodium citrate	4.0	33 % (v/v) PEG 400
	0.1 M potassium chloride			
F10	0.05 M zinc acetate	0.05 M MES	6.1	11 % (w/v) PEG 8000
G10	0.3 M magnesium nitrate	0.1 M Tris	8.0	22 % (w/v) PEG 8000
H10	0.1 M sodium chloride	0.1 M MES	6.0	33 % (v/v) PEG 400
	4 % (v/v) ethylene glycol			
A11	0.05 M sodium chloride	0.1 M sodium citrate	5.5	26 % (v/v) PEG 400
B11	0.1 M lithium sulphate	0.1 M glycine	9.3	30 % (v/v) PEG 400
C11	0.15 M potassium citrate	0.1 M sodium phosphate	Non e	22 % (w/v) PEG 6000
	0.05 M lithium citrate			
D11	0.001 M zinc sulphate	0.05 M HEPES	7.8	28 % (v/v) PEG 600
E11	0.1 M sodium chloride	0.1 M sodium phosphate	7.0	33 % (v/v) PEG 300
F11	0.1 M sodium chloride	0.05 M Bicine	9.0	3 % (v/v) PEG 300
G11	0.05 M zinc acetate	0.1 M sodium cacodylate	6.0	6.6 % (w/v) PEG 8000
	6 % (v/v) ethylene glycol			
H11	0.2 M lithium sulphate	0.1 M sodium citrate	3.5	28 % (v/v) PEG 400
A12	0.1 M sodium chloride	0.1 M Tris	7.5	11 % (w/v) PEG 4000
B12	0.05 M lithium sulphate	0.1 M tricine	7.4	7 % (w/v) PEG 3000
C12	0.2 M calcium chloride	0.1 M MES	6.5	33 % (v/v) PEG 400
D12	1 M sodium chloride	0.1 M sodium citrate	6.0	28 % (w/v) PEG 4000

E12	None	0.1 M HEPES	7.5	11 % (w/v) PEG 4000
F12	0.002 M zinc sulphate	0.08 M HEPES	7.0	25 % (v/v) Jeffamine ED2001
G12	0.001 M cadmium chloride	0.1 M MES	6.5	30 % (v/v) PEG 400
	0.03 M magnesium chloride			
H12	None	0.1 M bis-tris-propane	7.0	3.0 M sodium chloride

References

- Alberti, M., D. Burke and J. Hearst (2004). Structure and Sequence of the Photosynthesis Gene Cluster
- Allen, J. P., G. Feher, T. O. Yeates, H. Komiya and D. C. Rees (1987). "Structure of the reaction center from *Rhodobacter sphaeroides* R-26: the protein subunits." *Proc Natl Acad Sci U S A* 84(17): 6162-6166.
- Asherie, N. (2004). "Protein crystallization and phase diagrams." *Methods* 34(3): 266-272.
- Bahatyrova, S., R. N. Frese, C. A. Siebert, J. D. Olsen, K. O. van der Werf, R. van Grondelle, R. A. Niederman, P. A. Bullough, C. Otto and C. N. Hunter (2004). "The native architecture of a photosynthetic membrane." *Nature* 430(7003): 1058-1062.
- Bartley, G. E. and P. A. Scolnik (1989). "Carotenoid biosynthesis in photosynthetic bacteria. Genetic characterization of the *Rhodobacter capsulatus* CrtI protein." *J Biol Chem* 264(22): 13109- 13113.
- Berman, H. M., J. Westbrook, Z. Feng, G. Gilliland, T. N. Bhat, H. Weissig, I. N. Shindyalov and P. E. Bourne (2000). "The Protein Data Bank." *Nucleic Acids Research* 28(1): 235-242.
- Blankenship, R. E. (2013). *Molecular mechanisms of photosynthesis*, John Wiley & Sons.
- Blankenship, R. Madigan, M. and Bauer, C. *Anoxygenic Photosynthetic Bacteria.*, Springer Netherlands. 2: 1083-1106.
- Blundell, T. L. and L. N. Johnson (1976). *Protein Crystallography*, Academic Press.
- Borland, C. F., R. J. Cogdell, E. J. Land and T. G. Truscott (1989). "Bacteriochlorophyll a triplet state and its interactions with bacterial carotenoids and oxygen." *Journal of Photochemistry and Photobiology B: Biology* 3(2): 237-245.
- Bril, C. (1963). "Studies on bacterial chromatophores II. Energy transfer and photooxidative bleaching of bacteriochlorophyll in relation to structure in normal and carotenoid-depleted Chromatium." *Biochimica et Biophysica Acta* 66: 50-60.
- Brotosudarmo, T. H., R. Kunz, P. Bohm, A. T. Gardiner, V. Moulisova, R. J. Cogdell and J. Kohler (2009). "Single-molecule spectroscopy reveals that individual low-light LH2 complexes from *Rhodopseudomonas palustris* 2.1.6. have a heterogeneous polypeptide composition." *Biophys J* 97(5): 1491-1500.
- Brotosudarmo, T. H. P., A. M. Collins, A. Gall, A. W. Roszak, A. T. Gardiner, R. E. Blankenship and R. J. Cogdell (2011). "The light intensity under which cells are grown controls the type of peripheral light-harvesting complexes that are assembled in a purple photosynthetic bacterium." *Biochemical Journal* 440: 51-61.
- Brotosudarmo, T H et al. 2009. "Single-Molecule Spectroscopy Reveals That Individual Low-Light LH2 Complexes from *Rhodopseudomonas Palustris* 2.1.6. Have a Heterogeneous Polypeptide Composition." *Biophys J* 97(5): 1491–1500.
- Carey, A.-M., K. Hacking, N. Picken, S. Honkanen, S. Kelly, D. M. Niedzwiedzki, R. E. Blankenship, Y. Shimizu, Z.-Y. Wang-Otomo and R. J. Cogdell (2014). "Characterisation of the LH2 spectral variants produced by the photosynthetic purple sulphur bacterium *Allochrochromatium vinosum*." *Biochimica et Biophysica Acta (BBA) - Bioenergetics* 1837(11): 1849-1860.
- Caffrey, Martin, and Vadim Cherezov. 2009. "Crystallizing Membrane Proteins Using Lipidic Mesophases." *Nat. Protocols* 4(5): 706–31.
- Carpenter, E. P., K. Beis, A. D. Cameron and S. Iwata (2008). "Overcoming the challenges of membrane protein crystallography." *Current Opinion in Structural Biology* 18(5): 581-586.
- Chayen, N. E. (1998). "Comparative studies of protein crystallization by vapour-diffusion and microbatch techniques." *Acta Crystallographica Section D-Biological Crystallography* 54: 8-15.
- Clayton, R. K. (1980). *Photosynthesis. Physical mechanisms and chemical patterns.*
- Clayton, R. K. and R. Haselkorn (1972). "Protein components of bacterial photosynthetic membranes." *J Mol Biol* 68(1): 97-105.
- Codgell, R. J., J. Southall, A. T. Gardiner, C. J. Law, A. Gall, A. W. Roszak and N. W. Isaacs (2006). "How purple photosynthetic bacteria harvest solar energy." *Comptes Rendus Chimie* 9(2): 201-206.
- Cogdell, R. J., P. Fyfe, T. Howard, N. Fraser, N. Isaacs, A. Freer, K. McKluskey and S. Prince (2004). The Structure and Function of the LH2 Complex from *Rhodopseudomonas acidophila* Strain 10050, with Special Reference to the Bound Carotenoid
- Cogdell R. J. and Frank, H. (1985). Carotenoids in photosynthesis. *Pure and Applied Chemistry*. 57: 723.
- Cogdell, R. J., T. H. Brotosudarmo, A. T. Gardiner, P. M. Sanchez and L. Cronin (2010). "Artificial photosynthesis—solar fuels: current status and future prospects." *Biofuels* 1(6): 861- 876.
- Cogdell, R. J., P. K. Fyfe, S. J. Barrett, S. M. Prince, A. A. Freer, N. W. Isaacs, P. McGlynn and C. N. Hunter (1996). "The purple bacterial photosynthetic unit." *Photosynthesis Research* 48(1- 2): 55-63.
- Cogdell, R. J., A. Gall and J. Kohler (2006). "The architecture and function of the light-harvesting apparatus of purple bacteria: from single molecules to in vivo membranes." *Q Rev Biophys* 39(3): 227-324.
- Cogdell, R. J., A. T. Gardiner, H. Hashimoto and T. H. P. Brotosudarmo (2008). "A comparative look at the first few milliseconds of the light reactions of photosynthesis." *Photochemical & Photobiological Sciences* 7(10): 1150-1158.
- Cogdell, R. J., A. M. Hawthornthwaite, M. B. Evans, L. A. Ferguson, C. Kerfeld, J. P. Thornber, F. van Mourik and R. van Grondelle (1990). "Isolation and characterisation of an unusual antenna complex from the

- marine purple sulphur photosynthetic bacterium *Chromatium purpuratum* BN5500." *Biochimica et Biophysica Acta (BBA) - Bioenergetics* 1019(3): 239-244.
- Cogdell, R. J., T. D. Howard, R. Bittl, E. Schlodder, I. Geisenheimer and W. Lubitz (2000). "How carotenoids protect bacterial photosynthesis." *Philosophical Transactions of the Royal Society B: Biological Sciences* 355(1402): 1345-1349.
- Cogdell, R. J., T. D. Howard, N. W. Isaacs, K. McLuskey and A. T. Gardiner (2002). "Structural factors which control the position of the Q(y) absorption band of bacteriochlorophyll a in purple bacterial antenna complexes." *Photosynth Res* 74(2): 135-141.
- Cogdell, R. J., N. W. Isaacs, T. D. Howard, K. McLuskey, N. J. Fraser and S. M. Prince (1999). "How photosynthetic bacteria harvest solar energy." *J Bacteriol* 181(13): 3869-3879.
- Cogdell, R. J. and H. Scheer (1985). "Circular dichroism of Light Harvesting Complexes from Purple Photosynthetic bacteria*." *Photochemistry and Photobiology* 42(6): 669-678.
- Cohen-Bazire, G. and R. Y. Stanier (1958). "Inhibition of Carotenoid Synthesis in Photosynthetic Bacteria: Specific Inhibition of Carotenoid Synthesis in a Photosynthetic Bacterium and its Physiological Consequences." *Nature* 181(4604): 250-252.
- Cranston, L. J., A. W. Roszak and R. J. Cogdell (2014). "Crystallization and preliminary X-ray diffraction analysis of the peripheral light-harvesting complex LH2 from *Marichromatium purpuratum*." *Acta Crystallogr F Struct Biol Commun* 70(Pt 6): 808-813.
- Crounse, J. B., R. P. Feldman and R. K. Clayton (1963). "Accumulation of Polyene Precursors of Neurosporene in Mutant Strains of *Rhodospseudomonas sphaeroides*." *Nature* 198(4886): 1227-1228.
- Dau, H. and K. Sauer (1996). "Exciton equilibration and Photosystem II exciton dynamics — a fluorescence study on Photosystem II membrane particles of spinach." *Biochimica et Biophysica Acta (BBA) - Bioenergetics* 3(2): 175-190.
- Davidson, E. and R. J. Cogdell (1981). "The polypeptide composition of the B850 light-harvesting pigment—protein complex from *Rhodospseudomonas sphaeroides*, R26.1." *FEBS Letters* 132(1): 81-84.
- De Yoreo, J. J. and P. G. Vekilov (2003). "Principles of Crystal Nucleation and Growth." *Reviews in Mineralogy and Geochemistry* 54(1): 57-93.
- Deisenhofer, J., O. Epp, K. Miki, R. Huber and H. Michel (1985). "Structure of the protein subunits in the photosynthetic reaction centre of *Rhodospseudomonas viridis* at 3 Å resolution." *Nature* 318(6047): 618-624.
- Deisenhofer, J. and H. Michel (1989). "The photosynthetic reaction center from the purple bacterium *Rhodospseudomonas viridis* - NOBEL LECTURE, December 8, 1988." *Chemica Scripta* 29(3): 205-&.
- Doll, S. and A. L. Burlingame (2015). "Mass Spectrometry-Based Detection and Assignment of Protein Posttranslational Modifications." *ACS Chemical Biology* 10(1): 63-71.
- Donohue, T. J., P. J. Kiley and S. Kaplan (1988). "The *puf* operon region of *Rhodobacter sphaeroides*." *Photosynthesis Research* 19(1): 39-61.
- Drenth, J. (2007). *Principles of Protein X-Ray Crystallography*, Springer New York.
- Emsley, P., B. Lohkamp, W. G. Scott and K. Cowtan (2010). "Features and development of Coot." *Acta Crystallogr D Biol Crystallogr* 66(Pt 4): 486-501.
- Förster, T. (1948). "Zwischenmolekulare Energiewanderung und Fluoreszenz." *Annalen der Physik* 437(1-2): 55-75.
- Fowler, G. J., G. D. Sockalingum, B. Robert and C. N. Hunter (1994). "Blue shifts in bacteriochlorophyll absorbance correlate with changed hydrogen bonding patterns in lightharvesting 2 mutants of *Rhodobacter sphaeroides* with alterations at alpha-Tyr-44 and alpha-Tyr- 45." *Biochem J* 299 (Pt 3): 695-700.
- Frank, H., Young, A., Britton, G., Cogdell, R. (2006) "The Photochemistry of Carotenoids", Springer Netherlands. 8: 71-80.
- Frank, H. and R. J. Cogdell (1996). "Carotenoids in Photosynthesis." *Photochemistry and Photobiology* 63(3): 257-264.
- Fuller, R. C. and I. C. Anderson (1958). "Inhibition of Carotenoid Synthesis in Photosynthetic Bacteria: Suppression of Carotenoid Synthesis and its Effect on the Activity of Photosynthetic Bacterial Chromatophores." *Nature* 181(4604): 252-254.
- Gall, A., S. Henry, S. Takaichi, B. Robert and R. J. Cogdell (2005). "Preferential Incorporation of Coloured-carotenoids Occurs in the LH2 Complexes From Non-sulphur Purple Bacteria Under Carotenoid-limiting Conditions." *Photosynthesis Research* 86(1): 25-35.
- Gardiner, A. T., R. J. Cogdell and S. Takaichi (1993). "The effect of growth conditions on the light-harvesting apparatus in *Rhodospseudomonas acidophila*." *Photosynthesis Research* 38(2): 159- 167.
- Gardiner, A. T., R. C. MacKenzie, S. J. Barrett, K. Kaiser and R. J. Cogdell (1996). "The purple photosynthetic bacterium *Rhodospseudomonas acidophila* contains multiple *puc* peripheral antenna complex (LH2) genes: Cloning and initial characterisation of four beta/alpha pairs." *Photosynthesis Research* 49(3): 223-235.
- Gardiner, A. T., R. C. MacKenzie, S. J. Barrett, K. Kaiser and R. J. Cogdell (1996). "The purple photosynthetic bacterium *Rhodospseudomonas acidophila* contains multiple *puc* peripheral antenna complex (LH2) genes: Cloning and initial characterisation of four β/α pairs." *Photosynthesis Research* 49(3): 223-235.
- Ghosh, R., H. Hauser and R. Bachofen (1988). "Reversible dissociation of the B873 lightharvesting complex from *Rhodospirillum rubrum* G9+." *Biochemistry* 27(3): 1004-1014.

- Giegé, Richard. 2013. "A Historical Perspective on Protein Crystallization from 1840 to the Present Day." *FEBS Journal* 280(24): 6456–97. <http://dx.doi.org/10.1111/febs.12580>.
- Golecki, J. R., S. Ventura and J. Oelze (1991). "The architecture of unusual membrane tubes in the B800–850 light-harvesting bacteriochlorophyll-deficient mutant 19 of *Rhodobacter sphaeroides*." *FEMS Microbiology Letters* 77(2-3): 335-340.
- Gonçalves, R. P., J. Busselez, D. Lévy, J. Seguin and S. Scheuring (2005). "Membrane insertion of *Rhodospseudomonas acidophila* light harvesting complex 2 investigated by high resolution AFM." *Journal of Structural Biology* 149(1): 79-86.
- Grigoriev, I. V., H. Nordberg, I. Shabalov, A. Aerts, M. Cantor, D. Goodstein, A. Kuo, S. Minovitsky, R. Nikitin, R. A. Ohm, R. Otilar, A. Poliakov, I. Ratnere, R. Riley, T. Smirnova, D. Rokhsar and I. Dubchak (2011). "The Genome Portal of the Department of Energy Joint Genome Institute." *Nucleic Acids Research*.
- Guan, L., I. N. Smirnova, G. Verner, S. Nagamori and H. R. Kaback (2006). "Manipulating phospholipids for crystallization of a membrane transport protein." *Proceedings of the National Academy of Sciences of the United States of America* 103(6): 1723-1726.
- Hacking, K. (2015). Characterisation of the LH2 complexes of *Allochromatium vinosum*. PhD, University of Glasgow.
- Hall, T. A. (1999). "BioEdit: a user-friendly biological sequence alignment editor and analysis program for Windows 95/98/NT." *Nucleic Acids Symposium Series* 41: 95-98.
- Hayashi, H., T. Nozawa, M. Hatano and S. Morita (1981). "Circular dichroism of bacteriochlorophyll *a* in light harvesting bacteriochlorophyll protein complexes from *Chromatium vinosum*." *Journal of Biochemistry* 89(6): 1853-1861.
- Henry, S. L. and R. J. Cogdell (2013). Chapter Seven - The Evolution of the Purple Photosynthetic Bacterial Light-Harvesting System. *Advances in Botanical Research*. J. T. Beatty, Academic Press. Volume 66: 205-226.
- Hjelmeland, L. M. (1990). "Solubilization of native membrane proteins." *Methods Enzymol* 182: 253-264.
- Holten, D., M. W. Windsor, W. W. Parson and J. P. Thornber (1978). "Primary photochemical processes in isolated reaction centers of *Rhodospseudomonas viridis*." *Biochim Biophys Acta* 501(1): 112
- Horton, R. M., H. D. Hunt, S. N. Ho, J. K. Pullen and L. R. Pease (1989). "Engineering hybrid genes without the use of restriction enzymes: gene splicing by overlap extension." *Gene* 77(1): 61-68.
- Imhoff, J. F., J. Suling and R. Petri (1998). "Phylogenetic relationships among the Chromatiaceae, their taxonomic reclassification and description of the new genera *Allochromatium*, *Halochromatium*, *Isochromatium*, *Marichromatium*, *Thiococcus*, *Thiohalocapsa* and *Thermochromatium*." *International Journal of Systematic Bacteriology* 48(4): 1129-1143.
- Imhoff, J. F. and H. G. Trüper (1980). "*Chromatium purpuratum*, sp. nov., a new species of the Chromatiaceae." *Zentralblatt für Bakteriologie: I. Abt. Originale C: Allgemeine, angewandte und ökologische Mikrobiologie* 1(1): 61-69.
- Iwata, S. (2003). Methods and results in crystallization of membrane proteins, Internat'l University Line.
- Jensen, S. L., G. Cohen-Bazire, T. O. M. Nakayama and R. Y. Stanier (1958). "The path of carotenoid synthesis in a photosynthetic bacterium." *Biochimica et Biophysica Acta* 29(3): 477-498.
- Joanne Lemieux, M., R. A. F. Reithmeier and D.-N. Wang (2002). "Importance of detergent and phospholipid in the crystallization of the human erythrocyte anion-exchanger membrane domain." *Journal of Structural Biology* 137(3): 322-332.
- Katona, Gergely et al. 2003. "Lipidic Cubic Phase Crystal Structure of the Photosynthetic Reaction Centre from *Rhodobacter Sphaeroides* at 2.35 Å Resolution." *Journal of Molecular Biology* 331(3): 681–92.
- Kereiche, S., L. Bourinet, W. Keegstra, A. A. Arteni, J.-M. Verbavatz, E. J. Boekema, B. Robert and A. Gall (2008). "The peripheral light-harvesting complexes from purple sulfur bacteria have different 'ring' sizes." *FEBS Letters* 582(25–26): 3650-3656.
- Kerfeld, C A, J P Thornber, and T O Yeates. 1993. "Crystallization of Two Integral Membrane Pigment-Protein Complexes from the Purple-Sulfur Bacterium *Chromatium Purpuratum*." *Protein science : a publication of the Protein Society* 2(8): 1352–55.
- Kerfeld, Cheryl A, Todd O Yeates, and J Philip Thornber. 1994. "Purification and Characterization of the Peripheral Antenna of the Purple-Sulfur Bacterium *Chromatium Purpuratum*: Evidence of an Unusual Pigment-Protein Composition." *Biochemistry* 33(8): 2178–84
- Kiley, P. J. and S. Kaplan (1987). "Cloning, DNA sequence, and expression of the *Rhodobacter sphaeroides* light-harvesting B800-850- α and B800-850- β genes." *J Bacteriol* 169(7): 3268-3275.
- Kimber, M. S., F. Vallee, S. Houston, A. Necakov, T. Skarina, E. Evdokimova, S. Beasley, D. Christendat, A. Savchenko, C. H. Arrowsmith, M. Vedadi, M. Gerstein and A. M. Edwards (2003). "Data mining crystallization databases: knowledge-based approaches to optimize protein crystal screens." *Proteins* 51(4): 562-568.
- Kirk, J. T. O. (1994). *Light and Photosynthesis in Aquatic Ecosystems*, Cambridge University Press.
- Kirmaier, C. and D. Holten (1987). "Primary photochemistry of reaction centers from the photosynthetic purple bacteria." *Photosynthesis Research* 13(3): 225-260.
- Koepke, J., X. Hu, C. Muenke, K. Schulten and H. Michel "The crystal structure of the lightharvesting complex II (B800–850) from *Rhodospirillum rubrum*." *Structure* 4(5): 581-597.

- Kortlücke, C., K. Breese, N. Gad'on, A. Labahn and G. Drews (1997). "Structure of the puf operon of the obligately aerobic, bacteriochlorophyll alpha-containing bacterium *Roseobacter denitrificans* OCh114 and its expression in a *Rhodobacter capsulatus* puf puc deletion mutant." *Journal of Bacteriology* 179(17): 5247-5258.
- Laemmli, U. K. (1970). "Cleavage of structural proteins during the assembly of the head of bacteriophage T4." *Nature* 227(5259): 680-685.
- Lambs, L., M. Venturini, B. Decock-Le Reverend, H. Kozłowski and G. Berthon (1988). "Metal ion-tetracycline interactions in biological fluids. Part 8. Potentiometric and spectroscopic studies on the formation of Ca(II) and Mg(II) complexes with 4-dedimethylamino-tetracycline and 6-desoxy- 6-demethyl-tetracycline." *J Inorg Biochem* 33(3): 193-210. Landau, Ehud M., and Jürg P. Rosenbusch. 1996. "Lipidic Cubic Phases: A Novel Concept for the Crystallization of Membrane Proteins." *Proceedings of the National Academy of Sciences* 93(25): 14532-35.
- Law, Vivian et al. 2014. "DrugBank 4.0: Shedding New Light on Drug Metabolism." *Nucleic acids research* 42(Database issue): D1091-7.
- Law, C. J. and R. J. Cogdell (2007). The light-harvesting system of purple anoxygenic photosynthetic bacteria. *Primary Processes of Photosynthesis*, Part 1: 205-259.
- Lee, J. K., S. Q. Wang, J. M. Eraso, J. Gardner and S. Kaplan (1993). "Transcriptional regulation of puc operon expression in *Rhodobacter Sphaeroides*- Involvement of an integration host factor binding sequence." *Journal of Biological Chemistry* 268(32): 24491-24497.
- Li, J., D. Gilroy, D. M. Tiede and M. Gunner (1998). "Kinetic phases in the electron transfer from P+ QA-QB to P+ QAQB-and the associated processes in *Rhodobacter sphaeroides* R-26 reaction centers." *Biochemistry* 37(9): 2818-2829.
- Loftin, K. A., C. D. Adams, M. T. Meyer and R. Surampalli (2008). "Effects of ionic strength, temperature, and pH on degradation of selected antibiotics." *J Environ Qual* 37(2): 378-386.
- Lommen, M. A. and J. Takemoto (1978). "Comparison, by freeze-fracture electron microscopy, of chromatophores, spheroplast-derived membrane vesicles, and whole cells of *Rhodospseudomonas sphaeroides*." *J Bacteriol* 136(2): 730-741.
- Madigan, M. T. and D. O. Jung (2009). *An Overview of Purple Bacteria: Systematics, Physiology, and Habitats. The Purple Phototrophic Bacteria*. C. N. Hunter, F. Daldal, M. C. Thurnauer and J. T. Beatty. Dordrecht, Springer Netherlands: 1-15.
- Magdaong, N. M., A. M. LaFountain, J. A. Greco, A. T. Gardiner, A. M. Carey, R. J. Cogdell, G. N. Gibson, R. R. Birge and H. A. Frank (2014). "High efficiency light harvesting by carotenoids in the LH2 complex from photosynthetic bacteria: unique adaptation to growth under low-light conditions." *J Phys Chem B* 118(38): 11172-11189.
- Makhneva, Z., M. Bolshakov and A. Moskalenko (2008). "Heterogeneity of carotenoid content and composition in LH2 of the purple sulphur bacterium *Allochrochromatium minutissimum* grown under carotenoid-biosynthesis inhibition." *Photosynthesis Research* 98(1-3): 633-641.
- Makhneva, Z., M. Bolshakov and A. Moskalenko (2008). "Heterogeneity of carotenoid content and composition in LH2 of the purple sulphur bacterium *Allochrochromatium minutissimum* grown under carotenoid-biosynthesis inhibition." *Photosynth Res* 98(1-3): 633-641.
- Malik, K. A. (1983). "A modified method for the cultivation of phototrophic bacteria." *Journal of Microbiological Methods* 1(6): 343-352.
- Masclé-Allemand, C., K. Duquesne, R. Lebrun, S. Scheuring and J. N. Sturgis (2010). "Antenna mixing in photosynthetic membranes from *Phaeospirillum molischianum*." *Proceedings of the National Academy of Sciences* 107(12): 5357-5362.
- McCoy, Airlie J et al. 2007. "{it Phaser} Crystallographic Software." *Journal of Applied Crystallography* 40(4): 658-74. McDermott, G., S. M. Prince, A. A. Freer, A. M. Hawthornthwaite-Lawless, M. Z. Papiz, R. J. Cogdell and N. W. Isaacs (1995). "Crystal structure of an integral membrane light-harvesting complex from photosynthetic bacteria." *Nature* 374(6522): 517-521.
- McDermott, G., S. M. Prince, A. A. Freer, A. M. Hawthornthwaite-lawless, M. Z. Papiz, R. J. Cogdell and N. W. Isaacs (1995). "Crystal structure of an integral membrane slight harvesting complex from photosynthetic bacteria." *Nature* 374(6522): 517-521.
- McLuskey, K., S. M. Prince, R. J. Cogdell and N. W. Isaacs (2001). "The crystallographic structure of the B800-820 LH3 light-harvesting complex from the purple bacteria *Rhodospseudomonas acidophila* strain 7050." *Biochemistry* 40(30): 8783-8789.
- McPherson, A. (1990). "CURRENT APPROACHES TO MACROMOLECULAR CRYSTALLIZATION." *European Journal of Biochemistry* 189(1): 1-23. Michel, H. (1982). "Three-dimensional crystals of a membrane protein complex." *Journal of Molecular Biology* 158(3): 567-572.
- Michel, H., O. Epp and J. Deisenhofer (1986). "Pigment—protein interactions in the photosynthetic reaction centre from *Rhodospseudomonas viridis*." *The EMBO journal* 5(10): 2445.
- Miller, J. F., S. B. Hinchigeri, P. S. Parkes-Loach, P. M. Callahan, J. R. Sprinkle, J. R. Riccobono and P. A. Loach (1987). "Isolation and characterization of a subunit form of the light-harvesting complex of *Rhodospirillum rubrum*." *Biochemistry* 26(16): 5055-5062. Miller, K. R. (1982). "Three-dimensional

- structure of a photosynthetic membrane." *Nature* 300(5887): 53-55. Mitchell, P. (1961). "Coupling of Phosphorylation to Electron and Hydrogen Transfer by a ChemiOsmotic type of Mechanism." *Nature* 191(4784): 144-148.
- Moskalenko, A. A. and Z. K. Makhneva (2012). "Light-harvesting complexes from purple sulfur bacteria *Allochrochromatium minutissimum* assembled without carotenoids." *J Photochem Photobiol B* 108: 1-7.
- Moskalenko, A. A., Z. K. Makhneva, L. Fiedor and H. Scheer (2005). "Effects of carotenoid inhibition on the photosynthetic RC-LH1 complex in purple sulphur bacterium *Thiorhodospira sibirica*." *Photosynth Res* 86(1-2): 71-80.
- Newstead, S., S. Ferrandon and S. Iwata (2008). "Rationalizing alpha-helical membrane protein crystallization." *Protein Science* 17(3): 466-472.
- Newstead, S., S. Ferrandon and S. Iwata (2008). "Rationalizing α -helical membrane protein crystallization." *Protein Science* 17(3): 466-472.
- Niedzwiedzki, D. M., D. Bina, N. Picken, S. Honkanen, R. E. Blankenship, D. Holten and R. J. Cogdell (2012). "Spectroscopic studies of two spectral variants of light-harvesting complex 2 (LH2) from the photosynthetic purple sulfur bacterium *Allochrochromatium vinosum*." *Biochimica Et Biophysica Acta-Bioenergetics* 1817(9): 1576-1587.
- Niedzwiedzki, D. M. and Cranston, L., 2015. "Excited State Lifetimes and Energies of Okenone and Chlorobactene, Exemplary Keto and Non-Keto Aryl Carotenoids." *Physical Chemistry Chemical Physics* 17(20): 13245-56
- Nishimura, Y., K. Shimada, I. Yamazaki and M. Mimuro (1993). "Energy transfer processes in *Rhodopseudomonas palustris* grown under low-light conditions." *FEBS Letters* 329(3): 319-323.
- Nordberg, H., M. Cantor, S. Dusheyko, S. Hua, A. Poliakov, I. Shabalov, T. Smirnova, I. V. Grigoriev and I. Dubchak (2014). "The genome portal of the Department of Energy Joint Genome Institute: 2014 updates." *Nucleic Acids Res* 42(Database issue): D26-31.
- Oelze, J. and G. Drews (1972). "Membranes of photosynthetic bacteria." *Biochimica et Biophysica Acta (BBA) - Reviews on Biomembranes* 265(2): 209-239.
- Okamura, M. Y., L. A. Steiner and G. Feher (1974). "Characterization of reaction centers from photosynthetic bacteria. I. Subunit structure of the protein mediating the primary photochemistry in *Rhodopseudomonas spheroides* R-26." *Biochemistry* 13(7): 1394-1403.
- Ostermeier, C. and H. Michel (1997). "Crystallization of membrane proteins." *Current opinion in structural biology* 7(5): 697-701.
- Page, R. and R. C. Stevens (2004). "Crystallization data mining in structural genomics: using positive and negative results to optimize protein crystallization screens." *Methods* 34(3): 373-389.
- Papiz, M. Z., S. M. Prince, T. H., Cogdell R. J. and Isaacs N. W., (2003). "The structure and thermal motion of the B800-850 LH2 complex from *Rps.acidophila* at 2.0Å resolution and 100K: new structural features and functionally relevant motions." *J Mol Biol* 326(5): 1523-1538.
- Parkes-Loach, P. S., C. J. Law, P. A. Recchia, J. Kehoe, S. Nehrlich, J. Chen and P. A. Loach (2001). "Role of the core region of the PufX protein in inhibition of reconstitution of the core lightharvesting complexes of *Rhodobacter sphaeroides* and *Rhodobacter capsulatus*." *Biochemistry* 40(19): 5593-5601.
- Parkes-Loach, P. S., J. R. Sprinkle and P. A. Loach (1988). "Reconstitution of the B873 lightharvesting complex of *Rhodospirillum rubrum* from the separately isolated alpha- and betapolypeptides and bacteriochlorophyll a." *Biochemistry* 27(8): 2718-2727.
- Perlík, Václav et al. 2015. "Vibronic Coupling Explains the Ultrafast Carotenoid-to-Bacteriochlorophyll Energy Transfer in Natural and Artificial Light Harvesters." *Journal of Chemical Physics* 142(21): 234
- Pestka, Sidney. 1974. "[28] The Use of Inhibitors in Studies of Protein Synthesis." *Methods in Enzymology* 30: 261-82
- Polívka, T. and H. A. Frank (2010). "Molecular factors controlling photosynthetic light harvesting by carotenoids." *Acc Chem Res* 43(8): 1-1134.
- Polívka, T. and V. Sundström (2004). "Ultrafast Dynamics of Carotenoid Excited States-From Solution to Natural and Artificial Systems." *Chemical Reviews* 104(4): 2021-2072.
- Polli, D., G. Cerullo, G. Lanzani, S. De Silvestri, H. Hashimoto and R. J. Cogdell (2006). "Carotenoid-Bacteriochlorophyll Energy Transfer in LH2 Complexes Studied with 10-fs Time Resolution." *Biophysical Journal* 90(7): 2486-2497.
- Preusch, P. C., J. C. Norvell, J. C. Cassatt and M. Cassman (1998). "Progress away from 'no crystals, no grant'." *Nature structural biology* 5(1): 12-14.
- Prince, S. M., M. Z. Papiz, A. A. Freer, G. McDermott, A. M. HawthornthwaiteLawless, R. J. Cogdell and N. W. Isaacs (1997). "Apoprotein structure in the LH2 complex from *Rhodopseudomonas acidophila* strain 10050: Modular assembly and protein pigment interactions." *Journal of Molecular Biology* 268(2): 412-423.
- Prince, S M et al. 2003. "Detergent Structure in Crystals of the Integral Membrane LightHarvesting Complex LH2 from *Rhodopseudomonas Acidophila* Strain 10050." *Journal of Molecular Biology* 326(1): 307-15.
- Prive, G. G. (2007). "Detergents for the stabilization and crystallization of membrane proteins." *Methods* 41(4): 388-397.
- Qian, P., C. Neil Hunter and P. A. Bullough (2005). "The 8.5 Å Projection Structure of the Core RC-LH1-PufX Dimer of *Rhodobacter sphaeroides*." *Journal of Molecular Biology* 349(5): 948- 960.

- Rondonuwu, F. S., T. Taguchi, R. Fujii, K. Yokoyama, Y. Koyama and Y. Watanabe (2004). "The energies and kinetics of triplet carotenoids in the LH2 antenna complexes as determined by phosphorescence spectroscopy." *Chemical Physics Letters* 384(4–6): 364–371.
- Roszak, A. W., T. D. Howard, J. Southall, A. T. Gardiner, C. J. Law, N. W. Isaacs and R. J. Cogdell (2003). "Crystal structure of the RC-LH1 core complex from *Rhodospseudomonas palustris*." *Science* 302(5652): 1199–1202.
- Rummel, Gabriele et al. 1998. "Lipidic Cubic Phases: New Matrices for the Three-Dimensional Crystallization of Membrane Proteins." *Journal of Structural Biology* 121(2): 82–91.
- Sambrook, J. and E. F. Fritschy (2000). *Molecular Cloning: A Laboratory Manual* (Third Edition). Cold Spring Harbor, NY: Cold Spring Harbor Laboratory Press.
- Sauer, P. R. R., F. Lottspeich, E. Unger, R. Mentele and H. Michel (1996). "Deletion of a B800–850 Light-Harvesting Complex in *Rhodospirillum rubrum* DSM119 Leads to "Revertants" Expressing a B800–820 Complex: Insights into Pigment Binding." *Biochemistry* 35(20): 6500–6507.
- Savage, H., M. Cyrklaff, G. Montoya, W. Kühlbrandt and I. Sinning (1996). "Two-dimensional structure of light harvesting complex II (LHII) from the purple bacterium *Rhodovulum sulfidophilum* and comparison with LHII from *Rhodospseudomonas acidophila*." *Structure* 4(3): 243–252.
- Schafer, A., A. Tauch, W. Jäger, J. Kalinowski, G. Thierbach and A. Pühler (1994). "Small mobilizable multi-purpose cloning vectors derived from the *Escherichia coli* plasmids pK18 and pK19: selection of defined deletions in the chromosome of *Corynebacterium glutamicum*." *Gene* 145(1): 69–73.
- Scheer, H., W. A. Svec, B. T. Cope, M. H. Studier, R. G. Scott and J. J. Katz (1974). "Structure of bacteriochlorophyll b." *Journal of the American Chemical Society* 96(11): 3714–3716.
- Scheuring, S. and J. N. Sturgis (2009). "Atomic force microscopy of the bacterial photosynthetic apparatus: plain pictures of an elaborate machinery." *Photosynthesis Research* 102(2): 197–211.
- Scholes, G. D. (2003). "Long-range resonance energy transfer in molecular systems." *Annu Rev Phys Chem* 54: 57–87.
- Scholes, G. D., X. J. Jordanides and G. R. Fleming (2001). "Adapting the Förster Theory of Energy Transfer for Modeling Dynamics in Aggregated Molecular Assemblies." *The Journal of Physical Chemistry B* 105(8): 1640–1651.
- Sekine, F., K. Horiguchi, Y. Kashino, Y. Shimizu, L.-J. Yu, M. Kobayashi and Z.-Y. Wang (2012). "Gene sequencing and characterization of the light-harvesting complex 2 from thermophilic purple sulfur bacterium *Thermochromatium tepidum*." *Photosynthesis Research* 111(1): 9–18.
- Siebert, C. A., P. Qian, D. Fotiadis, A. Engel, C. N. Hunter and P. A. Bullough (2004). "Molecular architecture of photosynthetic membranes in *Rhodobacter sphaeroides*: the role of PufX." *The EMBO Journal* 23(4): 690–700.
- Silva, A. M. N., R. Vitorino, M. R. M. Domingues, C. M. Spickett and P. Domingues (2013). "Post-translational Modifications and Mass Spectrometry Detection." *Free Radical Biology and Medicine* 65: 925–941.
- Sistrom, W. R. and R. K. Clayton (1964). "Studies on a mutant of *Rhodospseudomonas sphaeroides* unable to grow photosynthetically." *Biochim Biophys Acta* 88: 61–73.
- Smyth, M. S. and J. H. J. Martin (2000). "x Ray crystallography." *Molecular Pathology* 53(1): 8–14.
- Sonoda, Y., S. Newstead, N.-J. Hu, Y. Alguel, E. Nji, K. Beis, S. Yashiro, C. Lee, J. Leung, A. D. Cameron, B. Byrne, S. Iwata and D. Drew (2011). "Benchmarking Membrane Protein Detergent Stability for Improving Throughput of High-Resolution X-ray Structures." *Structure* 19(1): 17–25.
- Sonoda, Y., S. Newstead, N.-J. Hu, Y. Alguel, E. Nji, K. Beis, S. Yashiro, C. Lee, J. Leung, A. D. Cameron, B. Byrne, S. Iwata and D. Drew (2011). "Benchmarking Membrane Protein Detergent Stability for Improving Throughput of High-Resolution X-ray Structures." *Structure (London, England: 1993)* 19(1): 17–25.
- Stackebrandt, E., R. G. E. Murray and H. G. Truper (1988). "PROTEOBACTERIA-CLASSIS NOV, A NAME FOR THE PHYLOGENETIC TAXON THAT INCLUDES THE PURPLE BACTERIA AND THEIR RELATIVES." *International Journal of Systematic Bacteriology* 38(3): 321–325.
- Stamouli, A., S. Kafi, D. C. G. Klein, T. H. Oosterkamp, J. W. M. Frenken, R. J. Cogdell and T. J. Aartsma (2005). "The Ring Structure and Organization of Light Harvesting 2 Complexes in a Reconstituted Lipid Bilayer, Resolved by Atomic Force Microscopy." *Biophysical Journal* 84(4): 2483–2491.
- Stark, W., W. Kühlbrandt, I. Wildhaber, E. Wehrli and K. Muhlethaler (1984). "The structure of the photoreceptor unit of *Rhodospseudomonas viridis*." *EMBO J* 3(4): 777–783.
- Stolz, J. F. (1990). *Structure of Phototrophic Prokaryotes*, Taylor & Francis.
- Tadros, M. H. and K. Waterkamp (1989). "Multiple copies of the coding regions for the light-harvesting B800–850 alpha- and beta-polypeptides are present in the *Rhodospseudomonas palustris* genome." *EMBO J* 8(5): 1303–1308.
- Tadros, Monier Habib et al. 1987. "Orientation of the B800–850, B870, and Reaction Center Polypeptides on the Cytoplasmic and Periplasmic Surfaces of *Rhodobacter capsulata* Membranes." *Biochemistry* 26(24): 7680–7687.
- Tate, C. G. (2010). *Practical Considerations of Membrane Protein Instability during Purification and Crystallisation. Heterologous Expression of Membrane Proteins: Methods and Protocols*. I. Mus-Veteau. Totowa, NJ, Humana Press: 187–203.
- Telfer, A., A. Pascal and A. Gall (2008). *Carotenoids in photosynthesis*. Carotenoids, Springer: 265–308.

- Tharia, H., T. Nightingale, M. Papiz and A. Lawless (1999). "Characterisation of hydrophobic peptides by RP-HPLC from different spectral forms of LH2 isolated from *Rps. palustris*." *Photosynthesis Research* 61(2): 157-167.
- Timmins, P. A., M. Leonhard, H. U. Weltzien, T. Wacker and W. Welte (1988). "A physical characterization of some detergents of potential use for membrane protein crystallization." *FEBS Letters* 238(2): 361-368.
- Toropygina, O. A., Z. K. Makhneva and A. A. Moskalenko (2005). "Reconstitution of Okenone into light harvesting complexes from *Allochrochromatium minutissimum*." *Biochemistry (Mosc)* 70(11): 1231-1237.
- van Neil, C. B. (1941). "The bacterial photosyntheses and their importance for the general problem of photosynthesis." *Advances in Enzymology and Related Subjects of Biochemistry* 1: 263-328.
- "UniProt: The Universal Protein Knowledgebase." 2017. *Nucleic Acids Research* 45(D1): D158– 69
- Vogl, K. and D. A. Bryant (2011). "Elucidation of the Biosynthetic Pathway for Okenone in *Thiodictyon* sp. CAD16 Leads to the Discovery of Two Novel Carotene Ketolases." *Journal of Biological Chemistry* 286(44): 38521-38532.
- Wacker, T., N. Gad'on, A. Becker, W. Mäntele, W. Kreutz, G. Drews and W. Welte (1986). "Crystallization and spectroscopic investigation with polarized light of the reaction center-B875 light-harvesting complex of *Rhodospseudomonas palustris*." *FEBS Letters* 197(1-2): 267-273.
- Walz, T. and R. Ghosh (1997). "Two-dimensional crystallization of the light-harvesting I - reaction centre photounit from *Rhodospirillum rubrum*1." *Journal of Molecular Biology* 265(2): 107-111.
- Wang, Z.-Y., M. Shimonaga, H. Suzuki, M. Kobayashi and T. Nozawa (2003). "Purification and Characterization of the Polypeptides of Core Light-Harvesting Complexes from Purple Sulfur Bacteria." *Photosynthesis Research* 78(2): 133-141.
- Weissgerber, T., R. Ziggann, D. Bruce, Y.-J. Chang, J. C. Detter, C. Han, L. Hauser, C. D. Jeffries, M. Land, C. Munk, R. Tapia and C. Dahl (2011). Complete genome sequence of *Allochrochromatium vinosum* DSM 180" *Standards in Genomic Sciences* 5(3): 311-330.
- Welte, W., T. Wacker, M. Leis, W. Kreutz, J. Shiozawa, N. Gad'on and G. Drews (1985). "Crystallization of the photosynthetic light-harvesting pigment-protein complex B800-850 of *Rhodospseudomonas capsulata*." *FEBS Letters* 182(2): 260-264.
- White, S. H. and W. C. Wimley (1999). Membrane protein folding and stability: Physical principles. *Annual Review of Biophysics and Biomolecular Structure*. 28: 319-365.
- Williams, K. P., B. W. Sobral and A. W. Dickerman (2007). "A robust species tree for the Alphaproteobacteria." *Journal of Bacteriology* 189(13): 4578-4586.
- Yang, J., M.-C. Yoon, H. Yoo, P. Kim and D. Kim (2012). "Excitation energy transfer in multiporphyrin arrays with cyclic architectures: towards artificial light-harvesting antenna complexes." *Chemical Society Reviews* 41(14): 4808-4826.
- Young, A. and G. Britton (2012). *Carotenoids in photosynthesis*, Springer Science & Business Media.
- Zuber, H. (1985). "Structure and function of light harvesting complexes and their polypeptides." *Photochemistry and Photobiology* 42(6): 821-844.